water

MDPI

Article

Modelling Peatland Productivity by Water Table Depth or Near-Surface Water Contents via the *DIMONA* Online Platform

Dimitre D. Dimitrov [1,*] and Peter M. Lafleur [2]

[1] Department of University Transfer, Faculty of Arts & Sciences, NorQuest College, 10215 108 St NW, Edmonton, AB T5J 1L6, Canada
[2] School of the Environment, Trent University, 1600 West Bank Drive, Peterborough, ON K9L 0G2, Canada
* Correspondence: dimitre@ualberta.ca; Tel.: +1-780-989-8882

Abstract: This study extends our previous work showing that a process-based (PB) model, the *DIMONA* PB model, could accurately simulate peatland soil water dynamics when driven by water table depth, d_{WT}, or by near surface soil water contents, θ. Here, we explore the model's ability to simulate the peatland canopy photosynthesis, growth, biomass, height, and gross primary productivity (GPP) of vascular plants and bryophytes—thus ecosystem GPP—using either of these drivers. The *DIMONA* PB model is embedded into the *DIMONA* online modelling platform, a web application capable of ingesting data from the Internet and performing machine learning (ML) modelling and Internet of Things (IoT) modelling complementary to PB modelling. We test whether the *DIMONA* PB model, driven by d_{WT} (Hypothesis 1) and by near-surface θ (Hypothesis 2), can successfully simulate peatland ecosystem GPP at the Mer Bleue bog (Ontario, Canada). Two model runs were generated, one driven by d_{WT} and another by near-surface θ. Both model runs performed with similar accuracy. Data fit for simulated on observed GPP reached 0.72 for R^2, 1.7 umol CO_2 m^{-2} s^{-1} for RMSE, and 0.88 for Willmott's index of agreement at an hourly time step and 0.91, 0.8 g C m^{-2} d^{-1}, and 0.92, respectively, at a daily time step. We use the output from the two model runs to examine whether the model's modifiers (i.e., equations) for water control can capture the specifics of contrasting hydrological conditions on peatland GPP (Hypothesis 3). Both model runs closely simulated the observed GPP to contrasting peatland hydrological conditions under similar meteorological forcing. We illustrate the ability of the *DIMONA* platform to facilitate the parameterization of *DIMONA* models for any geographic location, as well as its ability to perform IoT modelling of real-time photosynthesis at two site locations and ML modelling for ecosystem GPP as a complementary tool to PB modelling.

Keywords: process-based modelling; ecosystem and plant productivities; new modelling approach for plant water control on productivity; online modelling platform; peatlands

Academic Editor: Richard Smardon

Received: 8 November 2024
Revised: 27 December 2024
Accepted: 30 December 2024
Published: 7 January 2025

Citation: Dimitrov, D.D.; Lafleur, P.M. Modelling Peatland Productivity by Water Table Depth or Near-Surface Water Contents via the *DIMONA* Online Platform. *Water* **2025**, *17*, 134. https://doi.org/10.3390/w17020134

1. Introduction

Plant gross primary productivity, GPP, is a main component of the carbon (C) balance of natural ecosystems [1,2] and their agricultural counterparts [3], a global sink for atmospheric CO_2 [4], and the main driver of food production from agricultural crops [5] and agro-ecosystems [6]. In peatlands, GPP is the main source of soil C, which represents ~1/3 of the world's soil C or ~450–500 Pg organic C [7,8]. Since peatland GPP is sensitive to water table (WT) depths and water content in the peat profile [9,10], it is of primary importance to better understand the mechanisms behind this response, especially because climate change may impact hydrodynamic conditions in peatlands [2,11].

1.1. Advances and Limitations with Estimating GPP

Ecosystem GPP has been estimated by field observations, remote sensing, and/or modelling, each of which has advances and limitations. A major limitation of field observations is that sites with eddy covariance (EC) measurements are scarce, representing only small areas of the landscape that cannot be easily scaled up spatially [12,13], while the major limitations of remote sensing are the coarse temporal resolutions of GPP and their general inability to provide a detailed explanation of the processes that determine GPP [14].

To overcome the above limitations, modelling has been used in conjunction with field observations and remote sensing for the estimation, explanation, and prediction of GPP [15], and particularly GPP in peatlands [10]. However, many detailed models are usually data-intensive and parameter-expensive due to their detailed schemes for dynamic modelling of photosynthesis, leaf area index (LAI), and GPP, driven by sub-daily multivariable meteorological forcing, such as incoming short-wave radiation, I_{swr}, ambient air temperature, T_{air}, atmospheric relative humidity, RH, wind speed, v_w, and rain/show precipitation [10,16–19].

Simplistic models use empirical hydrological modifiers [20,21], and hydrologically sophisticated models explicitly simulate plant water relations [10,22], as their accurate representation is a key feature for modelling the GPP of peatlands [23–25]. Although empirical modifiers may work well, they generally lack the depth of process explanation under different ecological conditions. However, hydrologically sophisticated models are not only parameter-expensive and data-intensive but also bring additional uncertainty with their coupled simulations for soil water fluxes driven by precipitation, vertical and lateral drainage, and evapotranspiration via water potential gradients, as well as highly variable and, in many cases, unknown hydraulic conductivities [26,27].

1.2. Rationale of the Proposed Research

Simulated plant hydrology may not be easily reconciled with precipitation and soil hydrology due to the complexity and uncertainty of the latter, especially in peatlands [26,27], and the limited knowledge of plant hydrological properties in general [14]. Detailed model equations for plant water relations permit calculations of dynamic water fluxes. However, these calculations involve canopy, turgor, and/or osmotic water potential gradients for simulated plant species, constrained by axial resistances or conductances for primary and secondary vascular plant roots or bryophyte rhizoids, radial resistances or conductances from root/rhizoid surfaces to their internal axes, as well as from the surrounding soil to the surfaces of roots or rhizoids. In addition to the complexity of calculations, the required parameters for simulated plant water fluxes are normally taken from the literature or lab studies and may not necessarily reflect the plant properties at the sites of interest; they thereby may need to be adjusted, which increases modelling uncertainty [10]. Furthermore, many of the existing models are technology-demanding, especially if combined for large spatial scale simulations with other research software, e.g., Geographic Information Systems (GISs) [28] or various remote sensing products [29]. Even a single model run may require specialized knowledge of operating systems (such as Linux), Visual Studio, or CMD consoles instead of the more standard Windows or Mac environments. Thus, the computational skills needed for model applications often limit their wide use by researchers with no modelling background.

To overcome the above limitations, a process-based (PB) model, the *DIMONA* PB model, was developed for simulating the effects of plant water relations on GPP (Copyright © 2019 Dimitre Dikov Dimitrov, Edmonton, AB, Canada). The model introduces a series of modifiers for plant water control on GPP, which affect simulated photosynthesis, plant growth, root/rhizoid respiration, and nutrient uptake. They are especially designed to emphasize

soil hydrological properties that are measured at field sites, extractable by remote sensing, or accessible on designated websites or internet data repositories, rather than using the scarce and laboratory-derived plant-specific parameters. While the hydrological component of the *DIMONA* PB model were successfully tested in a peatland environment [26,27], the present study is focused on testing the plant components of the model that simulate GPP. To facilitate its use, the model was embedded within the namesake online ecosystem modelling and research platform *DIMONA* (Copyright © 2019 Dimitre Dikov Dimitrov, Edmonton, AB, Canada). *DIMONA* is an internet-based, easy-to-use, multi-purpose modelling and research platform designed as a web application.

1.3. Objectives and Hypotheses

The main objective of this study is to test a set of simple process-oriented modifiers for plant water control on GPP, together with the other equations and algorithms in the *DIMONA* PB model, for simulating peatland productivity. Another objective is to demonstrate the potential of and benefits from using the *DIMONA* online platform for research and modelling purposes. In this study, the *DIMONA* PB model is driven by meteorological forcing of I_{swr}, T_{air}, RH, v_w, and soil hydrology instead of precipitation. The related conceptual and modelling hypotheses are as follows:

Hypothesis 1. *As the water table (WT) depth, d_{WT}, was found to be a reliable predictor of soil water contents, θ, at various depths in unsaturated peat [26], d_{WT} together with I_{swr}, T_{air}, RH, and v_w can be used to accurately reproduce peatland ecosystem and plant productivities. Thus, we hypothesize that the DIMONA PB model driven by site observations of d_{WT} and meteorology will reliably simulate peatland productivities (i.e., GPP) through the soil– plant water continuum by circumventing combined uncertainties in local soil and plant hydrological properties.*

Hypothesis 2. *Following [27], d_{WT} can be predicted by near-surface θ in peat; thus, peatland ecosystem and plant productivities can be modelled accurately by inputs of near-surface θ together with I_{swr}, T_{air}, RH, and v_w. We hypothesize that near-surface peat θ observations measured can drive reliably simulations of peatland productivities.*

Hypothesis 3. *The simple process-oriented modifiers for the effects of plant–water relations on GPP driven by observed d_{WT} and near-surface θ capture the specifics of hydrological effects on peatland GPP.*

2. Materials and Methods

2.1. DIMONA Platform and Model

2.1.1. DIMONA Platform Overview

The DIMONA Ecosystem Modelling Platform, hereafter referred to as *DIMONA*, consists of the web application *DIMONA_online*, referred to as the *DIMONA* web application, which hosts the mathematical model *DIMONA*, referred as the *DIMONA* model. *DIMONA* is an acronym for **D**ynamic **I**ntegrated **M**odel for **O**rganism–e**N**vironment **A**nalysis (Copyright © 2019 Dimitre Dikov Dimitrov, Edmonton, AB, Canada). The *DIMONA* platform (Figure 1) is designed for the following purposes: (i) process-based (PB) scientific modelling with explanatory and predictive power (Figure 2a,b); (ii) Internet of Things (IoT) real-time modelling (Figure 3); (iii) machine learning (ML) data-driven predictive modelling (Figure 4); (iv) exploring and collecting data on the weather and climate, soil properties, hydrology, and biota (plants, animals, fungi) at any location on the globe by its geographic coordinates (Figure 5). The three modelling components of the *DIMONA* mathematical model are also referred to as the *DIMONA* PB, IoT, and ML models. For the above purposes, *DIMONA* connects with API websites, such as OpenWeatherMap (London, UK), Agro API (London, UK), Soil-

Grids REST (version 2.0), GBIF (version 1.0, Copenhagen, Denmark, Leaflet (version 1.9.4, Kyiv, Ukraine), or other websites and software as indicated in the *DIMONA* code.

In its current pilot version, *DIMONA* resides on an HP Pavilion Notebook workstation (laptop) with a hardware configuration of Intel(R) Core(TM) i5-7200U CPU @ 2.50 GHz 2.71 GHz Processor, 12 GB of RAM, and 64-bit operating system. The software environment hosting the *DIMONA* web application and model executables is MAMP 3.3.1 with a local Apache server and MySQL database server installed on the HP Pavilion laptop and playing the role of web server(s) when their ports are open and accessible on the internet via password-protected ngrok-stable-windows-amd64 internet tunnels. The front-end code, i.e., *DIMONA*'s website graphical user interface (GUI), is written in HTML5 (version 5.0), CSS3 (version 3.0), and JavaScript/jQuery (version ECMAScript 2019), and the back-end code for operating with the server and the database is written in the PHP7 (version 7.1.5) and MySQL (version 5.6.34) programming languages. The code of the *DIMONA* PB and IoT models is written in C++ (version ISO C++17) nd the code of the ML model in the C++ and Python3 (version 3.9.6) programming languages. Compiled C++ model executables (.exe) for the PB, IoT, and ML models and/or Python3 model executables (.py) for ML modelling via the TensorFlow (version 2.12.0) open-source ML framework are placed on a platform store accessible to all users, who can pick the model executables of interest and place them in their own user-created folders in the users' personal accounts (Figure 6a,b).

DIMONA's 5-tier architecture is described in detail in the Supplementary Material. Tier I serves the front end, i.e., *DIMONA*'s GUI, accessible from user/client personal computers (PC), from where they can reach *DIMONA* by using any browser, e.g., Google Chrome, Mozilla Firefox, etc. In the current *DIMONA* pilot version, the internet connection from the user's browser to *DIMONA* via ngrok internet tunnels is activated by the developer upon users' requests to generate a URL that is sent to them for working remotely. In its pilot capacity, *DIMONA* can handle a number of users working simultaneously in their own personal accounts. When exploring sites and data sources, *DIMONA* users do not need to have personal accounts; however, for all modelling activities, personal *DIMONA* accounts are required.

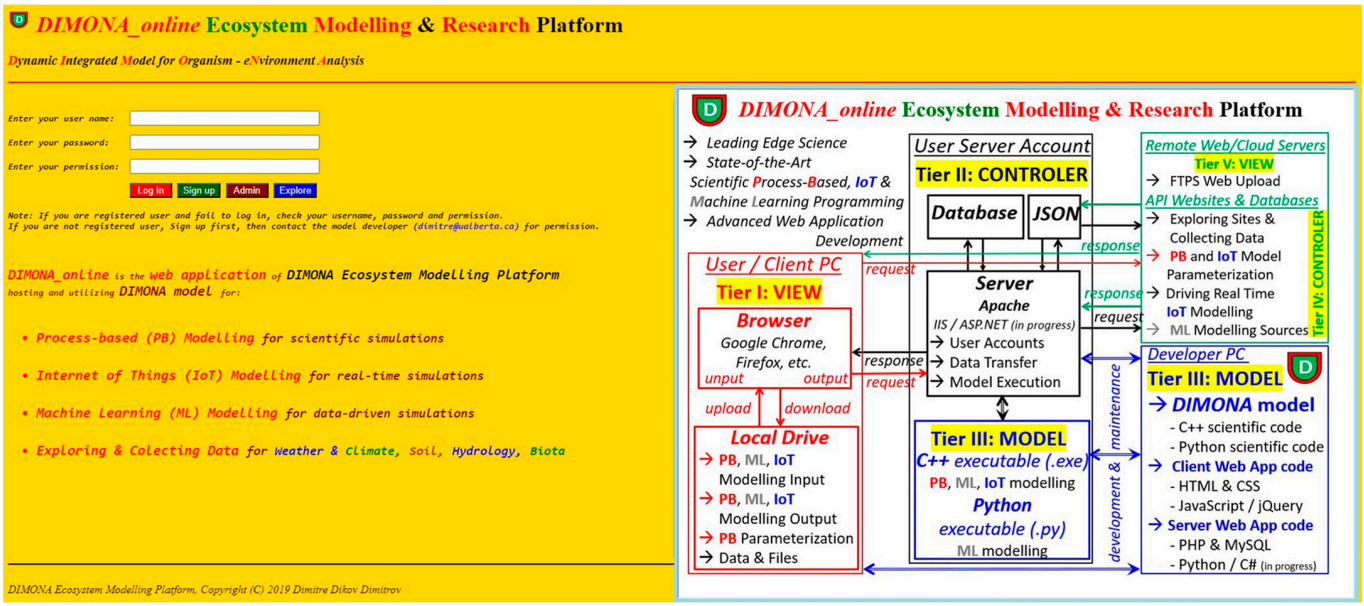

Figure 1. The main screen and schematic of the *DIMONA* platform. Model users can navigate to sign up/log into their personal accounts or just explore the connected online sources without personal accounts.

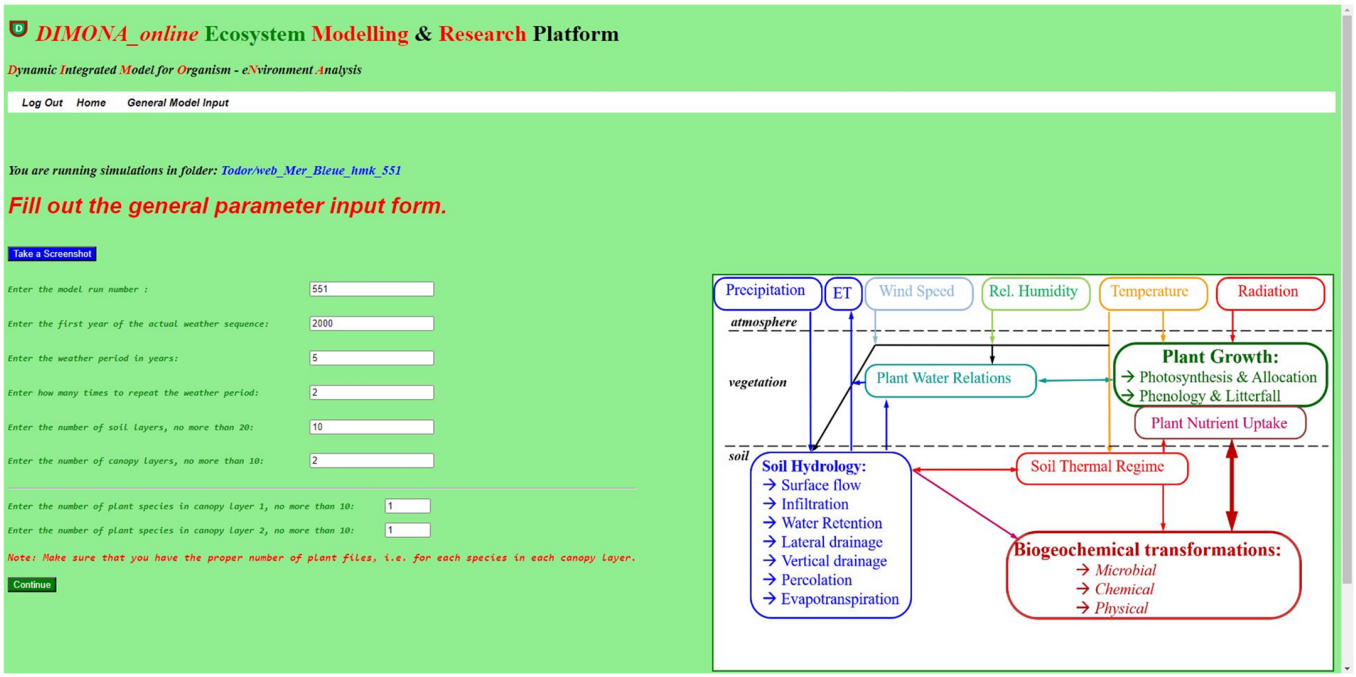

(**a**)

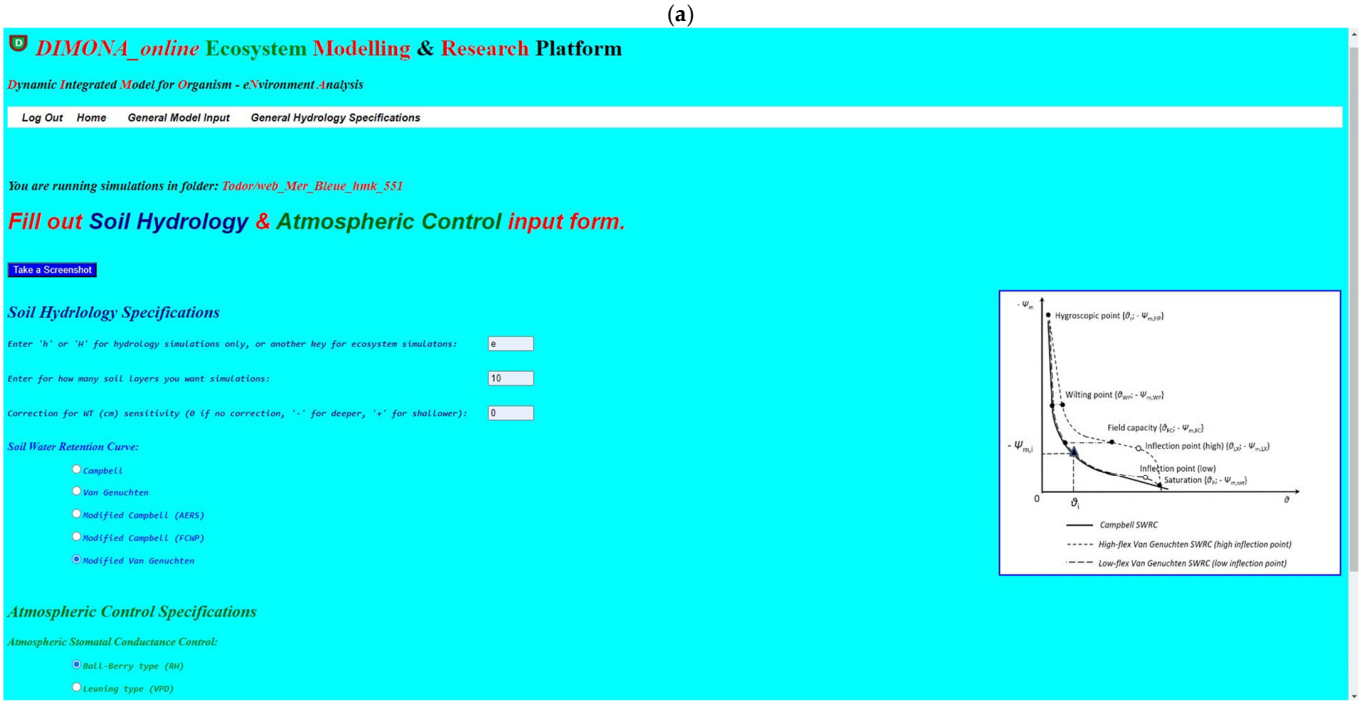

(**b**)

Figure 2. The general parameter screen (**a**) and the hydrology specifications screen (**b**) of the process-based (PB) model.

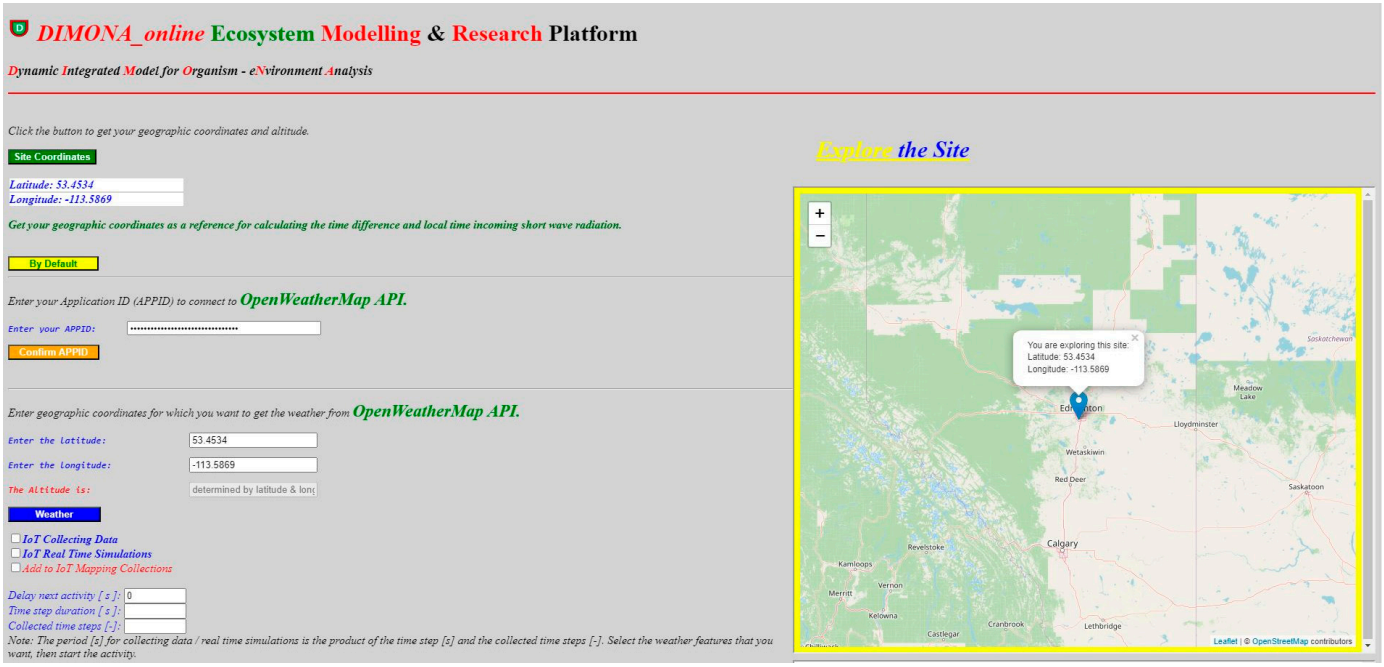

Figure 3. Part of the entrance screen for Internet of Things (IoT) modelling and/or exploring weather data at any geographic location around the world.

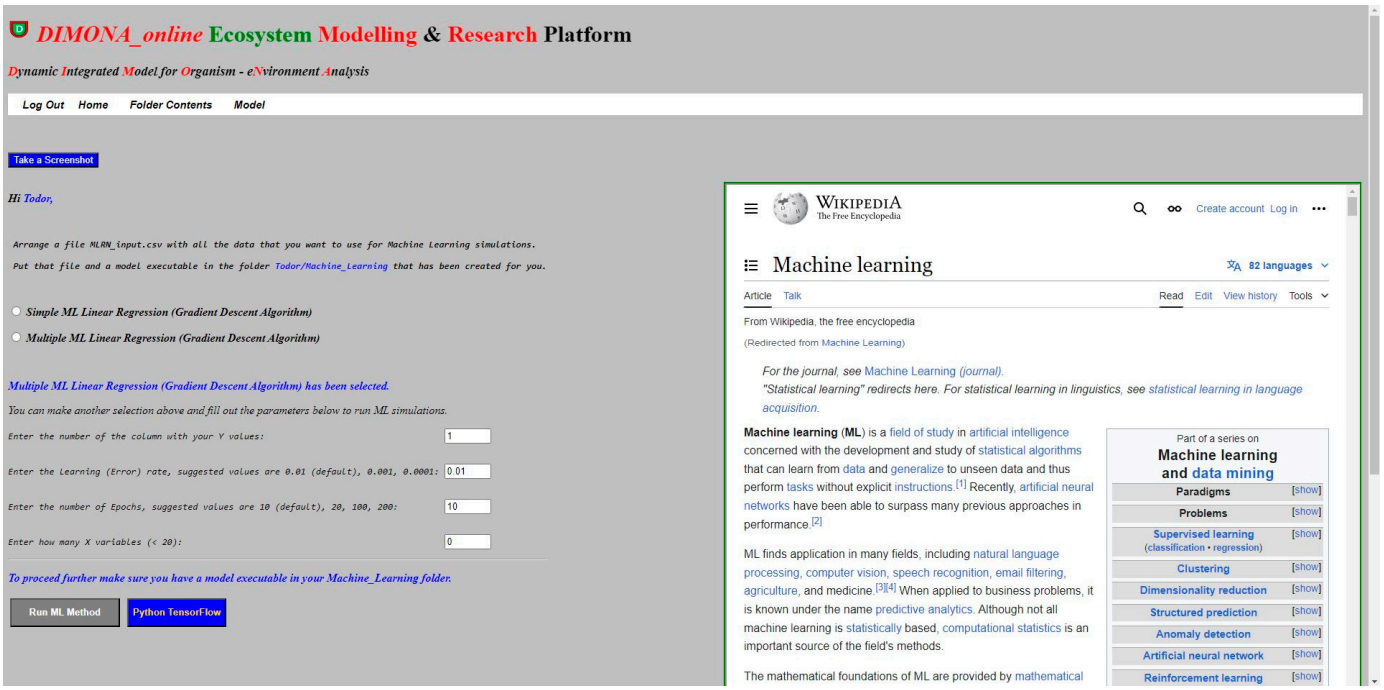

Figure 4. The entrance screen for machine learning (ML) modelling.

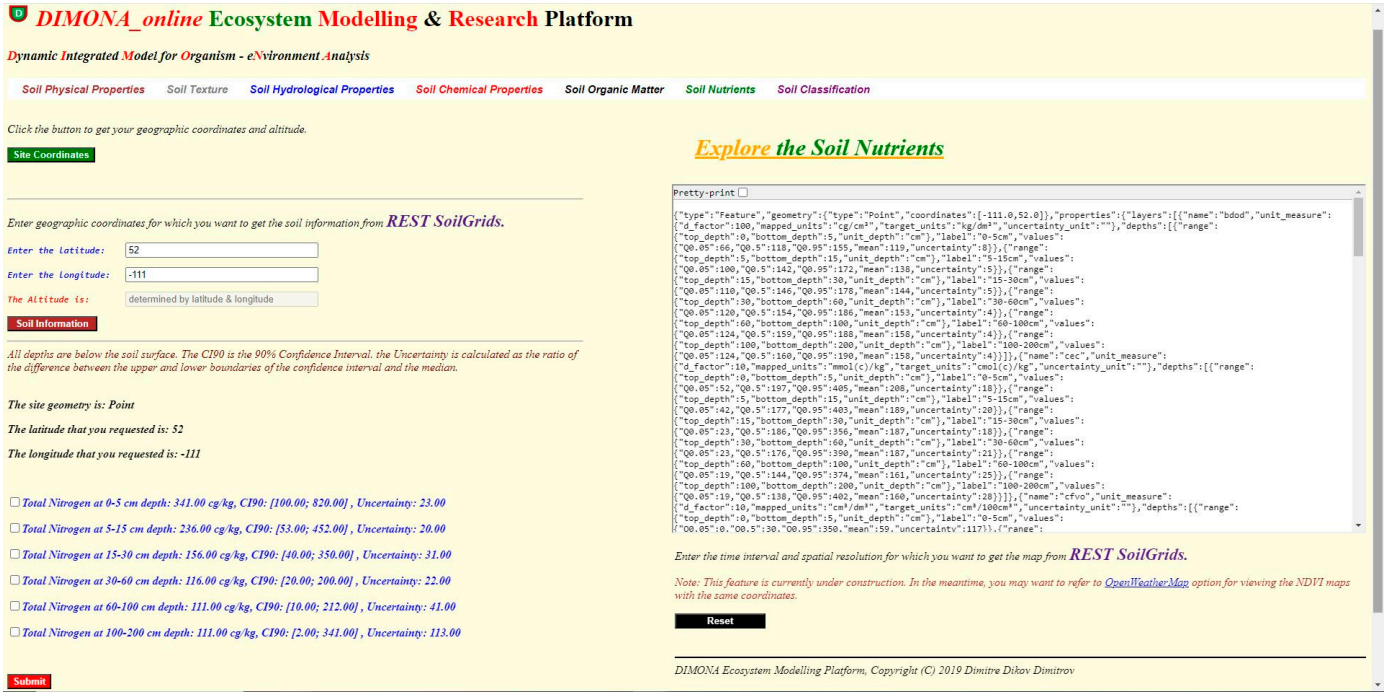

Figure 5. Data exploration screen for soil properties at preset geographic locations around the world.

Tier II serves the back end on the hosting server (Apache) with its database, dealing with user sign up and log in. Tier II creates and maintains users' personal accounts on the *DIMONA* server, allowing each user to remotely create, rename, copy, transfer, and delete different files and folders on their personal accounts. Tier II manages the upload of model input, drivers, parameters, and other files from the users' PC to the *DIMONA* server and download of model output from the *DIMONA* server to the users' PC after running the PB, IoT, or ML model executables. Tier III deals with interactions between *DIMONA*'s back end and the Developer's PC, where the programming and compiling of *DIMONA* model executables are performed. Tier III accommodates the deployment of compiled model executables on the *DIMONA* server and executing the .exe and .py files for remote model runs. Tier IV refers to other websites with API end points and external databases to/from which *DIMONA* requests/receives available .json files with model parameters, drivers, digital maps, or other data. The .json files received from the API websites are parsed by *DIMONA* for obtaining the data of interest. Through Tier IV, *DIMONA* has access to any geographic coordinates in the world via API websites, such as OpenWeatherMap for current weather data every few minutes, Agro Dashboard for Agricultural Monitoring, referred to as Agro API, for soil near-surface water contents and temperature every 12 h, SoilGrids REST API for soil physical and chemical properties, texture, organic matter, nutrients, and classification, and the Global Biodiversity Information Facility (GBIF) for plant, animal, and fungi species and ecological habitats.

Tier V allows users to upload, via the FTPS method with SSL or TLS protocols, model input and output, data, and parameter files from their personal *DIMONA* accounts directly to external websites, to which they have secured access, especially when the hard drive capacity allotted to each model user exceeds the limits of the pilot version.

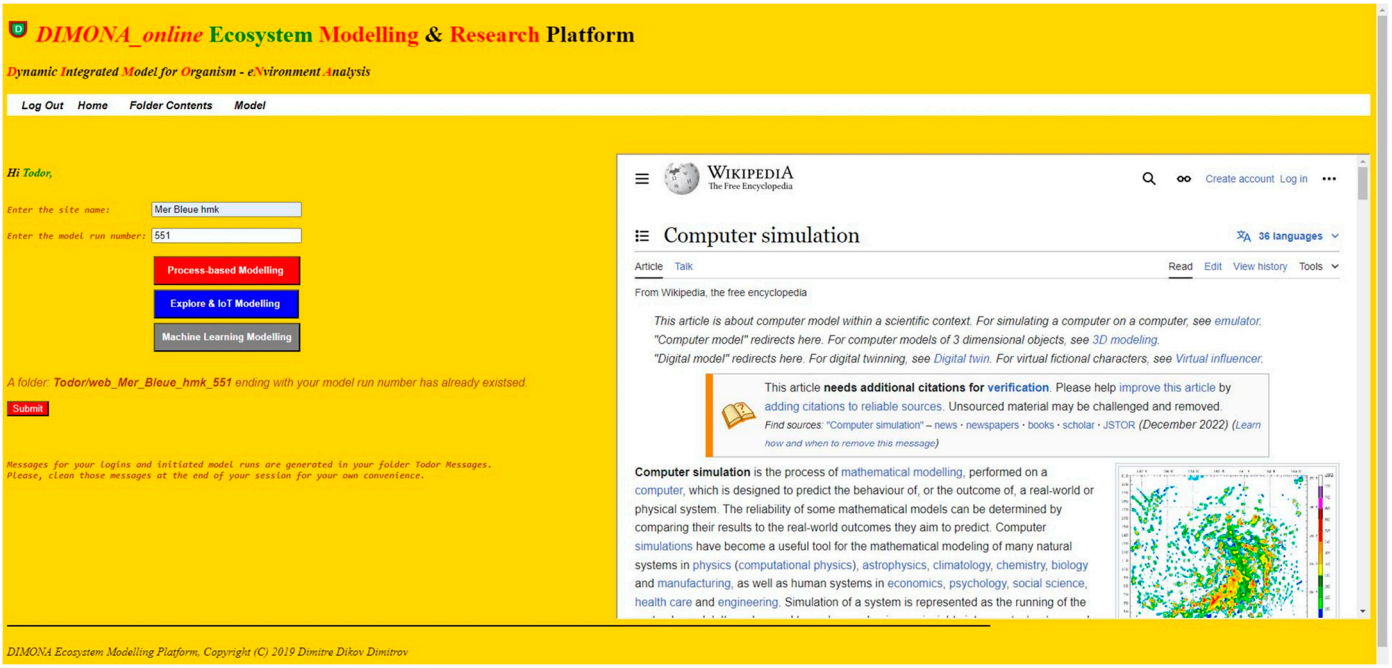

(**a**)

(**b**)

Figure 6. A user's personal account screen (**a**) and a user's folder (**b**) with other folders (in blue) and files (in red), and various options to upload or download model and data files and execute model simulations.

2.1.2. DIMONA Process-Based (PB) Model

The main processes and relations in the *DIMONA* PB model relevant to this study (Figure 7) are outlined below, with an emphasis on the simple process-oriented modifiers for plant water control on GPP through photosynthesis, plant growth, root/rhizoid respiration, and nutrient uptake. Model equations that are not explicitly stated in the manuscript are referred to by their numbers in the Supplementary Material, starting with the prefix S. All equation variables and parameters are explained in the Supplementary Material.

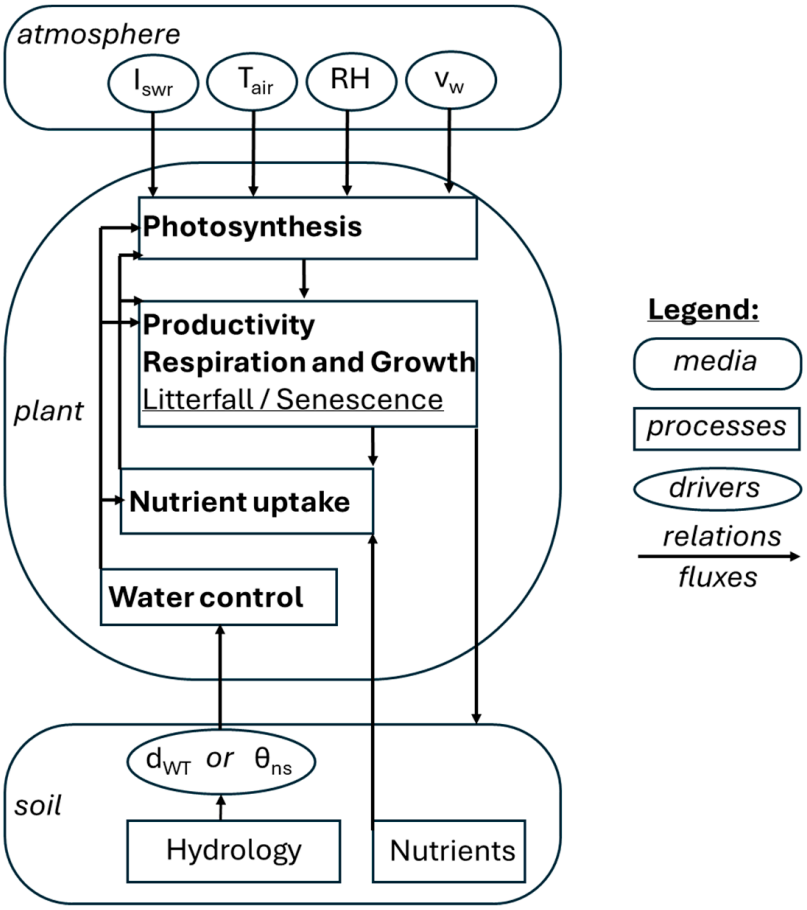

Figure 7. Model schematic of main processes and relations through simulated soil–plant–atmosphere continuum in *DIMONA* PB model.

Photosynthesis and C Fixation

DIMONA simulates the photosynthesis of vascular plants, e.g., coniferous and deciduous trees, evergreen and deciduous shrubs, grasses, agricultural crops, and bryophytes, e.g., *Sphagnum* moss. Simulations are at the canopy level per each simulated plant species. Simulated C fixation of vascular plants is based on the Farquhar biochemical model for photosynthesis [30,31], controlled by leaf temperature, T_L [32,33], and stomatal conductance through the ratio between internal and external leaf CO_2 concentrations [34], coupled to plant water status and external hydrological controls. The latter are the air relative humidity, RH, or atmospheric vapor pressure deficit (VPD), D_{VP}, represented by Ball–Berry- or Leuning-type equations, respectively [35–37]. Simulated C fixation of bryophytes is calculated by a rectangular hyperbola [20,38] controlled by T_L.

Simulated photosynthesis is driven by the incoming solar short-wave radiation, I_{swr}, partially reflected and attenuated through the canopy, ambient air temperature, T_a, RH, and wind speed, v_w, measured at 2 m above the canopy. It is also driven by soil hydrology through d_{WT} or near-surface θ, directly for vascular plants and indirectly for bryophytes, as outlined below and in the Supplementary Material. Simulations are conducted at hourly or less than hourly time steps for modelling the diurnal cycle of the photosynthesis, daily aggregations are also calculated. *DIMONA* can simultaneously simulate the photosynthesis and growth of a pre-set number of up to 10 plant species within the same canopy layer in up to 10 canopy layers (Figure 2a). The maximum numbers may be adjusted to >10 in the model code, if needed. With C3 vascular plants, relevant to this study, the ambient photosynthetic rate, A, is the minimum of the Rubisco-limited and the electron transport-limited CO_2 fixation rates A_C and A_J, respectively (Equation (S1.1.1.1)).A_J (Equation (S.1.1.1.2)) depends

on the ambient electron transport rate, J_m (Equation (S1.1.1.3)), and is constrained by the ratio c_x between the CO_2 concentration in intercellular spaces at the carboxylation sites of Rubisco activity, C_i, and the atmospheric CO_2 concentration, C_a (Equation (S1.1.5.1)). J_m is driven by I_{swr} attenuated through the canopy (Equations (S1.1.1.4) and (S1.1.2.2)), the effects of T_L (Equation (S1.1.1.5)), and plant water status (Equation (S1.1.1.6)). A_C (Equation (S.1.1.1.8)) depends on the ambient rate of carboxylation, V_m (Equation (S1.1.1.9)), and is constrained by c_x, as defined above (Equation (S1.1.5.1)). V_m is determined by the effects of T_L (Equation (S1.1.1.10)) and plant water status (Equation (S1.1.1.6)). Foliar respiration, R_d (Equation (S.1.1.6.1)), is determined by the effects of T_L and plant water status (Equations (S.1.1.6.2) and (S.1.1.6.3)).

The effects of T_L on A through A_C or A_J and on R_d are determined by T_a (Equations (S1.1.3.1) and (S1.1.3.7)), RH through D_{VP} (Equations (S1.1.3.1), (S1.1.4.4) and (S1.1.4.6)) and v_w (Equations (S1.1.3.1), (S1.1.3.5) and (S1.1.3.6)) via T_L (Equation (S1.1.3.1)). c_x (Equation (S1.1.5.1)) depends on leaves' boundary layer conductance, g_b (Equation (S1.1.5.2)), and hence on v_w (Equation (S1.1.5.3)) and stomatal conductance, g_s, which depends on RH (Equation (S1.1.5.5)) through the Ball–Berry method or D_{VP} via RH (Equation (S1.1.5.6)) through the Leuning method. Both g_b and ambient g_s for CO_2 and water vapor exchange (Equations (S1.1.5.7) and (S1.1.5.8)) are modelled at the canopy level. Thus, primary stomatal control is modelled through the feedback loop between c_x determining g_s by A via A_C or A_J (Equations (S1.1.1.1), (S1.1.5.5) and (S1.1.5.6)) and g_s determining c_x (Equation (S1.1.5.1)), and secondary stomatal control is modelled through RH or D_{VP} via RH (Equations (S1.1.5.5) and (S1.1.5.6)). The effect of plant water status (Equation (S1.1.1.6)) represents the non-stomatal control on photosynthesis and is expressed as the product of the effect of atmospheric water demand, which manifests through adaptations like cuticular conductance/resistance and depends on RH via D_{VP} (Equations (S1.1.4.2), (S1.1.4.3), (S1.1.4.4) and (S1.1.4.6)) and the ambient effect of soil water availability on photosynthesis, f_P, which is driven by soil water availability, $f_{\theta W}$ (Equations (S1.1.4.1), (S4.1.1.1) and (S4.4.1.1)) (Section Water Control on Plant Processes).

With bryophytes, the ambient photosynthetic rate, A_b, is constrained by the maximum photosynthetic rate, $A_{max,b}$, and driven by I_{swr}, as well as T_a, RH, and v_w via T_L in a rectangular hyperbola (Equation (S1.2.1.1)). $A_{max,b}$ is explicitly related to RH via a linear regression (Equation (S1.2.3.1)), thereby reflecting the sensitivity of bryophyte photosynthesis to the humidity of the surrounding air. Bryophyte foliar respiration, R_d (Equation (S1.2.4.1)), is proportional to $A_{max,b}$ and is controlled by T_a, v_w, and especially RH. The control of soil hydrology is exerted via bryophyte growth (Section Water Control on Plant Processes).

Plant Productivity, Growth, and Nutrient Uptake

The DIMONA PB model has a full suite of plant and soil biogeochemistry, tracking pools for key nutrients. For each plant species, the model simulates its vascular or bryophyte GPP (Equations (S2.1.1.1) and (S2.1.1.2)) controlled by nitrogen (N) and phosphorus (P) nutrient availability in leaves and the effect of soil water and air availability on vascular growth, f_θ (Section Water Control on Plant Processes). Furthermore, for each plant species, *DIMONA* PB simulates LAI (Equation (S2.1.1.3)) and net primary productivity, $NPP = GPP - R_a$ (Equation (S2.1.2.8)), where R_a is plant autotrophic respiration, such as $R_a = R_l + R_b + R_r$ (Equations (S2.1.2.1) and (S2.1.2.3)), and R_l (Equations (S2.1.2.2) and (S2.1.2.6)), R_b (Equations (S2.1.2.4) and (S2.1.27)), and R_r (Equation (S2.1.2.5)) are, respectively, the leaf respiration, stem respiration (with branches), and root/rhizoid respiration hydrology constrained by the combined effect of air availability to roots/rhizoids due to soil water and plant adaptations to wetland soil conditions, f_R (Section Water Control on Plant Processes). For each simulated plant species, *DIMONA* maintains pools of C

(Equations (S2.2.1.1), (S2.3.1.1) and (S2.4.1.1)), nitrogen, N (Equations (S2.2.1.2), (S2.3.1.2) and (S2.4.1.2)), and phosphorus, P (Equations (2.2.1.3), (S2.3.1.3) and (S2.4.1.3)), with structural and non-structural components for the three main plant components in the model, i.e., leaves, stems (with branches), and roots (including fine roots)/rhizoids.

Simulated plant growth and litterfall are driven by the balance between maintenance and growth respiration, as simulated plant growth is constrained by ambient photosynthetic C (photosynthate), N and P nutrient uptake, and plant water status. Thus, the growth of leaves, stems, and roots/rhizoids occurs in the model if R_l, R_b, and R_r are >maintenance respiration in leaves, stems, and roots/rhizoids (Equations (S2.2.2.1), (S2.3.2.1) and (S2.4.2.1)), which determines the growth respiration of leaves, stems, and roots/rhizoids (Equations (S2.2.2.2), (S2.3.2.2) and (S2.4.2.2)). Growth respiration causes an increment in leaves', stems', and roots/rhizoids' structural C pools via the corresponding growth yields (Equations (S2.2.2.3), (S2.3.2.3) and (S2.4.2.3)). The simulated litterfall of leaves, stems, and roots/rhizoids, respectively, occurs if R_l, R_b, and R_r are $\leq$ to the maintenance respiration of leaves, stems, and roots/rhizoids, which determines zero growth respiration resulting in a decrement in leaves', stems', and roots/rhizoids' structural C pools (Equations (S2.2.3.2), (S2.3.3.2) and (S2.4.3.2)). Simulated leaf senescence (no deciduous species are simulated in this study) is driven by a plant phenology module (Equation (S2.2.4.1)). Thus, updates of structural and non-structural C, N, and P pools occur in the model at each time step.

Water Control on Plant Processes

Plant water relations in the *DIMONA* PB model are represented as process-oriented modifiers (i.e., equations) for water control on plant processes, such as non-stomatal control on photosynthesis (Equations (S1.1.1.6) and (S1.1.4.1)), water control on plant productivity and growth (Equations (S2.1.1.1) and (S2.1.1.2)), and water control on root/rhizoid respiration (Equations (S2.1.2.5), (S2.1.2.6) and (S2.1.2.7)) and N and P nutrient uptake (Equation (S3.1.1.1), (S3.1.1.2) and (S3.1.1.3)). Respectively, these modifiers represent the effect of soil water availability on photosynthesis, the effect of soil water and air availability on plant productivity and growth, and the effect of air availability on root/rhizoid respiration and nutrient uptake, all of which directly and indirectly (via all affected plant processes) determine plant GPP and hence ecosystem GPP. These modifiers with their constituents, i.e., the soil water and air availability to plants, and the effect of air availability from adaptations to wetland soil conditions and their basic properties are briefly summarized below and presented in detail in the Supplementary Material. The modifiers are designed to provide simple and non-computationally intensive yet realistic plant water control mechanisms on productivity and growth, root/rhizoid respiration, and nutrient uptake and to avoid the largely unknown and uncertain physiological parameters of plant–water relations (Section 1.2). These modifiers directly relate plant water control to soil θ. This applies especially for θ in the near-surface peat layers, where most roots grow [39], and from which the entire peat profile hydrology could be dynamically estimated [27]. Thus, *DIMONA*'s modifiers allow the site to perform large-scale simulations of peatland GPP at any geographic location.

a. The Effect of Soil Water Availability on Photosynthesis

The modifier for the effect of soil water availability on the photosynthesis of vascular plants, f_P (Equation (S4.1.1.1)), constituting non-stomatal control on modelled photosynthesis (Equations (S1.1.1.6) and (S1.1.4.1)) is formulated as

$$f_P = f_{\theta W} \quad (1a)$$

where $f_{\theta W}$ represents soil water availability (d. Soil Water and Air Availability to Plants). Thus, the ambient effect of soil water availability on photosynthesis, $f_{\theta P}$, is calculated as the minimum of the effect of soil water availability on plant photosynthesis, f_P, and unity

$$f_{\theta P} = \min\{1;\ f_P\} \tag{1b}$$

thereby reflecting no hydrology constraints on photosynthesis at or above field capacity.

b. The Effect of Soil Water and Air Availability on Plant Productivity and Growth

The modifiers for the effect of soil water and air availability on plant productivity and growth for vascular plants and bryophytes are presented below. The effect of soil water and air availability on vascular plant growth, f_θ (Equation (S4.2.1.1a,b), is formulated as

$$f_\theta = \frac{{f_{\theta R}}^{0.001} {f_{\theta W}}^{1.8} + f_{\theta A} f_{\theta W}}{1 + f_{\theta A}} \quad \text{if } \overline{\theta} > \overline{\theta}_{FC} \tag{2a}$$

$$f_\theta = \frac{{f_{\theta R}}^{1.2} {f_{\theta W}}^{0.5} + f_{\theta A} f_{\theta W}}{1 + f_{\theta A}} \quad \text{if } \overline{\theta} \leq \overline{\theta}_{FC} \tag{2b}$$

where $f_{\theta W}$ is as defined above, $f_{\theta R}$ is the soil air availability to roots (d. Soil Water and Air Availability to Plants), and $f_{\theta A}$ is the effect of air availability on plant growth, root respiration, and nutrient uptake from the adaptations (if any) that a given vascular species may have for wetland soil conditions (e. The Effect of Air Availability on Plants from Adaptations to Wetland Soil Conditions). This effect may be due to adaptations such as enhanced rooting above the WT or genetic/inherent abilities to develop aerenchyma in stem and root tissues, grow adventitious roots above the waterlogged soil, or develop a rhizosphere oxygenation layer, etc., as outlined in the Supplementary Material. Equation (2a) represents f_θ in wet soil, i.e., when the average ambient water content of the unsaturated soil, $\overline{\theta}$, is above the field capacity, while Equation (2b) represents f_θ in dry soil, i.e., when $\overline{\theta}$ is $\leq$the field capacity. For vascular species that do not develop adaptations to wetland soils, $f_{\theta A} = 0$ (Equation (S.4.2.1.1c,d)).

The products of $f_{\theta R}$ and $f_{\theta W}$, as well as $f_{\theta A}$ and $f_{\theta W}$, in Equation (2a,b) reflect the combined effects of water and air availability on GPP (Equations (S2.1.1.1) and (S2.1.1.2)) and plant growth through constraining f_θ for the extreme conditions of water saturation and severe droughts. With soil drying, $f_{\theta W}$ declines such that with severe droughts, $f_{\theta W}$ approaches zero (d. Soil Water and Air Availability to Plants); hence, f_θ, and thereby GPP, approach zero and simulated plants can eventually die. With waterlogging, $f_{\theta R}$ approaches zero (d. Soil Water and Air Availability to Plants) and the ability of simulated plant species to survive is reflected by $f_{\theta A}$ (e. The Effect of Air Availability on Plants from Adaptations to Wetland Soil Conditions), such that if $f_{\theta A}$ is large enough, i.e., with adaptations to wetland soil conditions, plants sustain productivity and growth in the model. Respectively, if $f_{\theta A}$ is too small or zero, i.e., with insufficient or no adaptations to wetland soil conditions, then f_θ and thereby GPP approach zero and simulated plants eventually die. The exponent terms in Equations (1a,b) and (2a,b) are determined for the Mer Blue bog by trial and error and may differ for other plant species and sites, reflecting the specifics of growth for each plant species under different hydrological conditions.

For many bryophyte species, including *Sphagnum*, most of their living parts are above the soil and their rhizoids occupy the near-surface soil layers [23]. Hence, the modifier f_θ considers only the effect of soil water availability on bryophyte growth and is not considered limited by soil air. Thus

$$f_\theta = f_{\theta W} \tag{3}$$

reflecting the primary importance of water for bryophyte physiological processes.

c. The Effect of Air Availability on Root/Rhizoid Respiration and Nutrient Uptake

The modifier for the effect of soil air availability and air availability due to adaptations (if any) to wetland soils on vascular root respiration, f_R (Equation (S4.3.1.1)), is formulated as follows:

$$f_R = \frac{f_{\theta R} + f_{\theta A}}{1 + f_{\theta A}} \quad (4)$$

where $f_{\theta R}$ and $f_{\theta A}$ are as defined above. For many bryophytes, f_R (Equation (S4.3.1.2)) is formulated as

$$f_R = f_{\theta R} \quad (5)$$

With waterlogging, $f_{\theta R}$ approaches zero and the ability of simulated plant species to survive is reflected by $f_{\theta A}$. If $f_{\theta A}$ is large enough, i.e., with adaptations to wetland soil conditions, then f_R is sufficiently large to sustain R_r (Equation (S2.1.2.5)) and hence the biomass (Equation (S2.4.6.1)) and ambient area of roots/rhizoids (Equation (S2.4.6.2)), and thereby GPP (Equations (S2.1.1.1), (S2.1.1.2) via (S3.1.1.1), (S3.1.1.2) (S3.2.1.1), and (S3.3.1.1), (S3.3.1.2) and (S3.3.1.3)). Respectively, if $f_{\theta A}$ is too small or zero, then f_R and thereby GPP are too small or zero, and the simulated plants eventually die.

Unlike f_R, the modifier for the effect of air availability to roots/rhizoids on N and P nutrient uptake is formulated per soil layer i, denoted by $f_{U,i}$ (Equation (S4.3.1.3)):

$$f_{U,i} = \frac{f_{\theta R,i} + f_{\theta A}}{1 + f_{\theta A}} \quad (6)$$

where $f_{\theta A}$ is as defined above and $f_{\theta R,i}$ represents the soil air availability to roots in soil layer i (d. Soil Water and Air Availability to Plants). For many bryophyte species, e.g., *Sphagnum*, $f_{\theta A} = 0$ and $f_{U,i}$ (Equation (S4.3.1.4)) is

$$f_{U,i} = f_{\theta R,i} \quad (7)$$

Similarly to $f_{\theta R}$ for the entire soil profile, $f_{\theta R,i}$ for soil layer i approaches zero with waterlogging, such that the ability of simulated plant species to uptake N and P is affected by $f_{\theta A}$. If $f_{\theta A}$ is large enough, i.e., with adaptations to wetland soil conditions, $f_{U,i}$ is sufficiently large to sustain the root/rhizoid uptake of NH_4^+ (Equation (S3.1.1.1)), NO_3^- (Equation (S3.1.1.2)), and PO_4^{3-} (Equation (S3.2.1.1)) from soil layer i and thereby GPP (Equations (S2.1.1.1), (S2.1.1.2) via (S3.3.1.1), (S3.3.1.2) and (S3.3.1.3)) and plant growth. Respectively, if $f_{\theta A}$ is too small or zero, i.e., with insufficient or no adaptations to wetland soil conditions, then $f_{U,i}$ is too small, which negatively affects plant productivity and growth. As soil layers with decreasing $f_{U,i}$ prevail with progressive waterlogging, plant and ecosystem GPP may become too small or approach zero as simulated plant species eventually die in the model run.

d. Soil Water and Air Availability to Plants

Soil water availability, $f_{\theta W}$ (Equation (S4.4.1.1)), is estimated from the average ambient soil water content available for plants, $\overline{\theta}$, and the average soil water contents at field capacity and wilting point, $\overline{\theta}_{FC}$ and $\overline{\theta}_{WP}$, with these averages for the unsaturated soil profile. $f_{\theta W}$ is calculated as follows:

$$f_{\theta W} = \max\left\{0;\ \frac{\overline{\theta} - \overline{\theta}_{WP}}{\overline{\theta}_{FC} - \overline{\theta}_{WP}}\right\} \quad (8)$$

Thus, $f_{\theta W} = 0$ with $\overline{\theta} \leq \overline{\theta}_{WP}$ reflects no plant water uptake at or below wilting point, $0 < f_{\theta W} < 1$ with $\overline{\theta}_{WP} < \overline{\theta} < \overline{\theta}_{FC}$ reflects constrained plant water uptake between field capacity and wilting point, and $f_{\theta W} \geq 1$ with $\overline{\theta} \geq \overline{\theta}_{FC}$ reflects unconstrained plant water uptake at or above field capacity.

Soil air availability, $f_{\theta R}$ (Equation (S4.4.1.2)), is estimated from $\overline{\theta}$ and $\overline{\theta}_{FC}$ and the averages of soil total porosity, $\overline{\theta}_{TP}$, and macroporosity, $\overline{\theta}_{MP}$ (if any), for the unsaturated soil profile, as follows:

$$f_{\theta R} = \max\left\{0;\ \frac{(\overline{\theta}_{TP} - \overline{\theta}_{MP}) - \overline{\theta}}{(\overline{\theta}_{TP} - \overline{\theta}_{MP}) - \overline{\theta}_{FC}}\right\} \quad (9)$$

Thus, $f_{\theta R} = 0$ with $\overline{\theta} \geq \overline{\theta}_{TP} - \overline{\theta}_{MP}$ ($\overline{\theta}_{MP} \geq 0$) reflects no soil air for plant roots/rhizoids in saturated soil, $0 < f_{\theta R} \leq 1$ with $\overline{\theta} \geq \overline{\theta}_{FC}$ reflects constrained air availability in soil at or above field capacity, and $f_{\theta R} > 1$ with $\overline{\theta} < \overline{\theta}_{FC}$ reflects unconstrained air availability in soil below the field capacity.

For each soil layer i of the unsaturated soil profile, soil air availability, $f_{\theta R,i}$ (Equation (S4.4.1.3)), is estimated from the ambient soil water content available for the root/rhizoid water uptake, θ_i, soil total porosity, $\theta_{TP,i}$, soil macroporosity, $\theta_{MP,i}$ (if any), and soil water content at field capacity, $\theta_{FC,i}$, of that soil layer, as follows:

$$f_{\theta R,i} = \max\left\{0;\ \frac{(\theta_{TP,i} - \theta_{MP,i}) - \theta_i}{(\theta_{TP,i} - \theta_{MP,i}) - \theta_{FC,i}}\right\} \quad (10)$$

with $f_{\theta R,i}$ acting in a similar way to $f_{\theta R}$ above.

When soil approaches field capacity, $\overline{\theta} = \overline{\theta}_{FC}$, $f_{\theta W} = 1$ in Equation (8) (Equation (S4.4.1.1)) and $f_{\theta R} = 1$ in Equation (9) (Equation (S4.4.1.2)); hence, $f_\theta = (1 + f_{\theta A})/(1 + f_{\theta A}) = 1$ in Equations (2a,b) (Equation (S4.2.1.1a,b,c,d)) and $f_\theta = 1$ in Equation (3) (Equation (S4.2.1.2a,b)). Also, $f_R = (1 + f_{\theta A})/(1 + f_{\theta A}) = 1$ in Equation (4) (Equation (S4.3.1.1a,b)) and $f_R = 1$ in Equation (5) (Equation (S4.3.1.2a,b)), $f_{U,i} = (1 + f_{\theta A})/(1 + f_{\theta A}) = 1$ in Equation (6) (Equation (S4.3.1.3a,b)) and $f_{U,i} = 1$ in Equation (7) (Equation (S4.3.1.4a,b)). Thus, consistent with other studies [20,21], there are no hydrology limitations on plant growth, root/rhizoid respiration, and nutrient uptake when soil is at field capacity in the model.

e. The Effect of Air Availability on Plants from Adaptations to Wetland Soil Conditions

The modifier for the effect of air availability on plant productivity and growth, root respiration, and nutrient uptake from adaptations to wetland soils, $f_{\theta A}$ (Equations (S4.5.1.1) and (S4.5.1.2)), is

$$f_{\theta A} = 1 + max\left(0;\ \frac{d_{WT}}{d_{SL}}\right) \text{ if } \overline{\theta} > \overline{\theta}_{FC} \quad (11a)$$

$$f_{\theta A} = 1 - min\left(1;\ \frac{d_{WT}}{d_{SL}}\right) \text{ if } \overline{\theta} \leq \overline{\theta}_{FC} \quad (11b)$$

where d_{SL} is the depth of the entire soil profile (unsaturated and/or saturated). Thus, when $d_{WT} = 0$, then $f_{\theta A} = 1$, indicating plants with adaptations to wetland soils. When WT recedes down the soil profile, i.e., $d_{WT} > 0$, and increases with WT drawdown while $\overline{\theta} > \overline{\theta}_{FC}$, then $f_{\theta A}$ increases above unity, reflecting improved root activity, with receding WT and with adaptations to wet soils. When the soil becomes less wet, with $\overline{\theta} \leq \overline{\theta}_{FC}$, often accompanied by WT receding further down, then $f_{\theta A}$ also decreases, reflecting a diminishing role of adaptations with improved soil aeration, proportionally to d_{WT}/d_{SL}. Thus, $f_{\theta A} \to 0$ with WT approaching the bottom of the soil profile, or disappearing, i.e., with $d_{WT} \to d_{SL}$, reflecting no need for adaptations in the well-aerated soil.

Soil Hydrology

Previously, the hydrological module for peat in the *DIMONA* PB model (i.e., the PHM model) was applied to the Mer Bleue bog to simulate θ at various peat depths at a daily

time step driven by observed d_{WT} [26] and near-surface θ [27]. It is from these studies that the above modifiers were estimated at an hourly time step.

2.2. Site Description and Field Observations

The Mer Bleue bog (Figure 8) is ~2800 ha in area and is located ~15 km east of Ottawa, ON, Canada. The site has a pronounced microform hummock–hollow topography, with ~2/3 of the surface area occupied by hummocks and the remaining ~1/3 by hollows [24,26]. The groundcover is mainly Ericaceous shrubs, underlain by *Sphagnum fuscum* and *Sphagnum capillifolium* on hummocks and *Sphagnum magellanicum* and *Sphagnum angustifolium* on hollows [39–41]. Daily d_{WT} was measured during 1998–2004 in a well below the average hummock surface using a custom float and counterweight system attached to a potentiometer [24,40,42]. Daily near-surface θ was measured during 1999–2004 at 0.1 m below the hummock surface and at 0.03 m below the hollow surface using water content probes (model CS615, Campbell Scientific, Logan, UT, USA); their calibration and normalization are described in [24,40,42]. Hourly I_{swr}, T_{air}, RH, and v_w were continuously measured at 2 m above the canopy during 1998–2004 [24,42,43]. Hourly ecosystem GPP observations with daily aggregations for model–data comparisons were made available during 2000–2004, obtained by partitioning from measured eddy covariance (EC) NEE [24,42]. There were some GPP observations in 1999, but they were much fewer than those in each of the years 2000–2004, hence were not used in model–data comparisons.

Figure 8. A map of the Mer Bleue study area (**above**) with the microtopography of the Mer Bleue bog study site (**below**).

2.3. Model Experiments

Model runs were conducted at an hourly time step for each of the two microforms, i.e., hummocks and hollows. Hourly measurements of I_{swr}, T_{air}, RH, and v_w were used as meteorological drivers for the *DIMONA* PB model for testing Hypotheses 1, 2, and 3. Gap-filling for the missing values was performed by using data from the Environment Canada weather station at Macdonald–Cartier Ottawa Airport, located ~15 km away from the Mer Bleue bog [44]. Daily-observed d_{WT} below the average hummock surface was adjusted by +25 cm below the average hollow surface to account for hummock–hollow elevation differences [26]. Then, daily-observed d_{WT} was fragmented in the model into hourly values in hummocks and hollows, which were used as hydrological drivers to test Hypotheses 1 and 3. The daily near-surface θ observed in hummocks at 10 cm depth and in hollows at 3 cm depth was fragmented in the model into hourly values used as hydrological drivers in each microform to test Hypotheses 2 and 3. Simulations during days with missing or low-quality observed d_{WT} and/or near-surface θ values were omitted from the model–data comparisons whenever possible.

Model inputs of hourly I_{swr}, T_{air}, RH, and v_w, daily d_{WT} and near-surface θ, physiological parameters for the shrubs and *Sphagnum*, and site and soil parameters were uploaded as .csv files in the corresponding online folders in *DIMONA* (Figure 6b). Key parameters and their values used in this study for plant photosynthesis, productivity, and nutrient uptake are summarized in Table 1, while those for plant water control are given within the corresponding equations (Section Water Control on Plant Processes). The period of consecutive years with available hydrological and meteorological drivers and information on how many times that period should be repeated during simulations were entered online via the *DIMONA* GUI (Figure 2a). The number of repetitions is chosen by the model user such that the modelled ecosystem could reach equilibrium, i.e., when ecosystem NPP equals litterfall [39]. Thus, the period 1998–2004 of available hydrological and meteorological drivers was repeated twice within each model run, driven either by observed d_{WT} or near-surface θ, resulting in 14 years of simulations until ecosystem equilibrium was reached. Simulated ecosystem GPP in the last 5 years of simulations (i.e., the repeated 2000–2004 period) was used for testing Hypotheses 1, 2, and 3 by comparing model output vs. available EC-derived ecosystem GPP and other field observations.

Table 1. Selected parameters of *DIMONA* PB model for photosynthesis, plant productivity, growth, and nutrient uptake.

Quantity [1]	Meaning	Value	Units
D_{TJ}	Energy of deactivation for electron transport rate	200,000	J mol^{-1}
E_{SCO}	Activation energy for decline in Rubisco affinity for CO_2 with T	−24,460	J mol^{-1}
E_{TC}	Activation energy for $V_{max,25}$	65,000	J mol^{-1}
E_{TJ}	Activation energy for maximum electron transport rate	35,000	J mol^{-1}
$J_{max25,S}$ (25 °C)	Maximum summer electron transport rate at 25 °C	36.5	umol e^- m^{-2} s^{-1}
$J_{max25,P}$ (25 °C)	Maximum spring electron transport rate at 25 °C	17.5	umol e^- m^{-2} s^{-1}
$J_{max25,F}$ (25 °C)	Maximum fall electron transport rate at 25 °C	18.5	umol e^- m^{-2} s^{-1}
K_{C25} (25 °C)	Michaelis–Menten constant for Rubisco CO_2 fixation	275	umol mol^{-1}
K_{O25} (25 °C)	Michaelis–Menten constant for Rubisco O_2 utilization	420,000	umol mol^{-1}
$R_{d,light,25}$	Mitochondrial respiration in the light at 25 °C	1.3	umol CO_2 m^{-2} s^{-1}
S_{CO} (25 °C)	Relative CO_2/O_2 specificity factor for Rubisco	2800	bar bar^{-1}
S_{TJ}	Entropy with deactivation	650	J K^{-1} mol^{-1}
$V_{max25,S}$ (25 °C)	Maximum rate of carboxylation in summer at 25 °C	19.5	umol e^- m^{-2} s^{-1}
$V_{max25,P}$ (25 °C)	Maximum rate of carboxylation in spring at 25 °C	7.5	umol e^- m^{-2} s^{-1}

Table 1. *Cont.*

Quantity [1]	Meaning	Value	Units
$V_{max25,F}$ (25 °C)	Maximum rate of carboxylation in fall at 25 °C	7.5	umol e^- m^{-2} s^{-1}
Γ* at 25 °C	CO_2 compensation point in the absence of day respiration	44.7	umol mol^{-1}
s_{la}	Vascular plant-specific leaf area	66	cm^2 g^{-1}
$s_{la,b}$	Bryophyte-specific leaf area	180	cm^2 g^{-1}
R	Root area index (biome)	79.1	m^2 m^{-2}
R_{mb}	Stem maintenance respiration	1.5 (vasc) 0.5 (moss)	g C g DM^{-2} s^{-1}
R_{ml}	Leaf maintenance respiration	0.1 (vasc) 0.025 (moss)	g C g DM^{-2} s^{-1}
R_{mr}	Root/rhizoid maintenance respiration	0.2 (vasc) 0.05 (moss)	g C g DM^{-2} s^{-1}
Y_{Gb}	Stem growth yield	0.55 (vasc) 0.35 (moss)	-
Y_{Gl}	Leaf growth yield	0.55 (vasc) 0.15 (moss)	-
Y_{Gr}	Root/rhizoid growth yield	0.65 (vasc) 0.45 (moss)	-
K_{NH4}	Michaelis–Menten constant for NH_4^+ uptake by roots/rhizoids	0.4	g N m^{-3}
K_{NO3}	Michaelis–Menten constant for NO_3^- uptake by roots/rhizoids	0.35	g N m^{-3}
K_{PO4}	Michaelis–Menten constant for PO_4^{3-} uptake by roots/rhizoids	0.125	g P m^{-3}
$U_{NH4,max}$	Max root/rhizoid NH_4^+ uptake at 25 °C and non-limiting NH_4^+	1.39×10^{-6}	g N m^{-2} h^{-1}
$U_{NO3,max}$	Max root/rhizoid NO_3^- uptake at 25 °C and non-limiting NO_3^-	1.39×10^{-6}	g N m^{-2} h^{-1}
$U_{PO4,max}$	Max root/rhizoid PO_4^{3-} uptake at 25 °C and non-limiting PO_4^{3-}	2.1×10^{-7}	g P m^{-2} h^{-1}

[1] Detailed tables of *DIMONA* PB model variables and parameters with equations and sources are given in the Supplementary Materials.

Model runs for hummocks and hollows driven by observed d_{WT} or near-surface θ with various combinations of equations for soil water retention curves (SWRCs) and stomatal conductance chosen via *DIMONA* GUI (Figure 2b) to represent the soil water constraints (via simulated $\overline{\theta}$ and θ_i) and atmospheric water constraints (via simulated g_s) were conducted to show that the modifiers f_P, f_θ, f_R, and f_{Ui} work reasonably well, i.e., to test Hypotheses 1 and 2. Hummock d_{WT} was elevated by 25 cm to run for hollows. All model runs are summarized in Table 2 along with their model names, hydrological drivers (d_{WT} or near-surface θ), SWRCs (Van Genuchten or Campbell), and stomatal conductance equations (Ball–Berry or Leuning).

Table 2. Model runs for testing DIMONA PB model performance constrained by different soil water retention curves (SWRCs) and stomatal conductance equations. d_{WT} is depth from soil surface to water table (cm) and θ is near-surface soil water content (m^3 m^{-3}). Bolded are representative model runs used as representatives to test the hypotheses of this study in detail.

Model Run Name	Hydrological Driver	SWRC Equation [1]	Stomatal Conductance Equation
CBall_WT	d_{WT}	Log-transformed Campbell	Ball–Berry
CLng_WT	d_{WT}	Log-transformed Campbell	Leuning
VBall_WT	**d_{WT}**	**Log-transformed Van Genuchten**	**Ball–Berry**
VLng_WT	d_{WT}	Log-transformed Van Genuchten	Leuning
CBall_NS	near-surface θ	Log-transformed Campbell	Ball–Berry
CLng_NS	near-surface θ	Log-transformed Campbell	Leuning
VBall_NS	**near-surface θ**	**Log-transformed Van Genuchten**	**Ball–Berry**
VLng_NS	near-surface θ	Log-transformed Van Genuchten	Leuning

[1] SWRC equations as introduced in [26].

From the combinations of model runs in Table 2, two representative model runs, VBall_WT driven by d_{WT} and VBall_NS driven by near-surface θ both using the Ball–Berry conductance formulations, were selected to test Hypotheses 1, 2, and 3 in detail. Within

each model run, hummock and hollow GPP and NPP were obtained by summing hummock and hollow shrub and moss GPP and NPP. Ecosystem GPP and NPP were obtained by summing the hummock and hollow values, weighted, respectively, at 0.67 and 0.33 to reflect the microform surface coverage. Simulated ecosystem GPP was compared to observed eddy covariance (EC)-derived ecosystem GPP. Comparisons were made at hourly and at daily time steps, the latter to eliminate the effects of possible autocorrelation due to the diurnal pattern of hourly photosynthesis. Hourly-binned aggregations were analyzed too to show the general patterns.

2.4. Model Evaluation and Statistics

To evaluate the *DIMONA* PB model's performance, hourly and daily linear regressions of simulated on observed ecosystem hourly and daily GPP were conducted, and their slopes, intercepts, and R^2 were computed, together with root mean square errors, RMSEs, and Willmott's indexes of agreement, d [45]. The linear regressions were executed in Microsoft Excel, while Willmott's d and RMSE on R Studio Cloud [46]. The linear regressions were examined to assess the overall model performance, RMSE to estimate the overall model accuracy, and Willmott's d ($0 \leq d \leq 1$) to estimate the relative model accuracy with respect to the magnitude of observed values [45]. To strengthen the hypothesis tests and to demonstrate the generality of the *DIMONA* PB model, the statistics of the corresponding hourly linear regressions, RMSE, and Willmott's d values for the other model runs in Table 2 were also examined. Findings from previous field and modelling studies were compared to the *DIMONA* PB simulations.

3. Results

Simulated hourly and daily courses of ecosystem GPP by VBall_WT and VBall_NS followed the observed pattern over a range of moisture conditions (Figures 9–12). Hourly modelled GPP vs. EC-derived GPP were shown for the same calendar period DOY 214–227 (2 to 15 August), which was wet with average d_{WT} ~34 cm in the year 2000 (Figures 9a, 10a, 11a and 12a); dry with average d_{WT} ~59 cm in the year 2001 (Figures 9b, 10b, 11b and 12b); very dry with average d_{WT} ~62 cm in the year 2002 (Figures 9c, 10c, 11c and 12c); and moderately wet with average d_{WT} ~43 cm in the year 2003 (Figures 9d, 10d, 11d and 12d). Daily modelled GPP vs. EC-derived GPP were shown over 2000–2004 (Figures 10e and 12e). For both model runs, the hourly courses of GPP were partitioned into their ecosystem compartments, i.e., simulated GPP of shrubs and mosses at hummocks and hollows. Hourly GPP of hummock and hollow shrubs and moss were analyzed together with the hourly courses of their meteorological drivers I_{SWR}, T_{air}, RH, and v_w and hydrological drivers, d_{WT} for VBall_WT and near-surface θ at 10 cm depth in hummocks and 3 cm depth in hollows for VBall_NS, for the wet period DOY 214–227 in 2000 (Figures 13–15) and the dry period DOY 214–227 in 2001 (Figures 16–18).

3.1. Analyzing Productivity Simulations Under Wet Conditions

During the wet period DOY 214–227 in 2000, VBall_WT reproduced the hourly dynamics of hummock and hollow shrubs and moss GPP (Figure 13), which were in general agreement with hourly ecosystem GPP (Figure 9a). VBall_NS had similar results (Figures 11a and 14a,b,d), except for the dynamics of hourly hollow shrub GPP, which followed a different pattern (Figure 14c), as explained below. Increased GPP from DOY 214 to DOY 215 in VBall_WT hummocks and hollows (Figure 13) and VBall_NS hummocks (Figure 14a,b) was due to increased I_{SWR} (Figure 15a) (Equations (S1.1.1.4) and (S1.1.2.2)). Although the increase in I_{SWR} continued through to DOY 218, simulated shrub GPP decreased, except on DOY 218 in VBall_WT hollows (Figures 13a,c and 14a). That de-

crease was due to the constraining effect of decreasing RH from DOY 215 to DOY 218 (Figure 15c) depressing g_s (Equation (S1.1.5.5)) and reducing T_L with decreased T_{air} (Equations (S1.1.3.1), (S1.1.4.4) and (S1.1.4.6)) in the model. The decrease in simulated shrub GPP from DOY 218 to DOY 220 (Figures 13a,c and 14a) was due to decreasing I_{SWR}, while RH increased during this time (Figure 15a,b). As moss has no stomatal control, the I_{SWR} increase with a relatively high RH on DOY 216 (Figure 15a,c) resulted in increasing moss GPP in both VBall_WT and VBall_NS hummocks and hollows (Figures 13b,d and 14b,d) in the first three days of the period (Equations (S1.2.1.1) and (S1.2.3.1)). A subsequent I_{SWR} increase from DOY 221 to DOY 223 (Figure 15a) caused increases in shrub and moss GPP in hummocks and hollows in VBall_WT (Figure 13) and in shrub and moss GPP in hummocks (Figure 14a,b) and moss GPP in hollows (Figure 14d) in VBall_NS (Equations (S1.1.1.4) and (S1.1.2.2)).

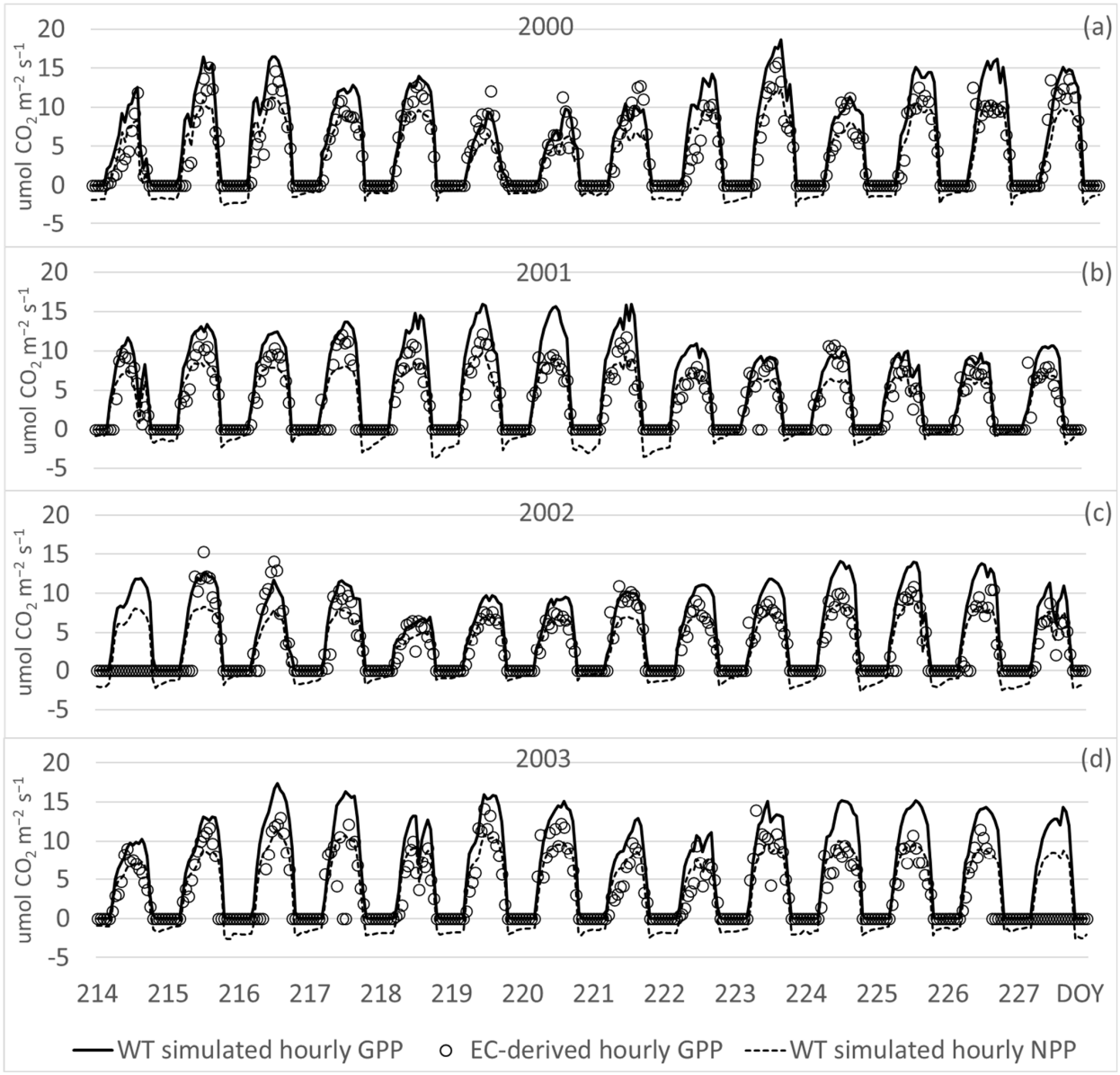

Figure 9. Hourly ecosystem gross primary productivity (GPP) and net primary productivity (NPP) at Mer Bleue bog during 2–15 August 2000 (**a**), 2001 (**b**), 2002 (**c**), and 2003 (**d**). Simulated GPP by VBall_WT model run driven by the observed depth to water table, d_{WT}, is compared vs. observed GPP derived from eddy covariance (EC) CO_2 exchange. DOY means day of year.

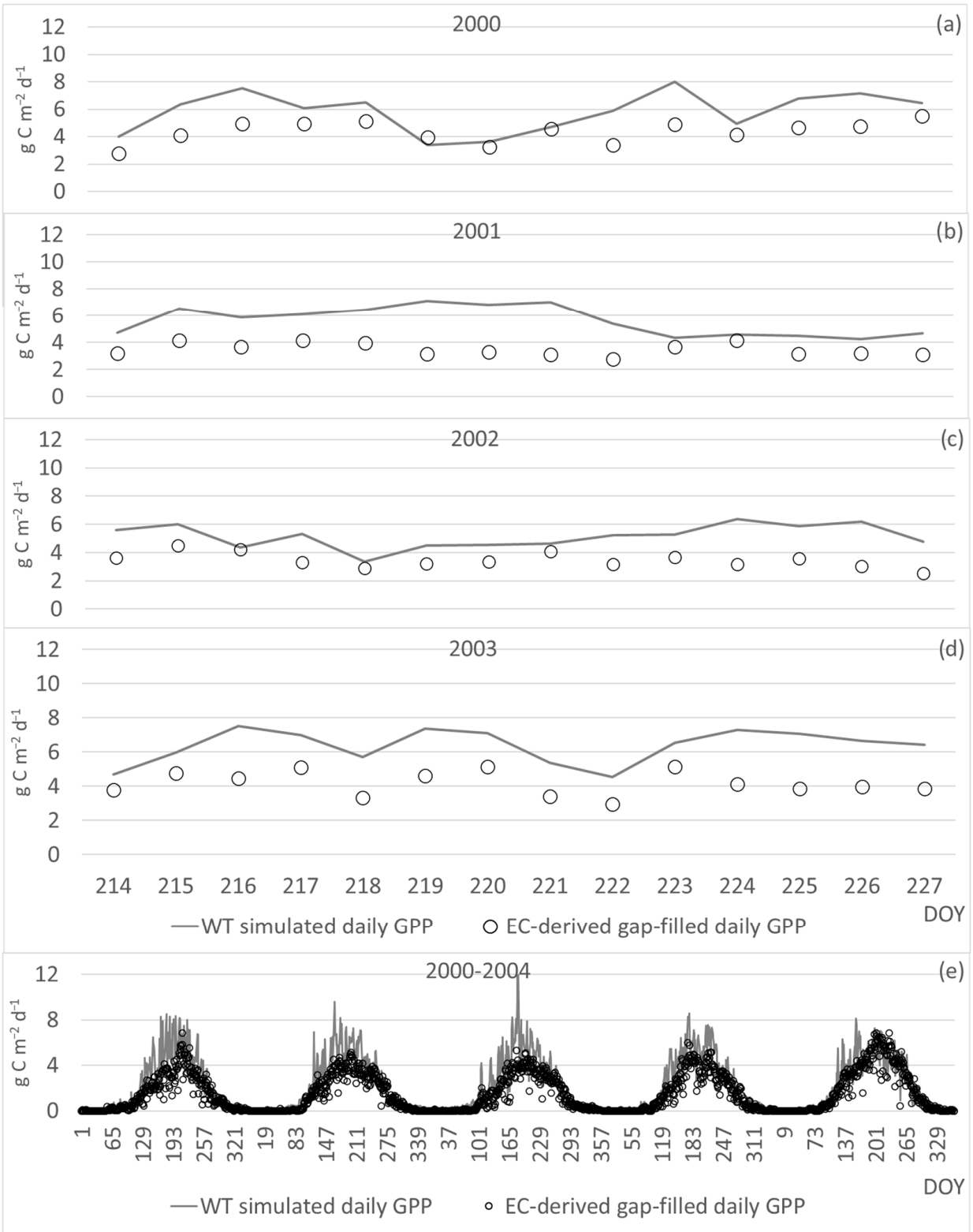

Figure 10. Daily ecosystem gross primary productivity (GPP) at Mer Bleue bog during 2–15 August 2000 (**a**), 2001 (**b**), 2002 (**c**), and 2003 (**d**) and the course of daily GPP in 2000–2004 (**e**). Simulated GPP by VBall_WT model run driven by the observed depth to water table, d_{WT}, is compared vs. observed GPP derived from eddy covariance (EC) CO_2 exchange. DOY means day of year.

The negative effect of low I_{SWR} on simulated GPP on DOY 222 (Equations (S1.1.1.4) and (S1.1.2.2)) was counteracted by the high v_w that day (Figure 15d), resulting in an increased g_b in the model (Equations ((S1.1.5.2) and (S1.1.5.3)), which caused an increase in

shrub GPP (Figures 13a,b and 14a). Compared to shrubs, moss GPP was reduced by the low I_{SWR} on DOY 222 (Equation (S1.2.1.1)) in both VBall_WT (Figure 13b,d) and VBall_NS (Figure 14b,d). The subsequent pronounced decline of shrub and moss GPP in hummocks and hollows on DOY 224 in both VBall_WT (Figure 13) and VBall_NS (Figure 14) was due to the significantly lower I_{SWR} and T_{air} that day (Figure 15a,b) and its effect on the model (Equations (S1.1.3.1), (S1.1.4.4) and (S1.1.4.6)).

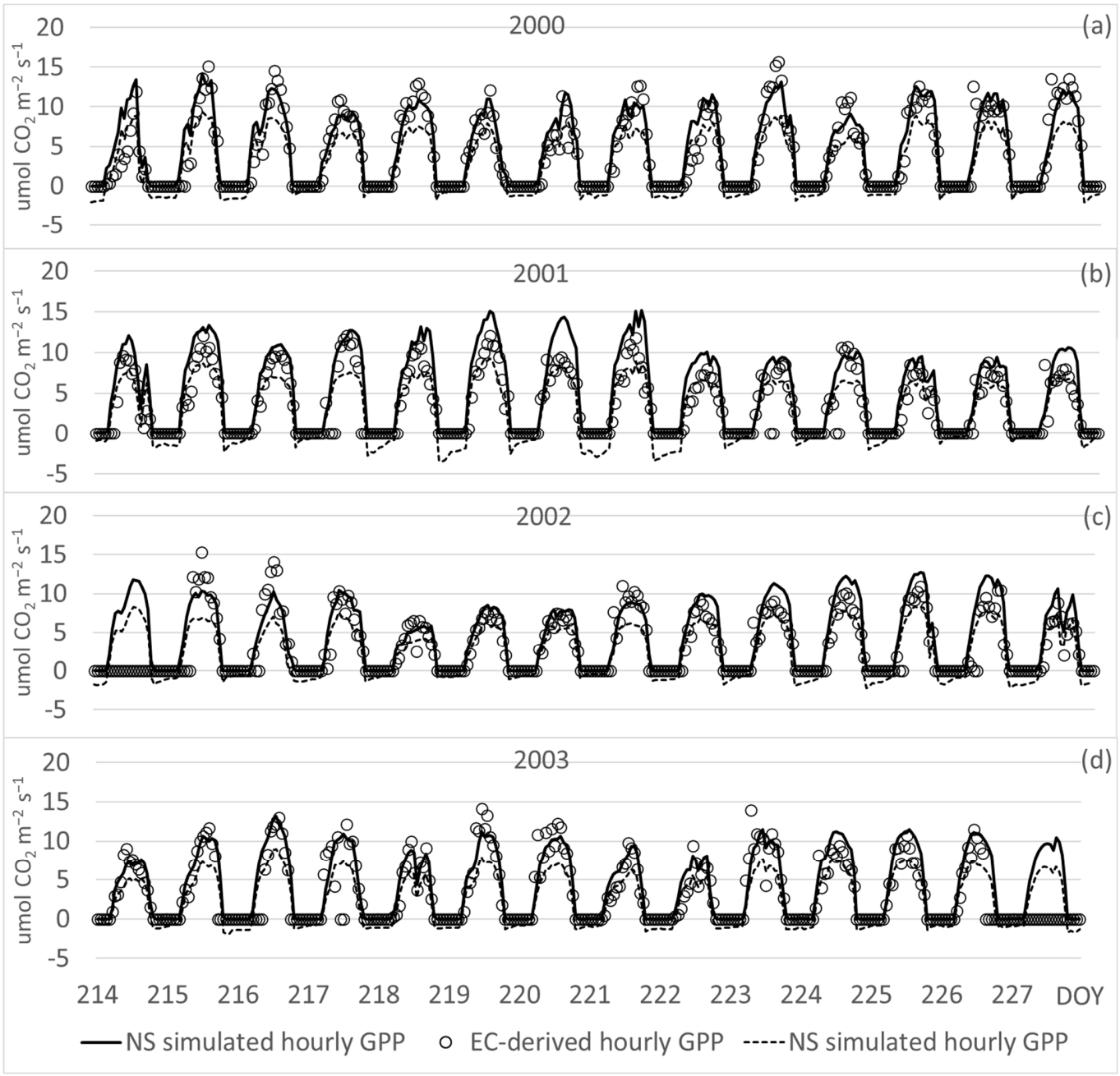

Figure 11. Hourly ecosystem gross primary productivity (GPP) and net primary productivity (NPP) at Mer Bleue bog during 2–15 August 2000 (**a**), 2001 (**b**), 2002 (**c**), and 2003 (**d**). Simulated GPP by VBall_NS model run driven by the observed near-surface soil water contents, θ, is compared vs. observed GPP derived from eddy covariance (EC) CO_2 exchange. DOY means day of year.

The stable, relatively high I_{SWR} and T_{air} and relatively low RH and v_w (Figure 15a–d) during the last three days of the period resulted in a moderately high GPP in VBall_WT and VBall_NS (Figures 13 and 14a,b,d).

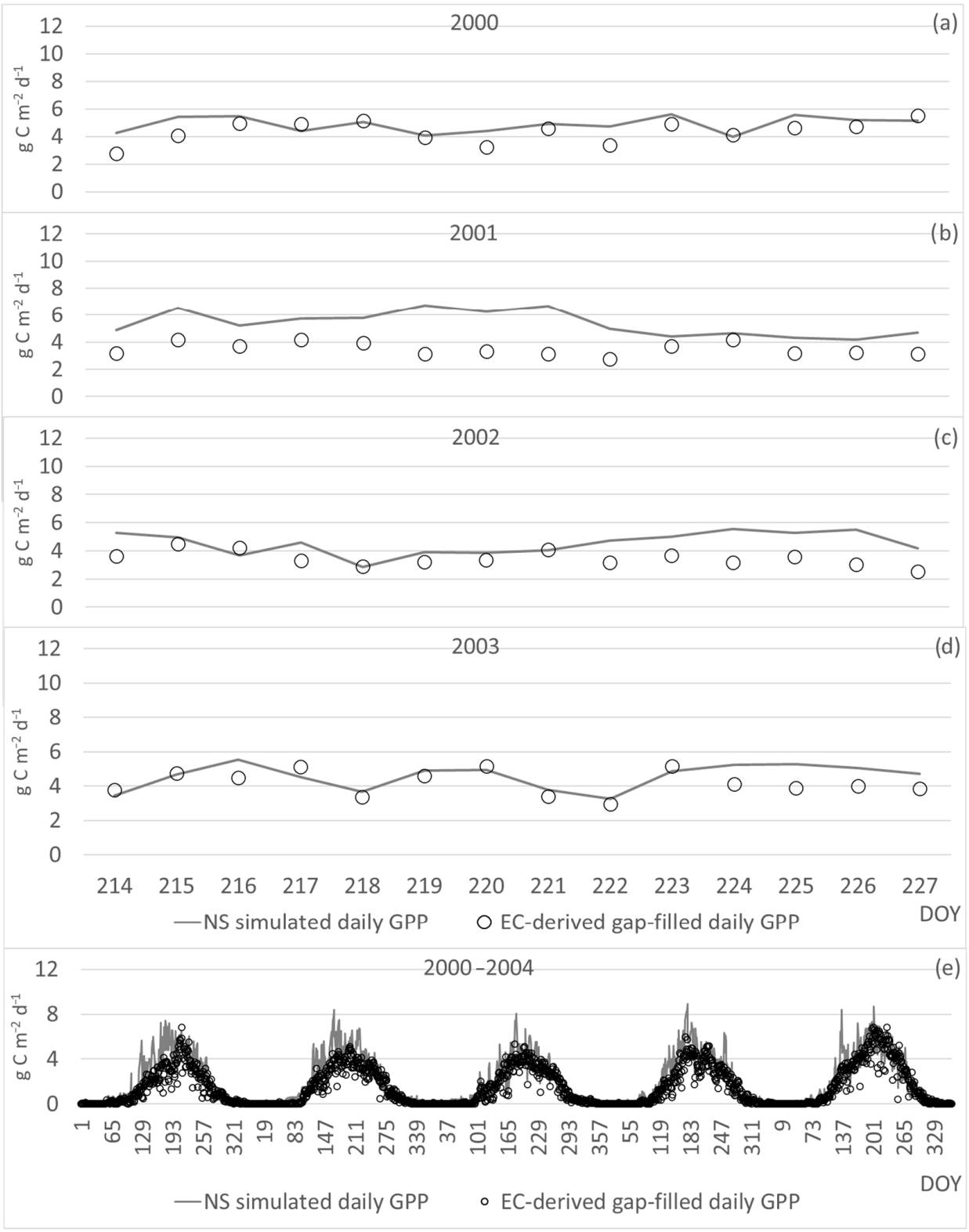

Figure 12. Daily ecosystem gross primary productivity (GPP) at Mer Bleue bog during 2–15 August 2000 (**a**), 2001 (**b**), 2002 (**c**), and 2003 (**d**), and the course of daily GPP in 2000–2004 (**e**). Simulated GPP by VBall_NS model run driven by the observed near-surface soil water contents, θ, is compared vs. observed GPP derived from eddy covariance (EC) CO_2 exchange. DOY means day of year.

In VBall_WT, d_{WT} in hummocks was ~34 cm below the hummock surface (Figure 15e), and d_{WT} in hollows was ~9 cm below the hollow surface. Thus, in unsaturated soil layers above WT, simulated θ in hollows was higher than that in hummocks (Equation (S6.1.1.4a,b)),

such that $\overline{\theta} \geq \overline{\theta}_{FC}$ and thereby soil air availability $f_{\theta R} < 1$ in Equation (9), while $f_{\theta A} > 1$ in Equation (11a), reflecting enhanced adaptations to wetland soil conditions. The combined effects of $f_{\theta R}$ and $f_{\theta A}$ in Equation (2a,b) resulted in similar, although slightly lower f_θ in hollows compared to f_θ in hummocks, where the higher $f_{\theta R}$ in Equation (9) reflecting higher air availability was offset by the lower $f_{\theta A} < 1$ in Equation (11b) reflecting fewer adaptations (with higher air availability). As a result, simulated shrub GPP in hollows (Figure 13c) was only slightly lower than simulated hummock shrub GPP (Figure 13a), which is consistent with the conservative response of vascular GPP to different WT levels observed in previous studies [10,41]. The f_θ in Equation (3) increased with increased water availability $f_{\theta W}$ in Equation (8), resulting in higher moss GPP (Equation ((S2.1.1.2a)) in hollows (Figure 13d) than in hummocks (Figure 13b), consistent with field observations [39].

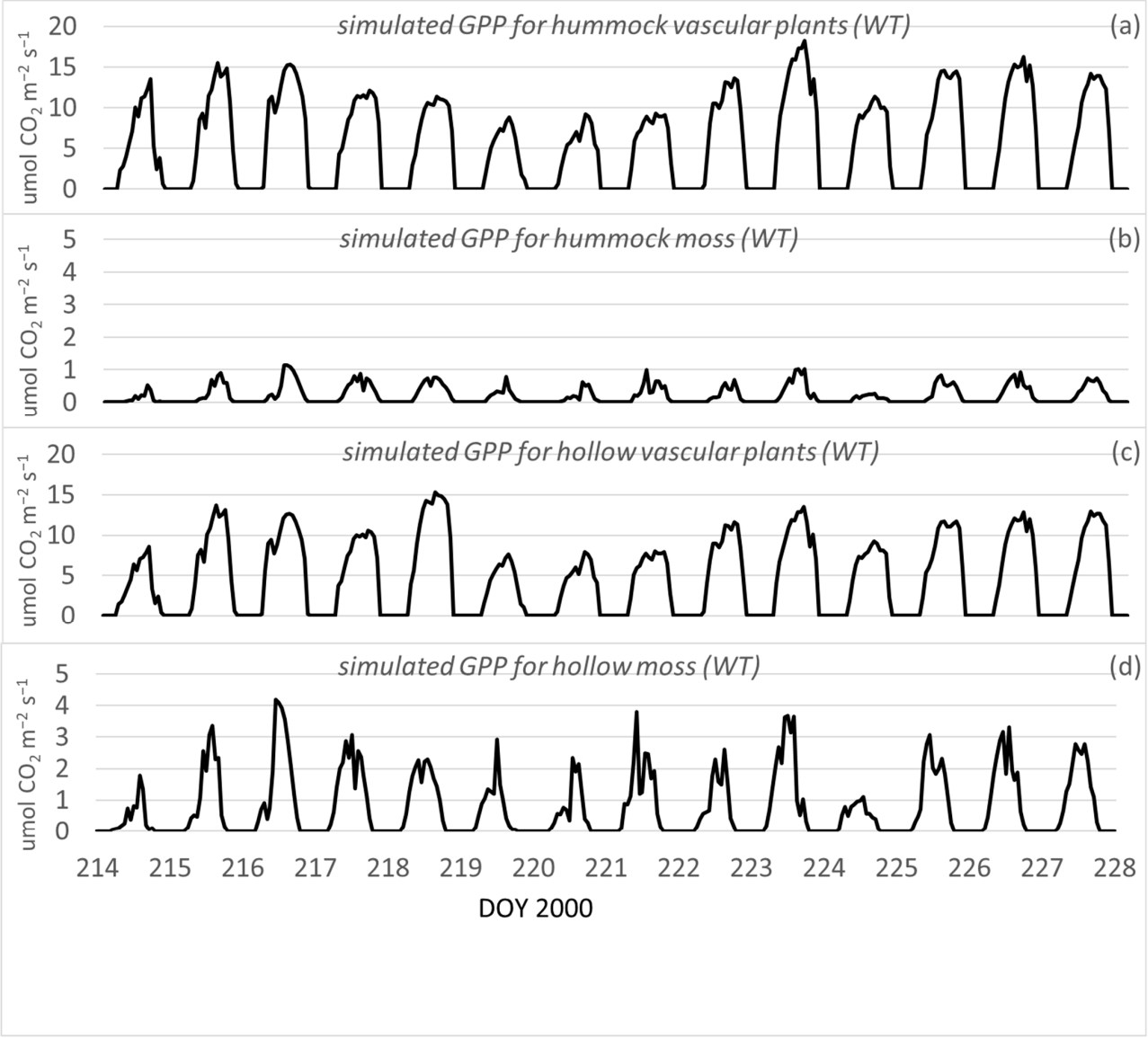

Figure 13. Hourly simulated GPP of hummock shrubs (**a**), hummock moss (**b**), hollow shrubs (**c**), and hollow moss (**d**) by VBall_WT model run driven by the observed depth to water table, d_{WT}, applied ro Mer Bleue bog during 2–15 August 2000. DOY means day of year.

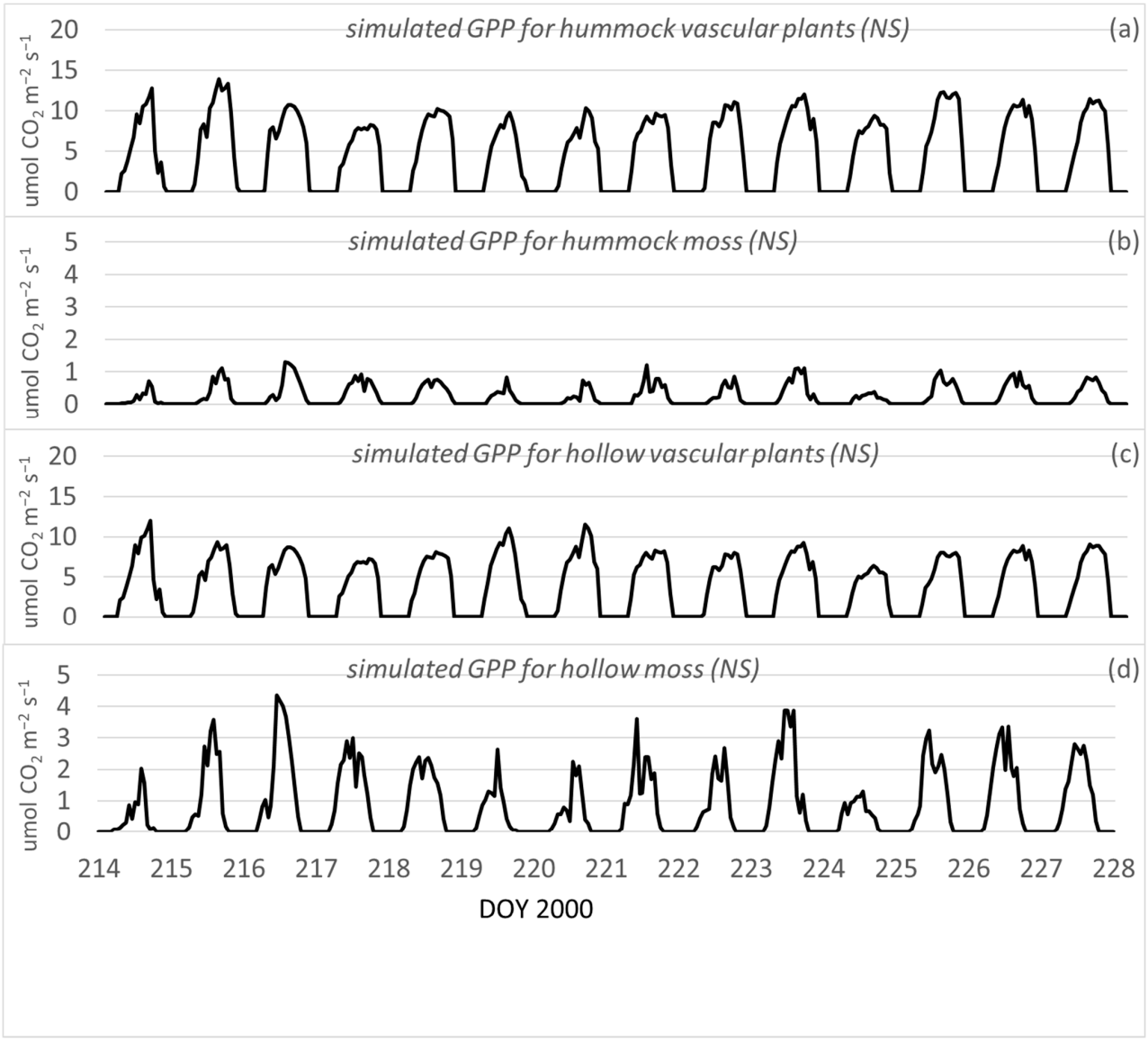

Figure 14. Hourly simulated GPP of hummock shrubs (**a**), hummock moss (**b**), hollow shrubs (**c**), and hollow moss (**d**) by VBall_NS model run driven by the observed near-surface soil water contents, θ, applied to Mer Bleue bog during 2–15 August 2000. DOY means day of year.

In VBall_NS, the high θ of the near-surface peat matrix in hollows compared to that in hummocks (Figure 15f), both with 0.8 m^3 m^{-3} macroporosity [26], resulted in pronounced reductions in hollow shrub GPP. The low soil air availability $f_{\theta R}$ in Equation (9) and relatively low $f_{\theta A}$ in Equation (11a,b) with d_{WT} close to the hollow surface (reflecting the general difficulties for plants in near-saturated soils, in contrast to higher $f_{\theta A}$ with moderately deep WT below the soil surface) caused a decline in f_{θ} in Equation (2a,b). The reduced f_{θ} caused markedly lower shrub GPP during days with higher hollow near-surface θ, i.e., DOY 215–218 and DOY 221–227, compared to GPP on DOY 214, DOY 219, and DOY 220, with lower near-surface θ (Figure 14c). The GPP of hummock shrub and moss and hollow moss in VBall_NS was similar to that in VBall_WT due to the mechanisms described above for VBall_WT. Overall, the contributions of hummock and hollow shrub and moss GPP resulted in the simulated ecosystem GPP closely following the observed GPP (Figure 11a).

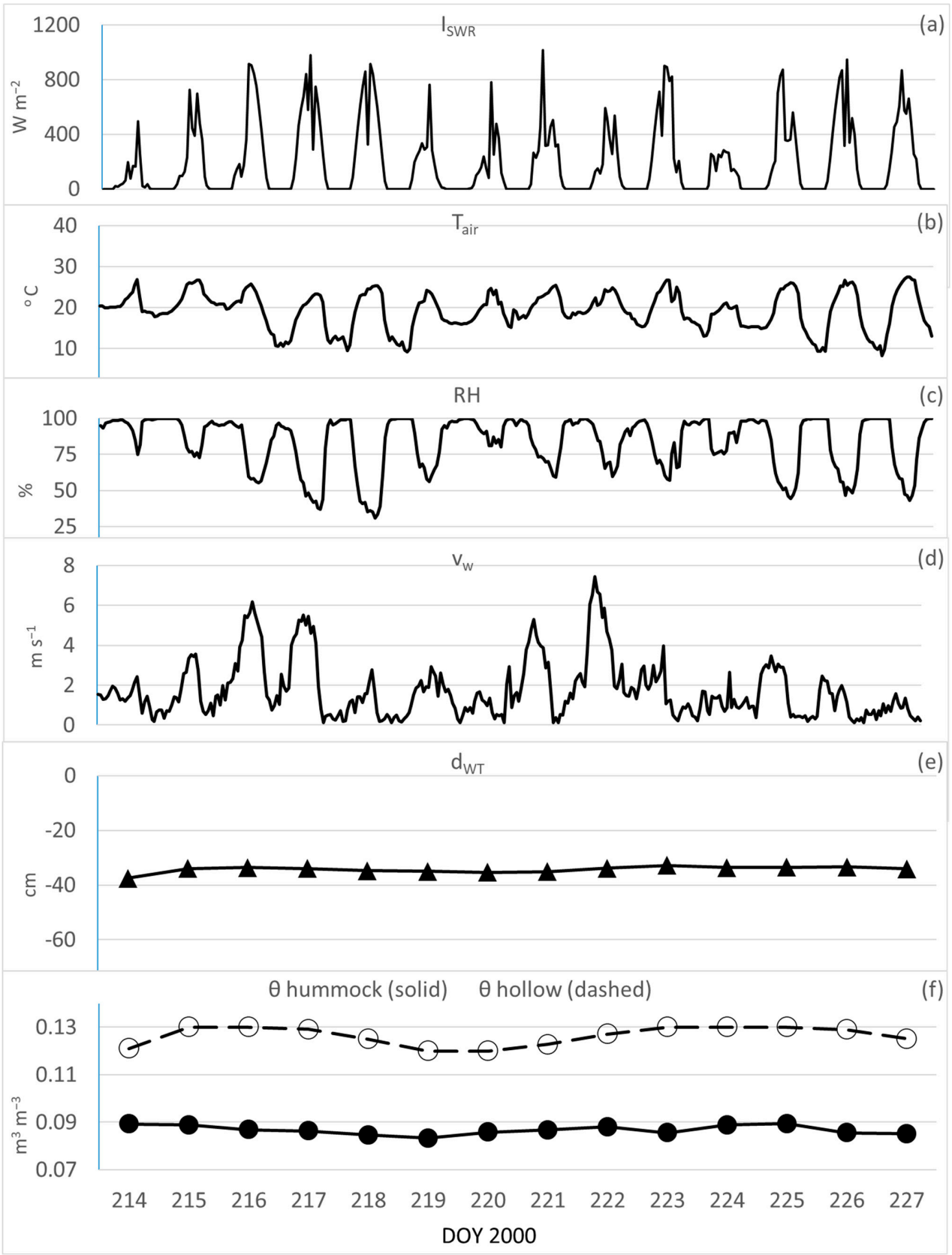

Figure 15. Hourly observed incoming short-wave radiation, I_{SWR} (**a**), air temperature, T_a (**b**), relative humidity, RH (**c**), wind speed, v_w (**d**), and daily observed depth to water table, d_{WT}, in hummocks assumed to be 25 cm below hollows (negative values mean below soil surface) (**e**), and near-surface soil water contents, θ, at 10 cm depth in hummocks and 3 cm depth in hollows (**f**), at Mer Bleue bog during 2–15 August 2000. DOY means day of year.

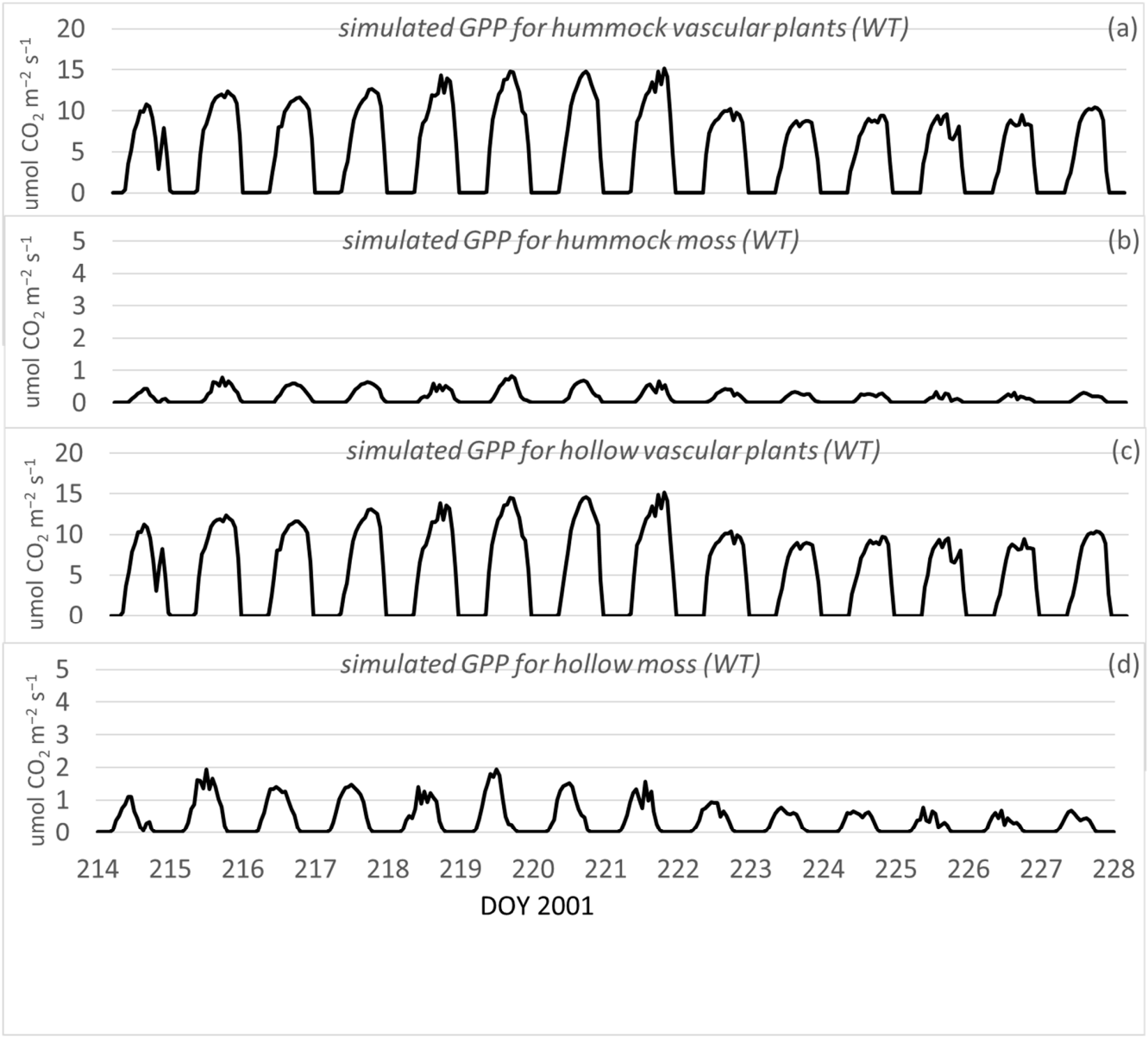

Figure 16. Hourly simulated GPP of hummock shrubs (**a**), hummock moss (**b**), hollow shrubs (**c**), and hollow moss (**d**) by VBall_WT model run driven by the observed depth to water table, d_{WT}, applied to Mer Bleue bog during 2–15 August 2001. DOY means day of year.

3.2. Analyzing Productivity Simulations Under Dry Conditions

During the dry period DOY 214–227 in 2001, both VBall_WT and VBall_NS reproduced hourly dynamics of hummock and hollow shrub and moss GPP in agreement with hourly ecosystem GPP (Figures 9b and 11b). The increased simulated GPP from DOY 214 to DOY 215 in VBall_WT and VBall_NS was due to increased I_{SWR} (Figure 18a) (Equations (S1.1.1.4) and (S1.1.2.2)). However, although the increase in I_{SWR} continued to DOY 216, simulated GPP decreased due to the constraining effect of decreasing RH from DOY 215 to DOY 216 (Figure 18c), which decreased g_s (Equation (S1.1.5.5)) and reduced T_L (Equations (S1.1.3.1), (S1.1.4.4) and (S1.1.4.6)). With no pronounced difference in I_{SWR} from DOY 217 to DOY 219 (Figure 18a), the simulated increase in GPP was caused by the combined effects of increased T_{air} and RH (Figure 18b,c) increasing T_L (Equations (S1.1.3.1), (S1.1.4.4) and (S1.1.4.6)), the effect of increased RH on increasing g_s (Equation (S1.1.5.5)), and the effect of increased v_w (Figure 18d) on increasing g_b (Equations (S1.1.5.2) and (S1.1.5.3)). Simulated GPP remained similar during DOY 220 and

DOY 221, with a slight decrease on DOY 220, which was more apparent for VBall_NS (Figure 17) than for VBall_WT (Figure 16). This behavior aligned with the slightly lower RH and v_w on that day compared to their values during the adjacent days and matched the observed ecosystem GPP (Figures 9b and 11b). The decline in simulated GPP on DOY 222 was caused by a combined effect of meteorological and hydrological drivers. Lower I_{SWR}, T_{air}, RH, and v_w (Figure 18a–d) values than those in the previous days contributed to a more pronounced decline in simulated hummock and hollow shrub GPP on DOY 222, which remained low until the end of the period on DOY 227 (Figure 16a,c and Figure 17a,c).

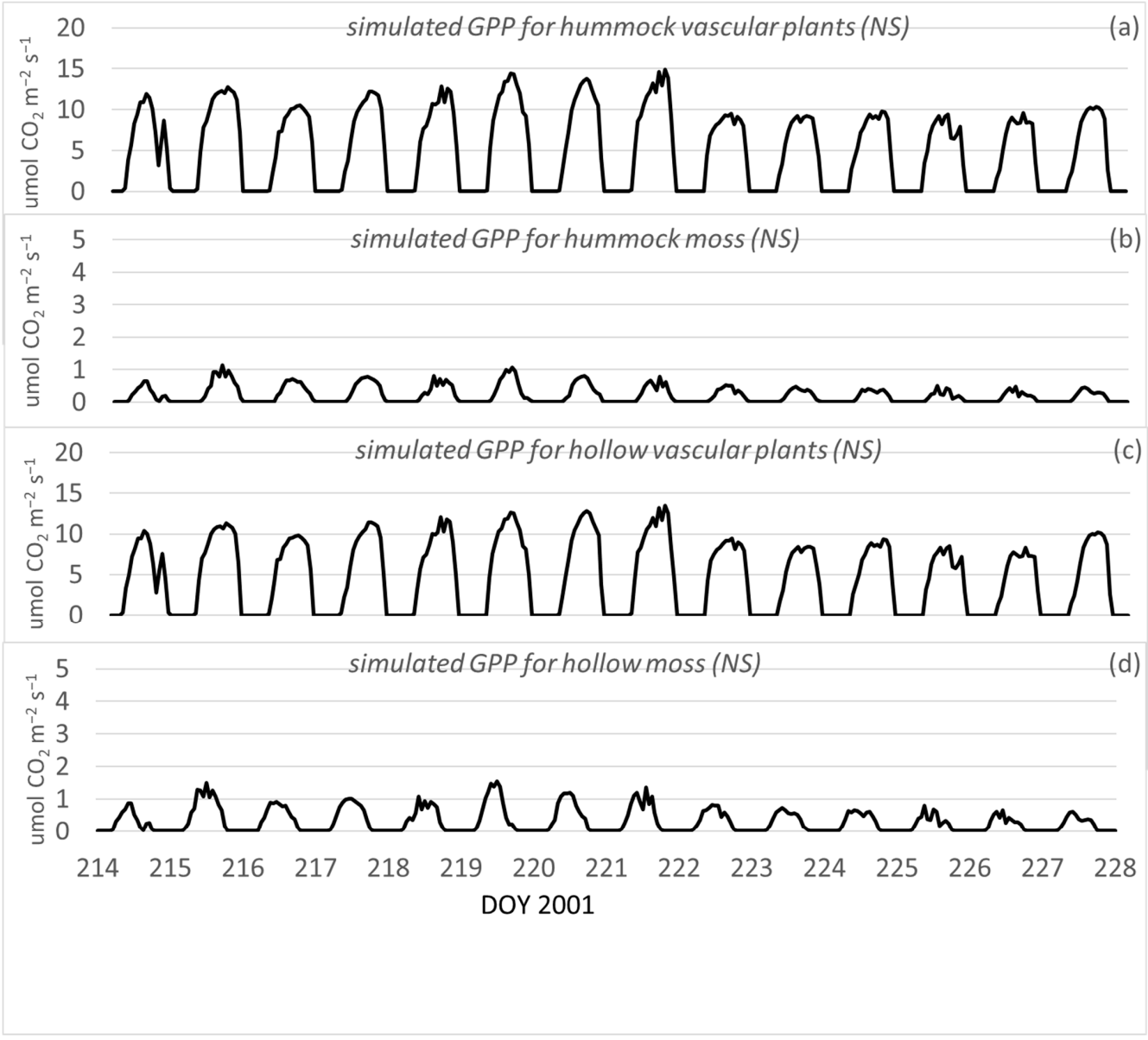

Figure 17. Hourly simulated GPP of hummock shrubs (**a**), hummock moss (**b**), hollow shrubs (**c**), and hollow moss (**d**) by VBall_NS model run driven by the observed near-surface soil water contents, θ, applied to Mer Bleue bog during 2–15 August 2001. DOY means day of year.

The effect of receding d_{WT} in VBall_WT (Figure 18e) and decreasing hummock and hollow near-surface θ in VBall_NS (Figure 18f) during this period is of particular note. In VBall_WT, on average, d_{WT} was ~59 cm below the hummock surface (respectively, ~34 cm below the hollow surface), but gradually declined to ~67 cm depth in hummocks (Figure 18e) (respectively, ~42 cm depth in hollows) towards the end of the period. As

the simulated $\overline{\theta}$ of the unsaturated peat above WT decreased with receding d_{WT}, the effect of vascular plants' adaptations to wetland soil $f_{\theta A}$ was initially around unity with $\overline{\theta}$, varying close to $\overline{\theta}_{FC}$ in Equation (11a,b), along with d_{WT} fluctuations in peat above ~60 cm in hummocks (respectively, ~40 cm in hollows) during DOY 214–221. However, with deeper WT drawdown during DOY 222–227 (Figure 18e), $f_{\theta A}$ declined in Equation (11b), reflecting the decreasing needs of the plants to maintain their adaptations with improved soil aeration. The latter was reflected in the model by increasing the air availability in the soil via $f_{\theta R}$ in Equation (9) and $f_{\theta Ri}$ in Equation (10). The combined behavior of $f_{\theta R}$ and $f_{\theta A}$ was counteracted, though, by the decreasing water availability $f_{\theta W}$ in Equation (8). This resulted in a similar f_{θ} in Equation (2a,b), with d_{WT} varying within the upper ~60 cm in hummocks and upper ~40 cm in hollows during DOY 214–221. However, with $f_{\theta W}$ becoming too low with WT drawdown below those depths, f_{θ} in Equation (2a,b) declined markedly during DOY 222–227. The same mechanism operated in VBall_NS, where the simulated low d_{WT} in hummocks and hollows was caused by the corresponding low near-surface θ [27]. The above mechanisms in VBall_WT and VBall_NS resulted in similar shrub GPP (S2.1.1.1a) in hummocks and hollows during DOY 214–221, which remained similar but lower during DOY 222–227 (Figures 16a,c and 17a,c).

The GPP lowering was properly captured by the *DIMONA* PB model through d_{WT} in VBall_WT, which was lower than ~60 cm in hummocks (Figure 18e) and ~40 cm in hollows, and through near-surface θ in VBall_NS, where it reached critical values in hummocks and hollows (Figure 18f). Both VBall_WT and VBall_NS performed in agreement with field studies that reported a general insensitivity of vascular plants to soil hydrology at Mer Bleue within most of the natural range of WT fluctuations [39,47], with the first signs of water stress caused by the drying of the upper peat layers when d_{WT} reached ~65 cm depth in hummocks [41].

Unlike vascular plants, the lack of adaptations and sensitivity of moss to soil hydrology via f_{θ} in Equation (3), f_R in Equation (5), $f_{U,i}$ in Equation (7), $f_{\theta R}$ in Equation (9), and $f_{\theta,i}$ in Equation (10) resulted in hummock moss GPP decreasing greatly compared to that in hollows in both model runs (Figures 16b,d and 17b,d), especially with the WT drawdown after DOY 222. Both hummock and hollow simulated moss GPP in the dry period of 2001 were lower compared to those in the wet period of 2000 (Figures 13b,d and 14b,d), consistent with previous findings that bog ecosystem GPP was primarily affected by soil hydrology via its moss component within the usual range of WT variation [10].

3.3. Representing the Specifics of Productivity Responses to Bog Hydrology

Both model runs were examined during two periods of similar meteorological forcing but contrasting hydrology. These were the 30-day periods DOY 235–264 in the dry year 2001 and the wet year 2004, with d_{WT} below the hummock surface 67 ± 3 cm and 38 ± 6 cm, respectively [10]. VBall_WT captured the hourly, daily, and hourly-binned courses of ecosystem GPP (Figure 19a–c) through their constituents, i.e., GPP of hummock shrubs and moss (Figure 20a,b) and hollow shrubs and moss (Figure 20c,d), during both periods. VBall_NS produced similar results for both periods (Figures 21 and 22). With similar meteorological forcing, the mechanisms explained above (Sections 3.2 and 3.3) resulted in lower simulated ecosystem GPP during the dry 2001 period compared to the wet 2004 period. In VBall_WT, the very deep WT varying between ~60 cm and ~70 cm depths in hummocks in Figure 1 in [12]—respectively, between ~40 cm and ~50 cm depths in hollows—caused a slight GPP decline in the 2001 period (Figure 20a,c). However, that decline was not pronounced because f_{θ} in Equation (2a,b) showed only a small reduction. Thereby, both hummock and hollow simulated shrub GPP in the 2001 period was similar to those in the 2004 period. VBall_NS performed similarly to VBall_WT (Figure 22a,c), as

both model runs were consistent with previous field studies that shrub GPP at Mer Bleue bog was not affected by soil hydrology until the WT receded below ~65 cm [39,41,47].

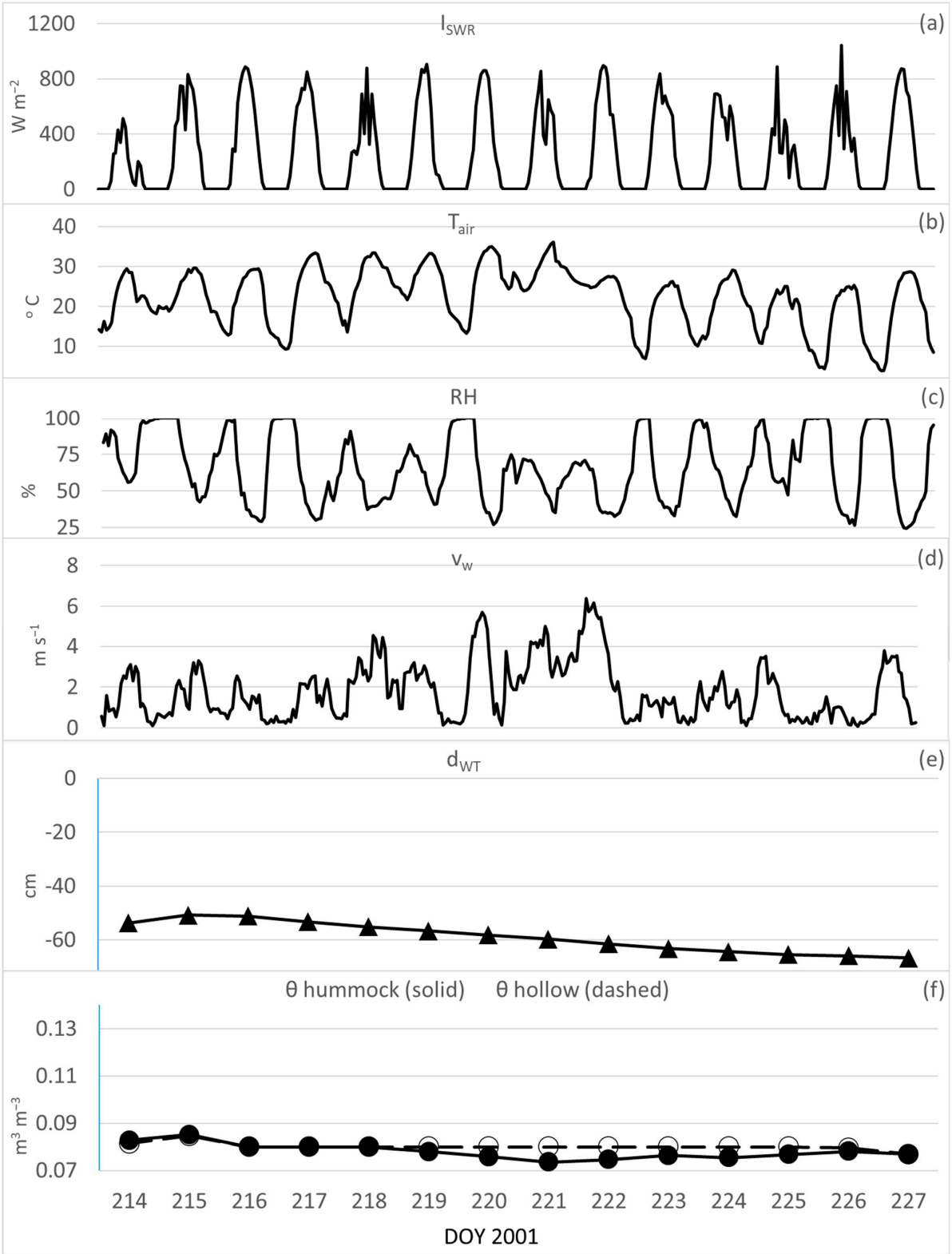

Figure 18. Hourly observed incoming short-wave radiation, I_{SWR} (**a**), air temperature, T_a (**b**), relative humidity, RH (**c**), wind speed, v_w (**d**), daily observed depth to water table, d_{WT}, in hummocks assumed to be 25 cm below hollows (negative values mean below soil surface) (**e**), and near-surface soil water contents, θ, at 10 cm depth in hummocks and 3 cm depth in hollows (**f**), at Mer Bleue bog during 2–15 August 2001. DOY means day of year.

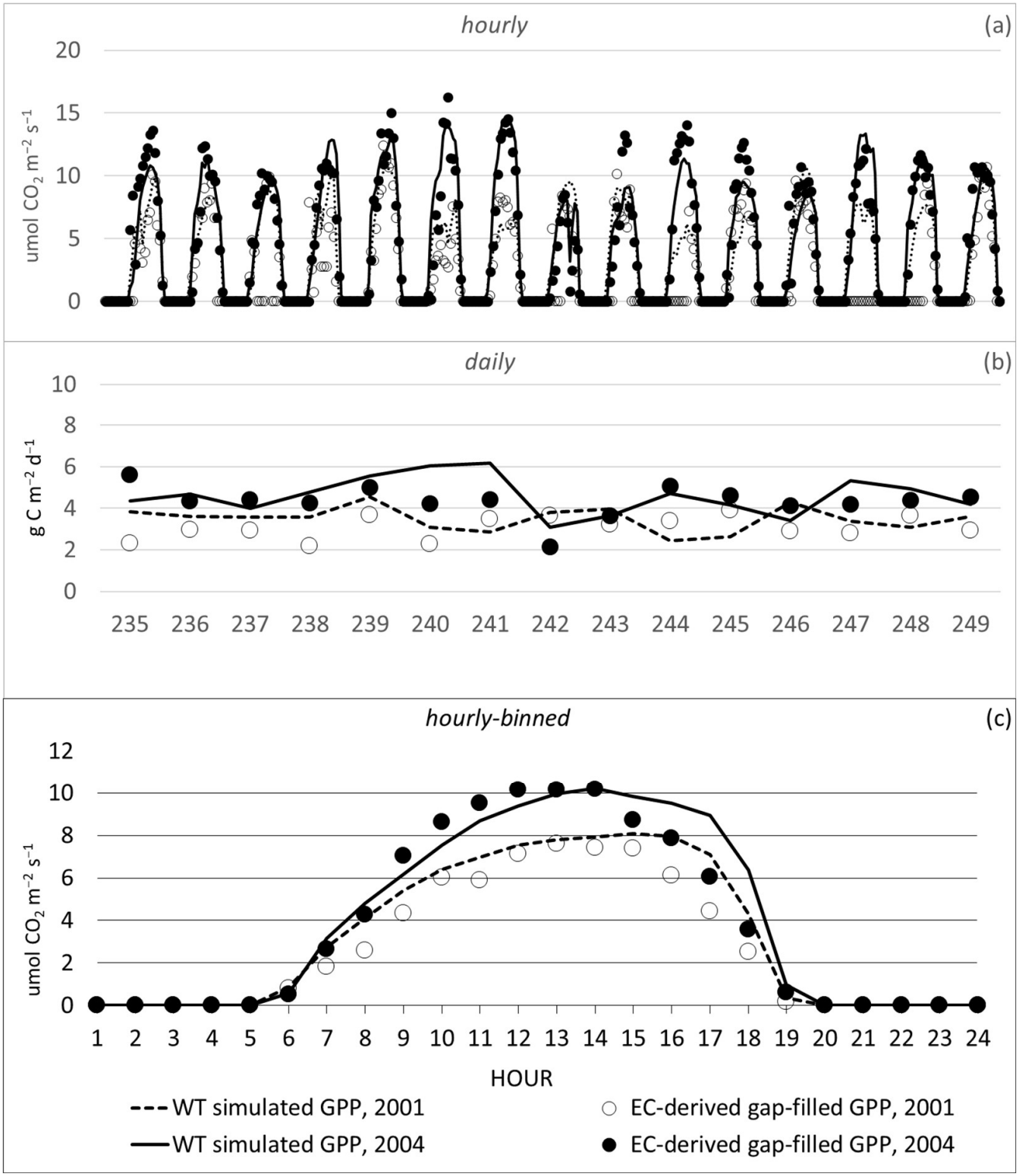

Figure 19. Hourly (**a**), daily (**b**), and hourly-binned (**c**) ecosystem gross primary productivity (GPP) at Mer Bleue bog. Simulated GPP by VBall_WT model run driven by the observed depth to water table, d_{WT}, is compared vs. observed GPP derived from eddy covariance (EC) CO_2 exchange. DOY means day of year. Hourly-binned values are given for 23 August to 21 September in 2001 and 2004, while hourly and daily values are given only for 23 August to 6 September in 2001 and 2004 due to scaling limitations.

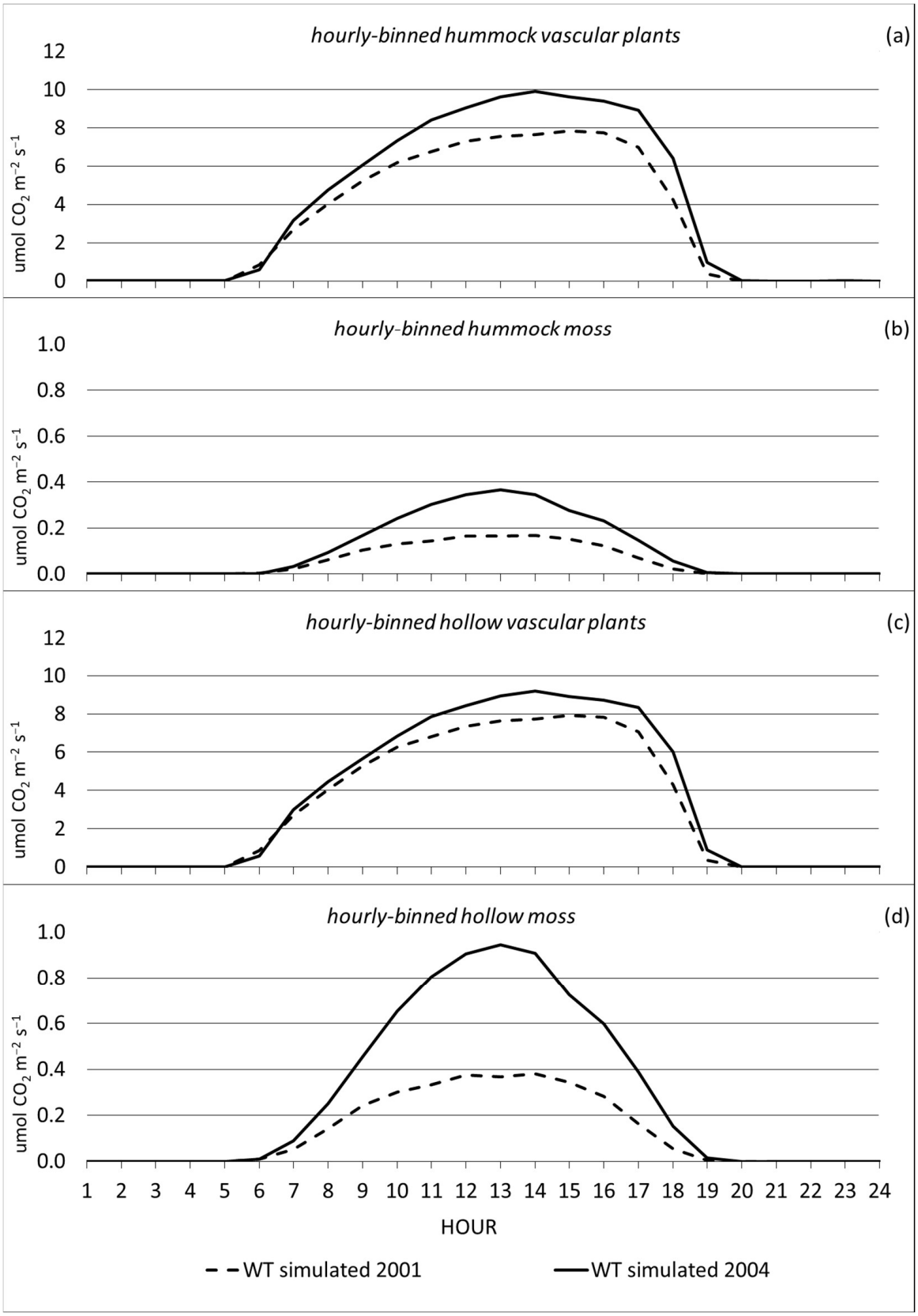

Figure 20. Hourly-binned simulated GPP of hummock shrubs (**a**), hummock moss (**b**), hollow shrubs (**c**), and hollow moss (**d**) by VBall_WT model run driven by the observed depth to water table, d_{WT}, applied to Mer Bleue bog during 23 August to 21 September in 2001 and 2004. DOY means day of year.

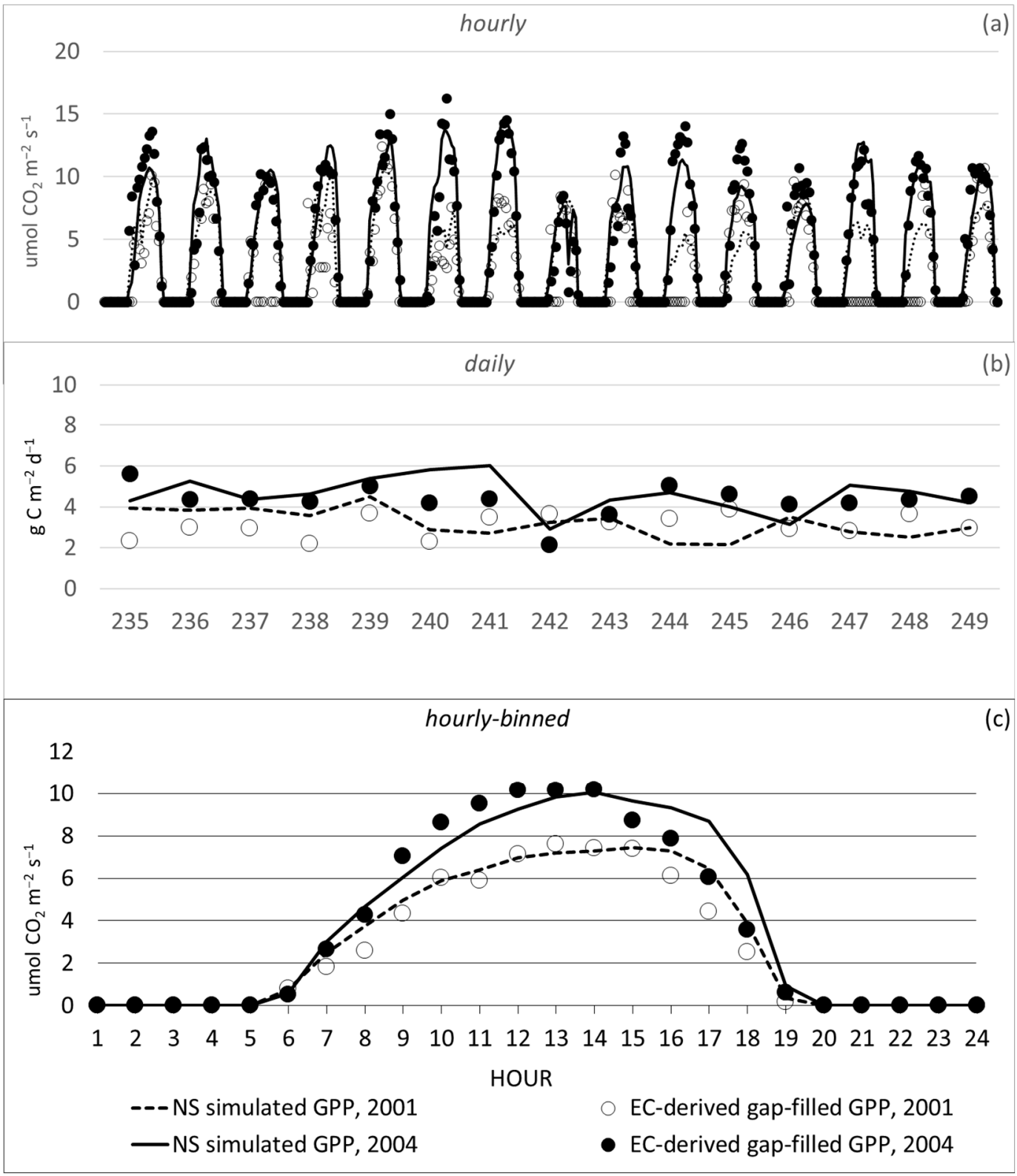

Figure 21. Hourly (**a**), daily (**b**), and hourly-binned (**c**) ecosystem gross primary productivity (GPP) at Mer Bleue bog. Simulated GPP by VBall_NS model run driven by the observed depth to water table, d_{WT}, is compared vs. observed GPP derived from eddy covariance (EC) CO_2 exchange. DOY means day of year. Hourly-binned values are given for 23 August to 21 September in 2001 and 2004, while hourly and daily values are given only for 23 August to 6 September in 2001 and 2004 due to scaling limitations.

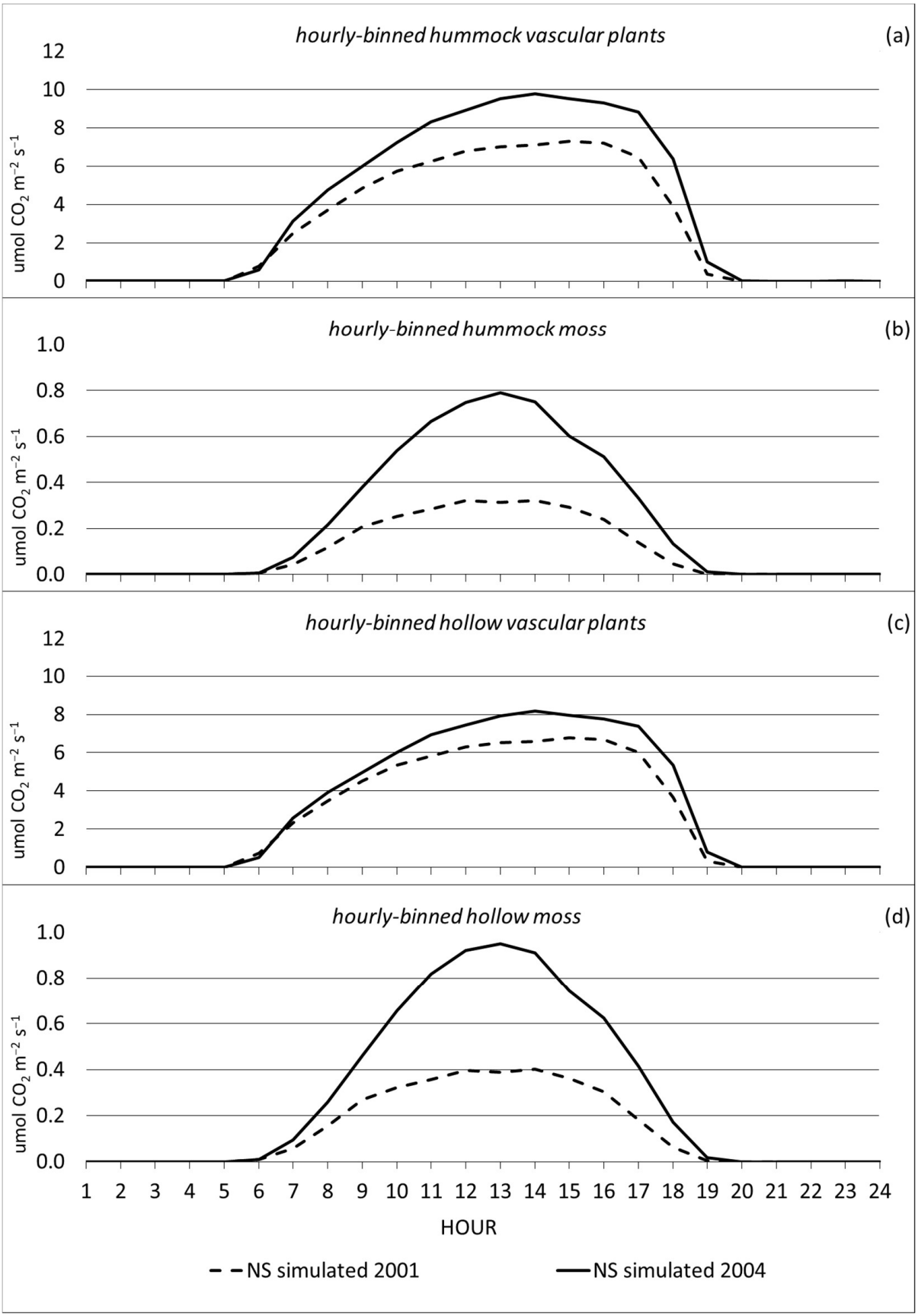

Figure 22. Hourly-binned simulated GPP of hummock shrubs (**a**), hummock moss (**b**), hollow shrubs (**c**), and hollow moss (**d**) by VBall_NS model run driven by the observed near-surface soil water contents, θ, applied to Mer Bleue bog during 23 August to 21 September in 2001 and 2004. DOY means day of year.

Both model runs were also compared to previous modelling work at the Mer Bleue bog which employed the *ecosys* model [22]. Hourly-binned hummock shrub GPP for the same periods (Figure 9b in [12]) previously simulated by *ecosys* was consistent in magnitude with the corresponding outcomes from VBall_WT and VBall_NS (Figures 20a and 22a). But the corresponding model performances for hollows differed.

Both *DIMONA* model runs produced higher values than the hourly-binned hollow shrub GPP in *ecosys*, reaching slightly above 3 umol CO_2 m^{-2} s^{-1} for 2001 and below 4 umol CO_2 m^{-2} s^{-1} for 2004 (Figure 9c in [12]). However, previous field studies reporting net photosynthetic capacities ~7 umol CO_2 m^{-2} s^{-1} at Mer Bleue bog hollows [39,48] suggest that the *DIMONA* model output might be closer to reality. Unlike shrubs, simulated moss GPP declined dramatically, by ~½ in both hummocks and hollows in VBall_WT and VBall_NS (Figures 20b,d and 22b,d), when comparing the 2004 period to the 2001 period. This was due to the pronounced decline in water availability $f_{\theta W}$ in Equation (8) for the upper two soil layers in the model, where rhizoids grow, hence producing a marked reduction in f_{θ} in Equation (3) for moss during the 2001 period. Compared to *ecosys* (Figure 10b,c in [12]), both VBall_WT and VBall_NS produced lower moss GPP rates in hummocks and hollows, but they were consistent with field observations.

Both VBall_WT and VBall_NS produced hummock moss GPP rates (Figures 20b and 22b) that were below, but comparable in magnitude to, the observed average values of maximum photosynthetic rate of *Sphagnum fuscum*, which occupies Mer Bleue bog hummocks [39], reported to reach ~1.7 umol CO_2 m^{-2} s^{-1} [49]. Also, both VBall_WT and VBall_NS produced hollow moss GPP rates (Figures 20d and 22d) that were below, though comparable to, the observed average values of maximum photosynthetic rates of *Sphagnum fallax* and *Sphagnum magellanicum*, which occupy Mer Bleue bog hollows [39], reported to reach ~4.3 umol CO_2 m^{-2} s^{-1} and ~2.7 umol CO_2 m^{-2} s^{-1}, respectively [49].

3.4. Evaluation of DIMONA PB Model Performance

The statistics of linear regressions of simulated on observed ecosystem GPP, as well as RMSE and Willmott's d values, are summarized for the 2000–2004 period and for each individual year for VBall_WT (Table 3), VBall_NS (Table 4), and the other runs listed in Table 2 (Table 5).

Table 3. Statistics for estimating the performance of the representative model run driven by water table depth (d_{WT}) as a hydrological driver, including slope a (unitless), intercept b (umol CO_2 m^{-2} s^{-1} for hourly time step, g C m^{-2} d^{-1} for daily time step), and coefficient of determination R^2 (unitless) of the linear regressions of simulated on eddy covariance (EC)-derived ecosystem GPP, root mean square error, RMSE (umol CO_2 m^{-2} s^{-1} for hourly time step, g C m^{-2} d^{-1} for daily time step), and Willmott's index of agreement, d (unitless).

Model Run Name	Period	Time Step	a	b	R^2	RMSE	d
VBall_WT	2000–2004	hourly	1.01	1.42	0.67	1.89	0.86
VBall_WT	2000	hourly	1.15	1.35	0.67	2.51	0.82
VBall_WT	2001	hourly	1.13	1.07	0.72	2.24	0.86
VBall_WT	2002	hourly	1.11	1.27	0.66	2.67	0.83
VBall_WT	2003	hourly	1.15	1.26	0.72	2.26	0.84
VBall_WT	2004	hourly	0.83	1.33	0.72	2.14	0.92
VBall_WT	2000–2004	daily	1.27	0.24	0.82	0.99	0.87
VBall_WT	2000	daily	1.41	0.22	0.82	0.99	0.85
VBall_WT	2001	daily	1.40	0.15	0.85	0.89	0.84

Table 3. *Cont.*

Model Run Name	Period	Time Step	a	b	R^2	RMSE	d
VBall_WT	2002	daily	1.46	0.09	0.80	1.07	0.84
VBall_WT	2003	daily	1.40	0.16	0.91	0.72	0.88
VBall_WT	2004	daily	1.01	0.26	0.85	0.86	0.94

For the entire 2000–2004 period, slopes varying between 1.01 and 1.02 for *DIMONA* hourly WT-driven model runs (Tables 3 and 5) and between 0.94 and 0.97 for hourly near-surface θ-driven model runs (Tables 4 and 5) are comparable to previous modelling studies with *ecosys* [10]. However, the corresponding intercepts in this study are larger by ~1 umol CO_2 m^{-2} s^{-1}. Respectively, R^2 varying between 0.67 and 0.69 and Willmott's d varying between 0.86 and 0.88 for *DIMONA* hourly WT-driven and near-surface θ-driven model runs are only slightly lower than those for *ecosys* [10], where the RMSE for modelled GPP was not reported.

The values of R^2 and Willmott's d improved for both VBall_WT and VBall_NS when individual years were analyzed, reaching 0.72 and 0.92, respectively (Tables 3 and 4). A slight decrease in intercepts was accompanied by a slight increase in slopes. However, the overestimation of simulated GPP was less than that reported for other models, varying between 20% and 61% [50], or even greater overestimations with satellite-derived GPP [51,52]. The slopes for the daily linear regressions with VBall_WT and VBall_NS were even larger (Tables 3 and 4), and artifacts of daily aggregations from hourly EC-derived GPP possibly played some role. Daily R^2 and Willmott's d values for VBall_WT and VBall_NS varied between 0.82 and 0.84 and between 0.87 and 0.91, respectively, for 2000–2004, with maximum values of 0.91 and 0.95, respectively, for individual years (Tables 3 and 4). These results suggest reasonable model performance at a daily time scale and no significant hourly autocorrelation.

Table 4. Statistics for estimating the performance of the representative model run driven by the near-surface soil water content (θ) as a hydrological driver, including slope a (unitless), intercept b (umol CO_2 m^{-2} s^{-1} for hourly time step, g C m^{-2} d^{-1} for daily time step), and coefficient of determination, R^2 (unitless), of the linear regressions of simulated on eddy covariance (EC)-derived ecosystem GPP, root mean square error, RMSE (umol CO_2 m^{-2} s^{-1} for hourly time step, g C m^{-2} d^{-1} for daily time step), and Willmott's index of agreement d (unitless).

Model Run Name	Period	Time Step	a	b	R^2	RMSE	d
VBall_NS	2000–2004	hourly	0.94	1.39	0.69	1.70	0.88
VBall_NS	2000	hourly	0.98	1.77	0.64	2.30	0.83
VBall_NS	2001	hourly	1.02	1.19	0.71	2.10	0.88
VBall_NS	2002	hourly	1.11	1.27	0.66	2.67	0.83
VBall_NS	2003	hourly	1.07	1.31	0.72	2.07	0.86
VBall_NS	2004	hourly	0.87	1.24	0.72	2.24	0.92
VBall_NS	2000–2004	daily	1.17	0.27	0.84	0.84	0.91
VBall_NS	2000	daily	1.25	0.36	0.82	0.89	0.87
VBall_NS	2001	daily	1.28	0.22	0.84	0.84	0.87
VBall_NS	2002	daily	1.16	0.12	0.85	0.72	0.93
VBall_NS	2003	daily	1.28	0.23	0.89	0.71	0.90
VBall_NS	2004	daily	1.03	0.24	0.87	0.83	0.95

Table 5. Statistics for estimating the performance of additional model runs driven by water table depth (d_{WT}) and near-surface soil water content (θ) as hydrological drivers, including slope a (unitless), intercept b (umol CO_2 m^{-2} s^{-1}), and coefficient of determination, R^2 (unitless), of the linear regressions of simulated on eddy covariance (EC)-derived ecosystem GPP, root mean square error, RMSE (umol CO_2 m^{-2} s^{-1}), and Willmott's index of agreement, d (unitless).

Model Run Name	Period	Time Step	a	b	R^2	RMSE	d
VLng_WT	2000–2004	hourly	1.01	1.43	0.67	1.89	0.86
CBall_WT	2000–2004	hourly	1.02	1.43	0.67	1.90	0.86
CLng_WT	2000–2004	hourly	1.02	1.44	0.67	1.91	0.86
VLng_NS	2000–2004	hourly	0.95	1.41	0.69	1.70	0.88
CBall_NS	2000–2004	hourly	0.96	1.40	0.69	1.72	0.88
CLng_NS	2000–2004	hourly	0.97	1.41	0.69	1.72	0.88

The *DIMONA* PB model's performance was further examined by comparing the model outcomes for ecosystem, shrub, and moss NPP, as well as shrub LAI, biomass, and height vs. available field and modelling reports. The model outcomes were determined as averages from the repeated 2000–2004 period in each model run (Section 2.3). The average simulated aboveground ecosystem NPP was 343 g C m^{-2} y^{-1} in VBall_WT and 318 g C m^{-2} y^{-1} in VBall_NS, both comparable to the field aboveground ecosystem NPP at Mer Bleue bog of 340 g C m^{-2} y^{-1} [39] and simulated by *ecosys* ecosystem NPP of 285 g C m^{-2} y^{-1} for the same site and period [10].

The average simulated aboveground shrub NPP was 301 g C m^{-2} y^{-1} in VBall_WT and 256 g C m^{-2} y^{-1} in VBall_NS, both higher than the field-determined aboveground shrub NPP of 160 g C m^{-2} y^{-1} at Mer Bleue bog. However, both VBall_WT and VBall_NS values of the aboveground shrub NPP were within the range of shrub aboveground NPP in bogs reported between 43 and 338 g C m^{-2} y^{-1} [39]. The average simulated aboveground shrub biomass was 652 g m^{-2} in VBall_WT and 526 g m^{-2} in VBall_NS, both within one standard deviation of reported aboveground shrub biomass at Mer Bleue bog, i.e., 506 ± 234 g m^{-2} [53]. For reference, *ecosys* predicted 408 g m^{-2} aboveground shrub biomass for the same site and period [10].

The average shrub LAI was 3.82 in VBall_WT and 3.1 in VBall_NS vs. the average shrub LAI from field observation of 1.6 ± 1.6 (±two standard deviations) [53,54]. However, shrub LAI at the Mer Bleue bog is highly variable and reported as >3 at various locations [55]. Also, simulated shrub canopy height was 35 cm in hummocks and 32 cm in hollows in VBall_WT and 31 cm in hummocks and 29 cm in hollows in VBall_NS, values which are slightly above the observed mean shrub canopy height of ~20 cm at Mer Bleue [53].

The average simulated moss NPP was 51 g C m^{-2} y^{-1} in VBall_WT and 77 g C m^{-2} y^{-1} in VBall_NS, both lower than the field moss NPP of 170 g C m^{-2} y^{-1} at Mer Bleue bog; however, both are within the range of moss NPP reported in bogs, which is between 17 and 380 g C m^{-2} y^{-1} [39], and comparable to the *ecosys*-simulated moss NPP of 87 g C m^{-2} y^{-1} for Mer Bleue [10]. Due to the specifics of *Sphagnum* growth, with no clear division of live and dead plant material [23], no comparisons for moss LAI, biomass, and height were made due to uncertainty in the evaluation of those features in the field [39].

4. Discussion

4.1. Findings for the Importance of Peatland Hydrology in the Context of Previous Research

Statistics for modelled vs. observed GPP (Tables 3–5) and comparisons of simulated vs. observed ecosystem shrub and moss NPP and shrub LAI, biomass, and canopy heights

(Section 3.4) suggest that modelling driven by near-surface θ performs slightly better than modelling driven by WT. As mentioned above, the reason for this is that compared to WT, observed near-surface θ better represented the simulated soil water contents within the top ~20 cm where moss rhizoids and vascular roots grow; thereby, it was a better reflection of the hydrological effects on their productivities. This aligns with previous findings that near-surface θ plays more important role than WT itself as a hydrological control on bog GPP due to the direct and pronounced effect of near-surface θ on moss productivity, although shrub productivity remains little affected by hydrology within the natural range of WT variation [10].

4.2. Advantages and Limitations of the Proposed PB Modelling Approach

The advantages of the proposed *DIMONA* PB modelling approach are mainly its simplicity and the applicability of the plant water control equations for photosynthesis, plant growth and productivity, root/rhizoid respiration, and nutrient uptake, i.e., Equations (1)–(11), referred to hereafter as representative for their general versions (Section S4 in the Supplementary Materials). Together with the simple hydrology equations for peat introduced earlier within the *DIMONA* platform [26,27,56], Equations (1)–(11) make process-based modelling with *DIMONA* tractable to most researchers, regardless of their previous modelling experience. Equations (1)–(11) are simple yet process-oriented, circumventing the computationally complex, data-intensive, and parameter-expensive plant–water relation algorithms usually coupled to 1D or 3D soil hydrology in complex ecosystem models [22,57,58]. Thus, the *DIMONA* PB model produces reasonable modelling outcomes while circumventing explicit but complicated simulations of water fluxes based on explicit plant physiological considerations.

Modelling of plant photosynthesis, growth, root respiration, and nutrient uptake—and hence GPP and NPP—using the proposed plant water control equations would allow the *DIMONA* PB model to be coupled to other hydrological models capable of producing the required moisture-related terms in Equations (1)–(11), thus further enhancing the applicability of *DIMONA*'s PB modelling approach. In addition, the proposed plant water control equations could be coupled to continuous field observations of θ at various depths in the soil profiles, from which the terms in Equations (1)–(11) could be dynamically computed, resulting in a hybrid data-fusion-like approach for modelling plant and ecosystem productivities. This makes DIMONA applicable to many other ecosystems.

Further to the above, there are several inherent advantages of the *DIMONA* PB model as part of the *DIMONA* online platform. The *DIMONA* platform is able to ingest globally available meteorological forcing, near-surface θ, and soil properties extracted from satellite imagery and/or provided via Internet data repositories or API websites, in addition to detailed, but scarce, field near-surface θ observations [27]. As such, the *DIMONA* PB model is globally applicable at the site level, as well as at the regional level, where simultaneous simulations at many sites over any polygons of interest are possible. Another advantage of the *DIMONA* PB model is its reduced computational time, e.g., the 14 years of simulations in each model run of this study (Table 2) were completed in less than 2 min via the *DIMONA* web application's GUI. The inherent limitations of the proposed approach are the scarcity of WT observations and hydrological parameters, which for other sites may differ from those reported for Mer Bleue.

4.3. Advantages of Using Modelling Platforms

4.3.1. Accessibility, Parameterization, and Exploring Data

Scientific models can become accessible and not technology-demanding for researchers without special modelling expertise when they are embedded into a modelling platform

such as *DIMONA*. The *DIMONA* GUI allows not only for straightforward upload and download of files with model drivers, specific parameters, and output, simple entry of general model parameters in a browser, and fast execution of model runs online, but also for various activities that may facilitate modelling and research, as suggested earlier (Section 2.1.1). *DIMONA* provides options to explore specialized websites that could be used for model parameterization or validation at various geographical locations (sites) worldwide. Such websites are SoilGrids REST [59] with data for soil bulk density and porosity, texture, chemical and nutrient properties, organic C and N contents, and soil classification categories; Agro API [60] with soil hydrology and temperature at 10 cm depth; OpenWeatherMap [61] with climate characteristics and various meteorological drivers; and the GBIF [62] with biota components, currently reached by *DIMONA* via ngrok internet tunnels [63]. While the above information could be found via browsing the Internet, a specialized modelling platform may reduce the time and efforts needed for this by providing direct links to specialized sources, plus additional options to explore and/or download the data of interest, which may result in an organized and easy way of parameterizing models or collecting research data.

4.3.2. Potential for Real-Time Simulations and Productivity Estimates

Websites with API endpoints allow model users to request/receive meteorological forcing and hydrological drivers at short user-specified intervals, e.g., each minute or second during a preset time interval, via the *DIMONA* online platform. This allows researchers to run the *DIMONA* IoT model for simulating real-time photosynthetic rates and plant and ecosystem productivities at any geographical coordinates worldwide. The *DIMONA* IoT model applies the PB model equations. The incoming hourly short-wave radiation at the land surface is not usually a widely reported variable. However, it can be approximated from inputs of hour (1 to 24), day (1 to 366), altitude (m), and the range of daily air temperature at the sites of interest [64,65], or it can requested/received after purchasing via websites such as Agro API.

The DIMONA IoT model can be applied to a single site or simultaneously to multiple sites. Thus, the model output for simulated real-time photosynthetic rates and/or plant and ecosystem productivities at one or more sites is provided as .json files produced in designated users' folders and visualized online as GUI figures and LeafLet [66]-generated maps dynamically populating designated screens in individual *DIMONA* user accounts. *DIMONA* IoT model performance was partially demonstrated for simulating the course of real-time shrub photosynthesis in California, US, every minute over a 20 min period [27,57].

To demonstrate how the *DIMONA* platform and IoT model could work for the Mer Bleue bog, meteorological drivers from the nearby Templeton meteorological station were requested by *DIMONA* and received via OpenWeatherMap API every minute over a 20 min period beginning at 9:25 a.m. on 8 September 2024. The *DIMONA* PB model generated the real-time rate of vascular, moss, and ecosystem photosynthesis for two geographical locations in the bog. One was in the upper bog interior with intact WT and the second was topographically lower towards the bog periphery, with WT affected by the nearby drainage ditch. Thus, the first location was at ~200 m and the second location was ~30 m away from the adjacent drainage ditch, following as close as possible the distances and directions along a previous study's field transect [53,55].

Although the meteorological inputs were the same for both locations, the daily near-surface θ, used as a hydrological driver, was set at 0.12 m^3 m^{-3} at the interior location and at 0.08 m^3 m^{-3} at the marginal location (Figure 23). These values were estimated from the average field WT depths at those locations during the 2005 and 2006 vegetation seasons [26,53,55]. The soil profiles at both locations were such that $\overline{\theta} \geq \overline{\theta}_{FC}$, i.e., $f_{\theta W} \geq 1$ in

Equation (8) and hence $f_{\theta P} \rightarrow 1$ in Equation (1b) via f_P in Equation (1a), thereby reflecting no hydrological limitations along the transect over the short IoT modelling period. This resulted in no difference in the average real-time IoT-simulated photosynthesis at the two locations (Figure 24). We show the course of the real-time IoT-simulated ecosystem photosynthesis rate (Figure 25a), together with the courses of photosynthesis rates of vascular plants (Figure 25b) and mosses (Figure 25c) at the upper location. They largely reflected the courses of the meteorological drivers (Figure 26). With unchanging I_{swr} over the 20 min period (Figure 26a), vascular plant photosynthesis (Figure 25b) increased with the increase in T_{air} (Figure 26b) at the end of the period, while moss GPP closely followed the course of RH (Figure 26c) together with that of T_{air}, which is especially visible near the end of the period (Figure 25c). As *DIMONA* IoT modelling is not the focus of this study, the above is not a constrained experiment, and no further details are considered here. Rather, the purpose of this demonstration of *DIMONA's* IoT modelling was to highlight the potential uses of the *DIMONA* modelling platform.

4.3.3. Potential for Machine Learning Modelling

As noted earlier, *DIMONA* has a machine learning model capability for studies where a process-based explanatory component is not in the prime objective, and especially where a reliable predictive power is needed based on meaningful physical, biological, or ecological predictors. Also, ML simulations may apply as an independent method to confirm the process-based modelling outcomes and the significance of the model drivers. Model users have two options for executing ML simulations via the *DIMONA* platform. One option is via the *DIMONA* ML model, coded in C++ as part of the *DIMONA* platform, for simple and multiple ML linear regressions by applying the method of gradient descend. The other option is via the TensorFlow framework installed as an open-source library, together with Python 3.9, on the Apache server hosting the *DIMONA* platform. Both options are facilitated through the *DIMONA* GUI, which makes them accessible to researchers with limited ML experience (Figure 4).

To demonstrate the potential of the *DIMONA* platform for ML research, the *DIMONA* ML model was trained for hourly GPP modelling on the hourly records of I_{swr}, T_{air}, RH, v_w, and d_{WT} during 1999–2001 and then tested against 2002–2004 data. The statistics of linear regressions of simulated on observed ecosystem GPP, RMSE, and Willmott's d values are summarized for the 2002–2004 period and for each individual year for the *DIMONA* ML model (Table 6). To illustrate the performance of the ML model, model outcomes for three 2-week periods, i.e., DOY 214–227 (2 to 15 August) in 2002 and 2003 and DOY 235–248 (23 August to 5 September) in 2004, were compared vs. available observations (Figure 27a–c). The outcomes for 2002 showed comparable R^2, RMSE, and d values (Table 6) to both PB models (Tables 3 and 4) and a reasonable fit to observations (Figure 27a), with the 2002 data as a testing set alone constituting ~25% of the data for the 1999–2002 period. However, the statistics and outcomes for 2003, and especially 2004 (Table 6, Figure 27b,c), showed a deteriorating pattern, as the testing set of 2003, and especially 2004, become more distant from the training set. This pattern was also visible with decreasing slopes, R^2 and d values, and large intercepts and RMSE (Table 6), when compared to both PB models in 2003 and 2004 (Tables 3 and 4), Thus, both PB models outperformed the ML model over the entire period of comparison, i.e., 2000–2004 (Tables 3 and 4) and 2002–2004 (Table 6). However, this behavior of the ML model might suggest that using larger data sequences consisting of more years, especially for training purposes, and enhancing the ML experiment with cross-validation for time series could improve the model's performance [67,68]. As ML modelling is not in the focus of this study, no further details are considered here. Instead, this demonstration is made simply to highlight the potential uses of the *DIMONA* modelling

platform, as well as to demonstrate ML modelling as an alternative and/or complementary predictive method to PB modelling. While ML frameworks like TensorFlow [69] are now largely available on the Internet, running simulations on *DIMONA* may not only facilitate the process for less experienced users but may also make ML simulations directly comparable to and benefitting from concurrent PB simulations conducted simultaneously on the same platform.

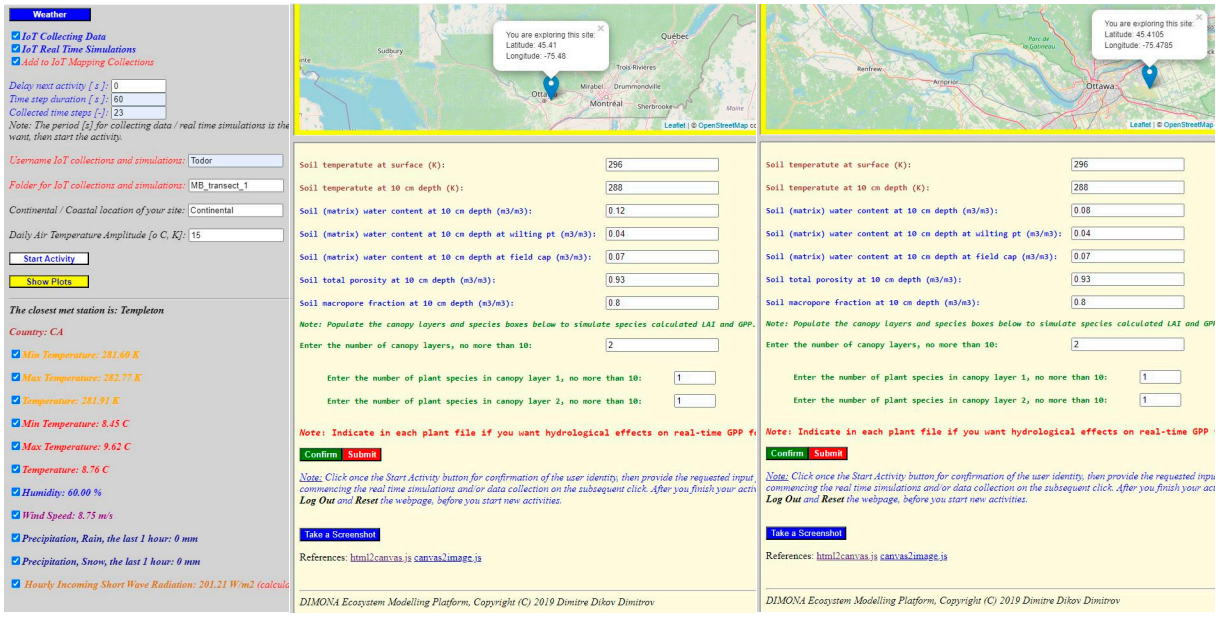

Figure 23. The meteorological inputs for both locations (to the **left**), soil hydrology parameterization with daily near-surface θ at the upper transect location (in the **middle**), and soil hydrology parameterization with daily near-surface θ at the lower transect location (to the **right**).

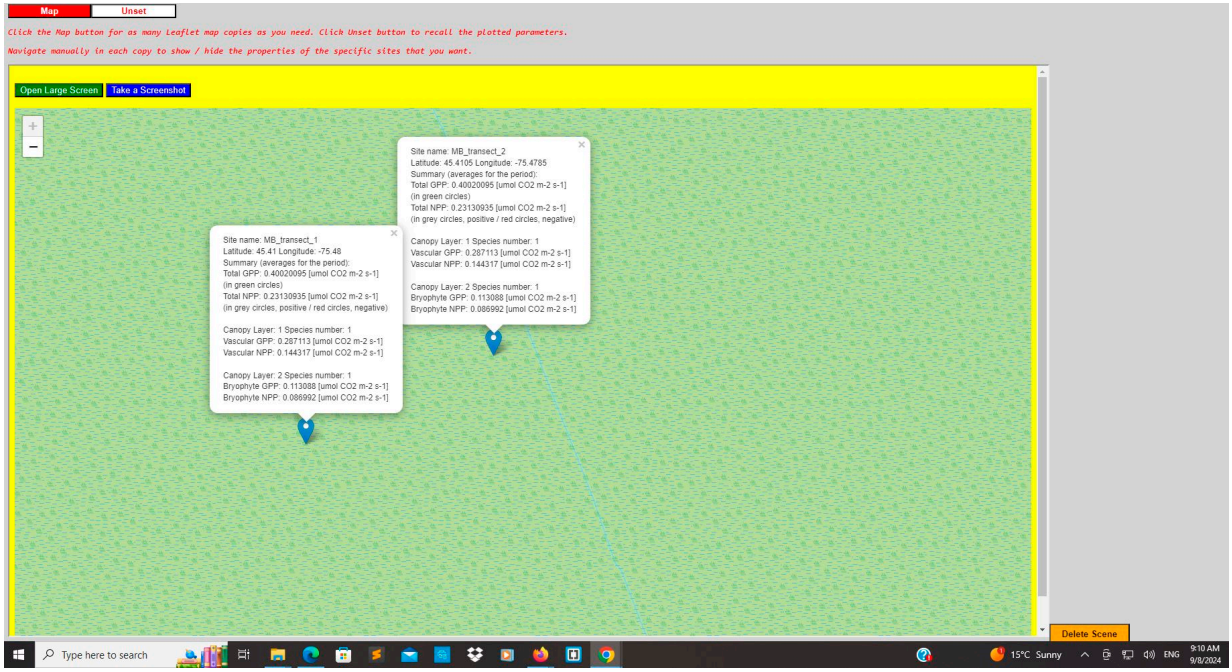

Figure 24. The average real-time IoT-simulated vascular, bryophyte, and ecosystem photosynthesis rates in umol CO_2 m^{-2} s^{-1} at the **upper** (**left**) and **lower** (**right**) transect locations. Values obtained every minute during a 20 min period of real-time simulations are averaged over that period in the morning of 8 September 2024 at Mer Bleue bog via the *DIMONA* platform.

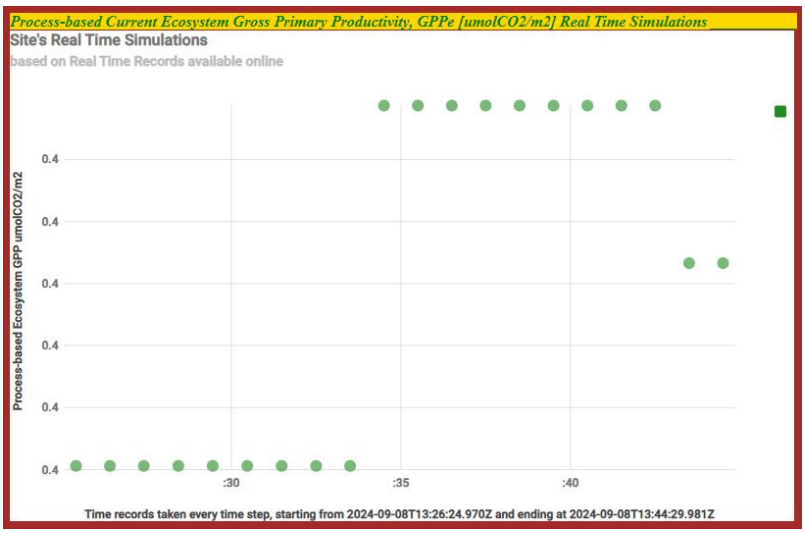

(**a**)

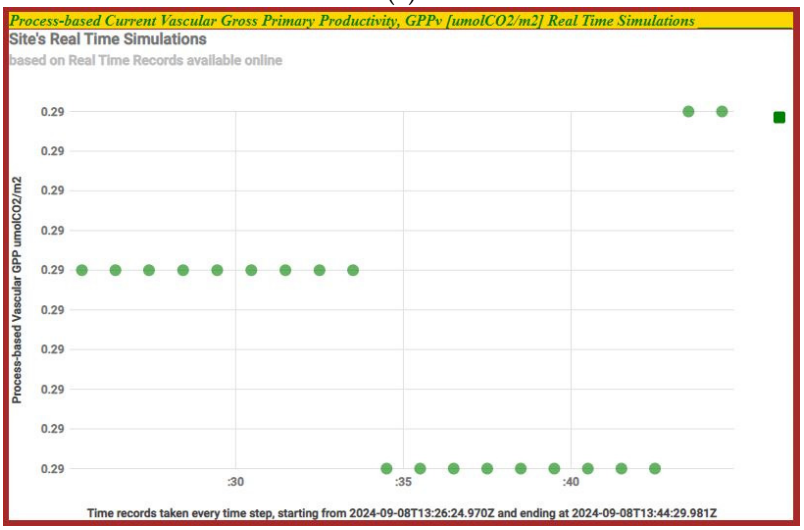

(**b**)

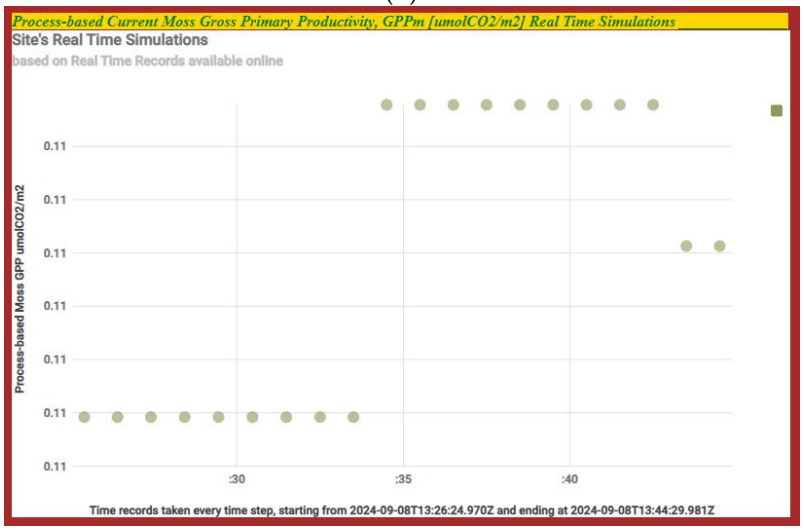

(**c**)

Figure 25. Screenshots of *DIMONA* online figures with real-time ecosystem (**a**), vascular (**b**), and moss (**c**) photosynthesis rates in umol CO_2 m^{-2} s^{-1} simulated every minute (the circles) over a 20 min interval in the morning of 8 September 2024 at Mer Bleue bog by the *DIMONA* IoT model. The square in the upper right corner is an artifact of the graphing software and should be ignored.

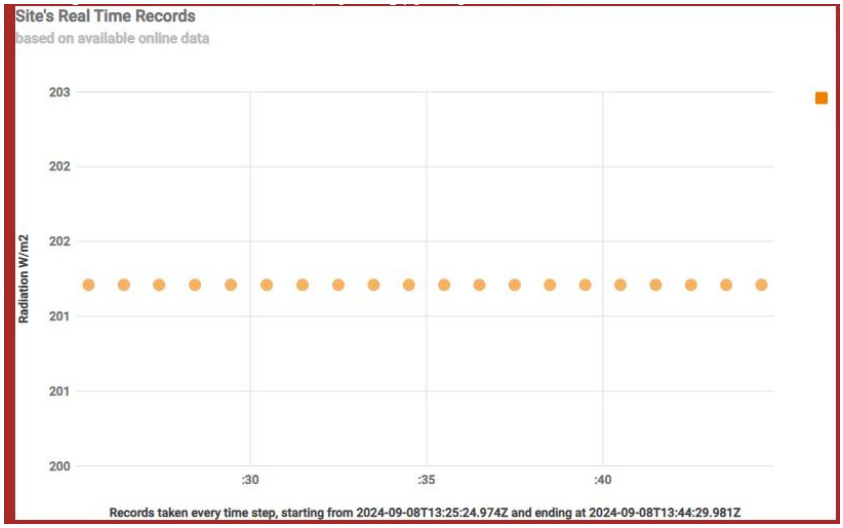

(**a**)

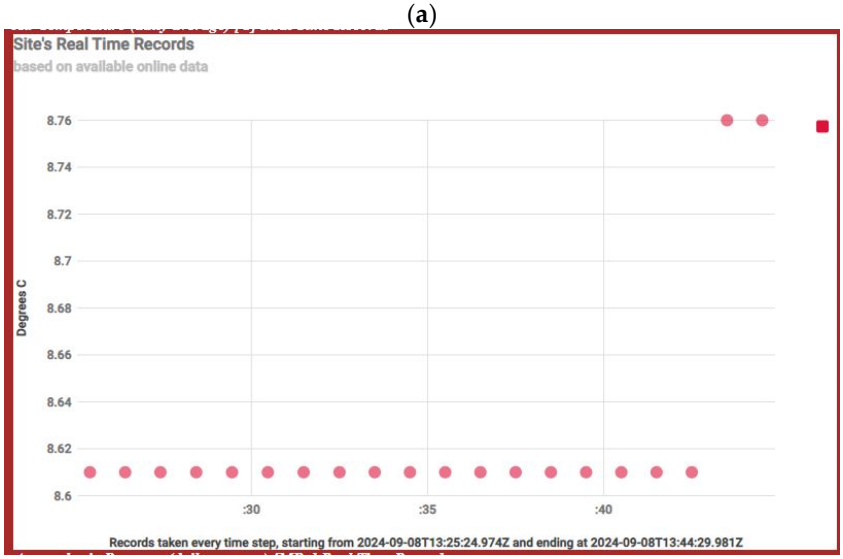

(**b**)

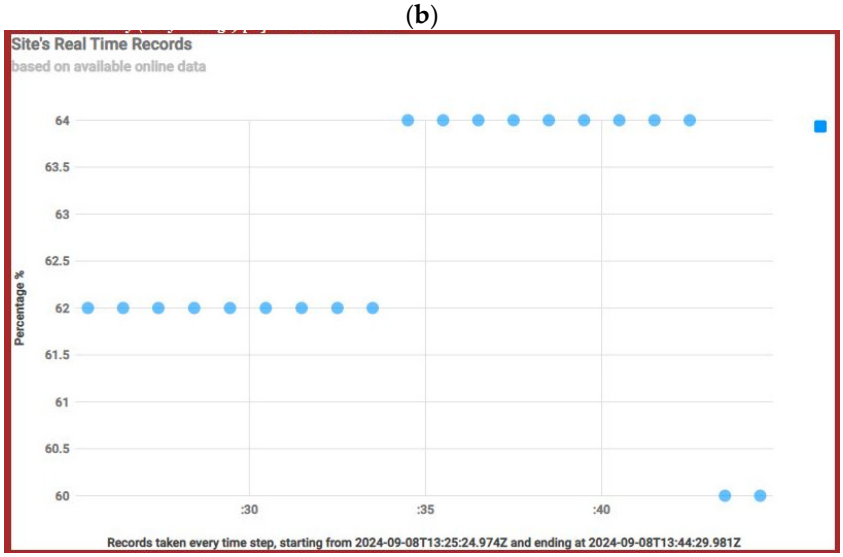

(**c**)

Figure 26. Screenshots of *DIMONA* online figures for incoming short-wave radiation (**a**), air temperature (**b**), and relative humidity (**c**) requested online by the *DIMONA* platform and received via OpenWeatherMap API every minute (the circles) over a 20 min interval in the morning of 8 September 2024 at Mer Bleue bog. The square in the upper right corner is an artifact of the graphing software and should be ignored.

Table 6. Statistics for estimating the performance of the *DIMONA* ML model run on machine learning regression for incoming short-wave radiation (I_{swr}), ambient air temperature (T_{air}), atmospheric relative humidity (RH),wind speed (v_w), and water table depth (d_{WT}), including slope a (unitless), intercept b (umol CO_2 m^{-2} s^{-1}), and coefficient of determination R^2 (unitless) of the linear regressions of simulated on eddy covariance (EC)-derived ecosystem GPP, root mean square error, RMSE (umol CO_2 m^{-2} s^{-1}), and Willmott's index of agreement, d (unitless).

Model Run Name	Period	Time Step	a	b	R^2	RMSE	d
MLRN	2002–2004	hourly	0.58	2.05	0.60	2.30	0.86
MLRN	2002	hourly	0.73	1.90	0.70	1.82	0.88
MLRN	2003	hourly	0.69	1.94	0.63	1.90	0.86
MLRN	2004	hourly	0.48	1.84	0.63	2.51	0.80

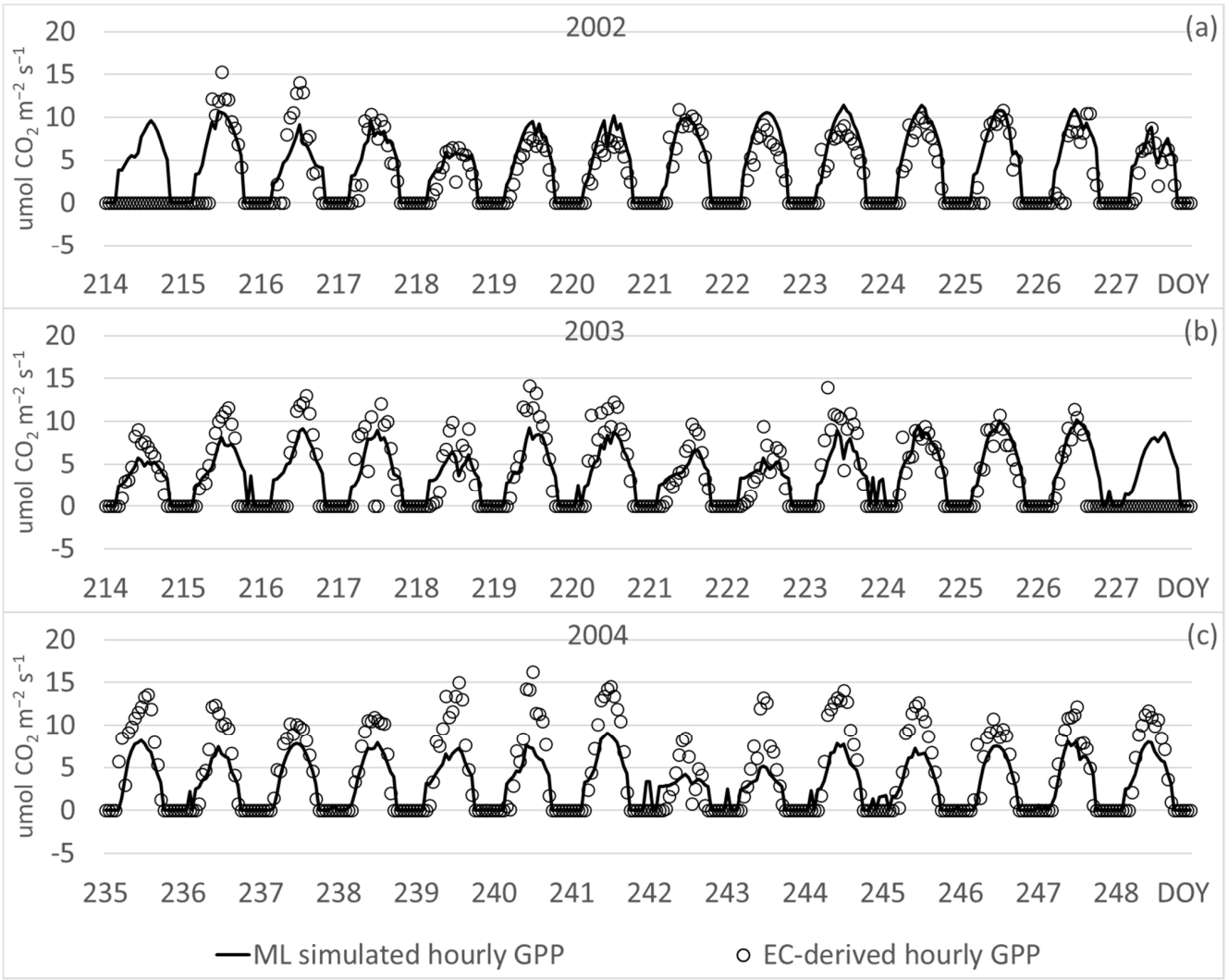

Figure 27. Hourly ecosystem gross primary productivity (GPP) at Mer Bleue bog during 2-week periods of 2 to 15 August in 2002 (**a**) and 2003 (**b**) and during 23 August to 5 September in 2004 (**c**). Simulated GPP by *DIMONA* ML model, based on machine learning multiple linear regression, is compared vs. observed GPP derived from eddy covariance (EC) CO_2 exchange. DOY means day of year.

5. Conclusions

This study introduces the *DIMONA* PB model, which is a process-based model embedded into the namesake *DIMONA* online modelling platform that facilitates model accessibility and application. The *DIMONA* PB model, driven by meteorological and hydrological data and constrained by site, soil, and plant parameters, is shown to perform reasonably well for simulating the vascular, bryophyte, and ecosystem productivities in a northern peatland at hourly and daily time steps. The model relies on a set of simple yet process-oriented modifiers (equations) for water control on photosynthesis, plant growth processes, root/rhizoid respiration, and nutrient uptake. These modifiers show a potential for being generally applicable to wet and dry natural peatlands, peatlands used for agricultural purposes, drained peatlands, and peatland transition zones. Moreover, as they are directly related to soil water contents, these modifiers could be applicable not only to peatlands but also to mineral soil natural ecosystems and agricultural crops. Their simplicity circumvents the complicated and demanding multi-parameter equations for plant–water relations in many process-based models. Further, this study demonstrates that both WT (Hypothesis 1) and near-surface soil θ (Hypothesis 2) are reliable hydrological model drivers for peatland GPP, but near-surface soil θ performed slightly better than WT as a driver for hydrological control on productivity. The model results also demonstrated that the equations and algorithms of the *DIMONA* PB model were able to capture the specifics of the peatland productivity response under varying hydrologic conditions (Hypothesis 3).

With the recently introduced simplified methods and widely available near-surface soil θ data extracted via satellite imagery and/or available on repository websites, the *DIMONA* PB model embedded in the *DIMONA* modelling platform is applicable on a global basis for any peatland at the site level or peatland polygons at the spatial level. Further, the *DIMONA* platform accommodates model accessibility, data exploration, and model parameterization on a global basis. *DIMONA* can obtain real-time estimates of productivity and hydrology by IoT modelling, where real-time meteorological and hydrological data are derived from websites with API endpoints. *DIMONA* also allows for ML modelling of ecosystem productivities and other features, especially where predictability is the focus, rather than explanatory power of the models. Thus, the multifaceted study presented here proposes not only a process-based model and a new modelling approach for plant water control on productivities, as well as an online software tool for their facilitation and wide application, but also a broader concept for ecological modelling that involves Internet of Things and machine learning modelling, complementary to and benefiting from process-based modelling.

Supplementary Materials: The following supporting information can be downloaded at https://www.mdpi.com/article/10.3390/w17020134/s1. References [70–120] are cited in the supplementary materials.

Author Contributions: Conceptualization, D.D.D.; Methodology, D.D.D.; Software, D.D.D.; Validation, D.D.D.; Formal Analysis, D.D.D.; Investigation, D.D.D.; Resources, D.D.D. and P.M.L.; Data Curation, P.M.L.; Writing—Original Draft Preparation, D.D.D.; Writing—Review and Editing, P.M.L.; Visualization, D.D.D.; Project Administration, D.D.D.; Funding Acquisition, P.M.L. All authors have read and agreed to the published version of the manuscript.

Funding: Data were collected with funding from the Canadian Carbon Program and the Fluxnet Canada Research Network (FCRN) through its major sponsors, the Natural Sciences and Engineering Council of Canada (NSERC), the Canadian Foundation for Climate and Atmospheric Sciences, and BIOCAP Canada.

Data Availability Statement: The data presented in this study are available on request from the corresponding author.

Acknowledgments: The authors wish to thank the anonymous reviewers and editors for their useful comments and suggestions, which resulted in improvements in this manuscript.

Conflicts of Interest: The authors declare no conflicts of interest.

Abbreviations

A	Ambient photosynthetic rate of vascular plants
A_b	Ambient photosynthetic rate of bryophytes
$A_{max,b}$	Maximum photosynthetic rate of bryophytes
A_C	Rubisco-limited CO_2 fixation rates of vascular plants
A_J	Electron transport-limited CO_2 fixation rates of vascular plants
a	Slope (linear regression)
API	Application programming interface
b	Intercept (linear regression)
C	Carbon
CO_2	Carbon dioxide
C_i	CO_2 concentration in intercellular spaces at carboxylation sites of Rubisco activity of vascular plants
c_x	Ratio between CO_2 concentration in intercellular spaces at carboxylation sites of Rubisco activity and atmospheric CO_2 concentration
CPU	Central Processing Unit
C3	3—carbon atom carbon fixation pathway (85% of plants on Earth)
DOY	Day of year
D_{VP}	Atmospheric vapor pressure deficit
d	Willmott's index of agreement
d_{SL}	Depth of the entire soil profile
d_{WT}	Water table depth
DIMONA	**D**ynamic **I**ntegrated **M**odel for **O**rganism—e**N**vironment **A**nalysis
EC	Eddy covariance technique
ER	Ecosystem Respiration
f_P	Effect of soil water availability on the photosynthesis of vascular plants
f_R	Effect of soil air availability and/or air availability with adaptations to wetlands on root/rhizoid respiration
$f_{U,i}$	Effect of air availability to roots/rhizoids due to soil water and/or adaptations to wetlands in soil layer i on N and P nutrient uptake
f_θ	Effect of soil water and air availability on plant growth
$f_{\theta A}$	Effect of air availability on plant growth, root respiration, and nutrient uptake derived from adaptations to wetland soil conditions
$f_{\theta P}$	Ambient effect of soil water availability on photosynthesis
$f_{\theta R}$	Soil air availability to roots/rhizoids
$f_{\theta R,i}$	Air availability to roots/rhizoids in soil layer i
$f_{\theta W}$	Soil water availability to plants
GIS	Geographic information system
GPP	Gross primary productivity
GUI	Graphical user interface
g_b	Leaf boundary layer conductance
g_s	Stomatal conductance of vascular plants
I_{swr}	Incoming solar short-wave radiation at 2 m above the canopy
i	Index
IoT	Internet of Things
J_m	Ambient electron transport rate of vascular plants
ML	Machine learning

N	Nitrogen
NEE	Net ecosystem exchange
NH_4^+	Ammonium
NO_3^-	Nitrate
NPP	Net ecosystem productivity
P	Phosphorus
PC	Personal computer
PB	Process-based (modelling)
PO_4^{3-}	Phosphate
R_a	Autotrophic respiration
R_b	Hydrology-constrained stem respiration (with branches)
R_d	Foliar respiration
R_l	Hydrology-constrained leaf respiration
R_r	Hydrology-constrained root/rhizoid respiration
RH	Atmospheric relative humidity at 2 m above the canopy
RAM	Random-access memory
R^2	Coefficient of determination (linear regression)
RMSE	Root mean square error
SWRC	Soil water retention curve
T_a	Air temperature at 2 m above the canopy
T_L	Leaf temperature
URL	Uniform resource locator
VPD	Atmospheric vapor pressure deficit (conceptual)
V_m	Ambient rate of carboxylation of vascular plants
v_w	Wind speed at 2 m above the canopy
WT	Water table (conceptual)
1D	One-dimensional
3D	Three-dimensional
θ	Soil water content
θ_i	Ambient water content of soil layer i of the unsaturated part of the soil profile
$\theta_{FC,i}$	Ambient soil water content at field capacity of soil layer i of the unsaturated part of the soil profile
$\theta_{TP,i}$	Ambient soil total porosity (if any) of soil layer i of the unsaturated part of the soil profile
$\overline{\theta}$	Average ambient soil water content of the unsaturated part of the soil profile
$\overline{\theta}_{FC}$	Average soil water content at field capacity of the unsaturated part of the soil profile
$\overline{\theta}_{MP}$	Average soil macroporosity (if any) of the unsaturated part of the soil profile
$\theta_{MP,i}$	Ambient soil macroporosity (if any) of soil layer i of the unsaturated part of the soil profile
$\overline{\theta}_{TP}$	Average soil total porosity of the unsaturated part of the soil profile
$\overline{\theta}_{WP}$	Average soil water content at wilting point of the unsaturated part of the soil profile

References

1. Yvon-Durocher, G.; Jones, J.I.; Trimmer, M.; Woodward, G.; Montoya, J.M. Warming alters the metabolic balance of ecosystem. *Philos. Trans. R. Soc. B* **2010**, *365*, 2117–2126. [CrossRef] [PubMed]
2. Goldstein, A.; Turner, W.R.; Spawn, S.A.; Anderson-Teixeira, K.J.; Cook-Patton, S.; Fargione, J.; Gibbs, H.K.; Griscom, B.; Hewson, J.H.; Howard, J.F.; et al. Protecting irrecoverable carbon in Earth's ecosystems. *Nat. Clim. Chang.* **2020**, *10*, 287–295. [CrossRef]
3. Gangopadhyay, P.K.; Shirsath, P.B.; Dadhwal, V.K.; Aggrawal, P.K. A new two-decade (2001–2019) high-resolution agricultural primary productivity dataset for India. *Sci. Data* **2022**, *9*, 730. [CrossRef] [PubMed]
4. Duan, H.; Zhou, S.; Jiang, K.; Bertram, C.; Harmsen, M.; Kriegler, E.; Van Vuuren, D.P.; Wang, S.; Fujimori, S.; Tavoni, M.; et al. Assessing China's efforts to pursue the 1.5 °C warming limit. *Science* **2021**, *372*, 378–385. [CrossRef]

5. Zhang, Q.; Cheng, Y.-B.; Lyapustin, A.I.; Wang, Y.; Zhang, X.; Suyker, A.; Verma, S.; Shuai, Y.; Middleton, E.M. Estimation of crop gross primary production (GPP): II. Do scaled MODIS vegetation indices improve performance? *Agric. For. Meteorol.* **2015**, *200*, 1–8. [CrossRef]
6. Liu, Q.; Sun, X.; Wu, W.; Liu, Z.; Fang, G.; Yang, P. Agroecosystem services: A review of concepts, indicators, assessment methods and future research perspectives. *Ecol. Indic.* **2022**, *142*, 109218. [CrossRef]
7. Yu, Z.C.; Campbell, C.; Vitt, D.H.; Bond, G.C.; Apps, M.J. Carbon sequestration in western Canadian peat highly sensitive to Holocene wet-dry climate cycles at millennial timescales. *Holocene* **2003**, *13*, 801–808. [CrossRef]
8. Loisel, J.; Yu, Z.C.; Beilman, D.W.; Camill, P.; Alm, J.; Amesbury, M.J.; Anderson, D.; Andersson, S.; Bochicchio, C.; Barber, K.; et al. A database and synthesis of northern peatland soil properties and Holocene carbon and nitrogen accumulation. *Holocene* **2014**, *24*, 1028–1042. [CrossRef]
9. Weltzin, J.F.; Pastor, J.; Harth, C.; Bridgham, S.D.; Updegraff, K.; Chapin, C.T. Response of bog and fen plant communities to warming and water table manipulations. *Ecology* **2000**, *81*, 3464–3478. [CrossRef]
10. Dimitrov, D.D.; Grant, R.F.; Lafleur, P.M.; Humphreys, E.R. Modelling the effects of hydrology on gross primary productivity and net ecosystem productivity at Mer Bleue bog. *J. Geophys. Res.—Biogeosciences* **2011**, *116*, G04010. [CrossRef]
11. Fenner, N.; Freeman, C. Drought-induced carbon loss in peatlands. *Nat. Geosci.* **2011**, *4*, 895–900. [CrossRef]
12. Wei, Y.; Liu, S.; Huntzinger, D.N.; Michalak, A.M.; Viovy, N.; Post, W.M.; Schwalm, C.R.; Schaefer, K.; Jacobson, A.R.; Lu, C.; et al. The North American carbon program multi-scale synthesis and terrestrial model intercomparison project—Part 2: Environmental driver data. *Geosci. Model Dev.* **2014**, *7*, 2875–2893. [CrossRef]
13. Sitch, S.; Friedlingstein, P.; Gruber, N.; Jones, S.D.; Murray-Tortarolo, G.; Ahlstrom, A.; Doney, S.C.; Graven, H.; Heinze, C.; Huntingford, C.; et al. Recent trends and drivers of regional sources and sinks of carbon dioxide. *Biogeosciences* **2015**, *12*, 653–679. [CrossRef]
14. Wang, Y.; Braghierre, R.K.; Longo, M.; Norton, A.J.; Kohler, P.; Doughty, R.; Yin, Y.; Bloom, A.A.; Frankenberg, C. Modeling Global Vegetation Gross Primary Productivity, Transpiration and Hyperspectral Canopy Radiative Transfer Simultaneously Using a Next Generation Land Surface Model—CliMA Land. *J. Adv. Model. Earth Syst.* **2023**, *15*, e2021MS002964. [CrossRef]
15. Schaefer, K.; Arain, A.; Chen, J.; Davis, K.; Dimitrov, D.; Golaz, N.; Hollinger, D.; Humphreys, E.; Lafleur, P.; Migliavacca, M.; et al. A model-data comparison of Gross Primary Productivity: Results from the North American Carbon Program Site Synthesis. *J. Geophys. Res.—Biogeosciences* **2012**, *117*, G03010. [CrossRef]
16. Dimitrov, D.D.; Grant, R.F.; Lafleur, P.M.; Humphreys, E.R. Modelling the effects of hydrology on ecosystem respiration at Mer Bleue bog. *J. Geophys. Res.—Biogeosciences* **2010**, *115*, G04043. [CrossRef]
17. Grant, R.F.; Baldocchi, D.D.; Ma, S. Ecological controls on net ecosystem productivity of a seasonally dry annual grassland under current and future climates: Modelling with ecosys. *Agric. For. Meteorol.* **2012**, *152*, 189–200. [CrossRef]
18. Grant, R.F.; Neftel, A.; Calanca, P. Ecological controls on N_2O emission in surface litter and near-surface soil of a managed grassland: Modelling and measurements. *Biogeosciences* **2016**, *13*, 3549–3571. [CrossRef]
19. Mezbahuddin, M.; Grant, R.F.; Flanagan, L.B. Modelling hydrological controls on variations in peat water content, water table depth, and surface energy exchange of a boreal Western Canadian fen peatland. *J. Geophys. Res.—Biogeosciences* **2016**, *121*, 2216–2242. [CrossRef]
20. Frolking, S.; Roulet, N.T.; Moore, T.R.; Lafleur, P.M.; Bubier, J.L.; Crill, P.M. Modelling the seasonal to annual carbon balance of Mer Bleue bog, Ontario, Canada. *Glob. Biogeochem. Cycles* **2002**, *16*, 1030. [CrossRef]
21. St-Hilaire, F.; Wu, J.; Roulet, N.T.; Frolking, S.; Lafleur, P.M.; Humphreys, E.R.; Arora, V. McGill wetland model: Evaluation of a peatland carbon simulator developed for global assessments. *Biogeosciences* **2010**, *7*, 3517–3530. [CrossRef]
22. Grant, R.F. A review of the Canadian ecosystem model ECOSYS. In *Modeling Carbon and Nitrogen Dynamics for Soil Management*; Shaffer, M., Ed.; CRC Press: Boca Raton, FL, USA, 2001; pp. 173–264. [CrossRef]
23. Clymo, R.S. Peat. In *Mires: Swamp, Bog, Fen and Moor General Studies*; Ecosystems of the, World; Gore, A.J.P., Ed.; Elsevier: Amsterdam, The Netherlands, 1983; Volume 4A, pp. 159–224.
24. Lafleur, P.M.; Roulet, N.T.; Bubier, J.L.; Frolking, S.; Moore, T.R. Interannual variability in the peatland-atmosphere carbon dioxide exchange at an ombrotrophic bog. *Glob. Biogeochem. Cycles* **2003**, *17*, 1036. [CrossRef]
25. Sulman, B.N.; Desai, A.R.; Cook, B.D.; Saliendra, N.; Mackay, D.S. Contrasting carbon dioxide fluxes between a drying shrub wetland in Northern Wisconsin, USA, and nearby forests. *Biogeosciences* **2009**, *6*, 1115–1126. [CrossRef]
26. Dimitrov, D.D.; Lafleur, P.M. Revisiting water retention curves for simple hydrological modelling of peat. *Hydrol. Sci. J.* **2020**, *66*, 252–267. [CrossRef]
27. Dimitrov, D.D.; Lafleur, P.; Sonnentag, O.; Talbot, J.; Quinton, W.L. Hydrology of peat estimated from near-surface water contents. *Hydrol. Sci. J.* **2022**, *67*, 1702–1721. [CrossRef]
28. Morin, T.H.; Riley, W.J.; Grant, R.F.; Mekonen, Z.; Stefanik, K.C.; Sanchez, A.C.R.; Mulhare, M.A.; Villa, J.; Wrighton, K.; Bohrer, G. Water level changes in Lake Erie drive 21st century CO2 and CH4 fluxes from a coastal temperate wetland. *Sci. Total Environ.* **2022**, *821*, 153087. [CrossRef]

29. Mortelmans, J.; Felsberg, A.; De Lannoy, G.J.M.; Veraverbeke, S.; Field, R.D.; Andela, N.; Bechtold, M. Improving the fire weather index system for peatlands using peat-specific hydrological input data. *Nat. Hazards Earth Syst. Sci.* **2024**, *24*, 445–464. [CrossRef]
30. Farquhar, G.D.; von Caemmerer, S.; Berry, J.A. A biochemical model of photosynthetic CO_2 assimilation in leaves of C3 species. *Planta* **1980**, *149*, 78–90. [CrossRef]
31. Farquhar, G.D.; von Caemmerer, S. Modelling of photosynthetic response to environmental conditions. In *Physiological Plant Ecology II. Water Relations and Carbon Assimilation*; Encyclopedia of Plant Physiology; Lange, O.L., Nobel, P.S., Osmond, C.B., Ziegler, H., Eds.; Springer: Berlin/Heidelberg, Germany; New York, NY, USA, 1982; Volume 12B, pp. 549–588.
32. Campbell, G.S.; Norman, J.M. *An Introduction to Environmental Biophysics*; Springer Science & Business Media: Berlin/Heidelberg, Germany, 1998. [CrossRef]
33. Lee, A.; Upshurch, G., Jr.; Murchie, E.H.; Lomax, B.H. Leaf energy balance modelling as a tool to infer habitat preference in the early angiosperms, Proceedings B. *R. Soc. Publ.* **2015**, *282*, 20143052. [CrossRef]
34. Baldocchi, D. An analytical solution for coupled leaf photosynthesis and stomatal conductance models. *Tree Physiol.* **1994**, *14*, 1069–1079. [CrossRef]
35. Ball, J.T. An analysis of stomatal conductance. Ph.D. Thesis, Stanford University, Stanford, CA, USA, 1988.
36. Ball, J.T.; Woodrow, I.E.; Berry, J.A. A Model Predicting Stomatal Conductance and its Contribution to the Control of Photosynthesis under Different Environmental Conditions. In *Progress in Photosynthesis Research*; Biggins, J., Ed.; Springer: Dordrecht, The Netherlands, 1987. [CrossRef]
37. Leuning, R. A critical appraisal of a combined stomatal photosynthesis model for C3 plants. *Plant Cell Environ.* **1995**, *18*, 339–355. [CrossRef]
38. Cui, X.; Gu, S.; Wu, J.; Tang, Y. Photosynthetic response to dynamic changes of light and air humidity in two moss species from the Tibetan Plateau. *Ecol. Res.* **2009**, *24*, 645–653. [CrossRef]
39. Moore, T.R.; Bubier, J.L.; Frolking, S.E.; Lafleur, P.M.; Roulet, N.T. Plant biomass and production and CO2 exchange in an ombrotrophic bog. *J. Ecol.* **2002**, *90*, 25–36. [CrossRef]
40. Lafleur, P.M.; Moore, T.R.; Roulet, N.T.; Frolking, S. Ecosystem respiration in a cool temperate bog depends on peat temperature but not on water table. *Ecosystems* **2005**, *8*, 619–629. [CrossRef]
41. Lafleur, P.M.; Hember, R.A.; Admiral, S.W.; Roulet, N.T. Annual and seasonal variability in evapotranspiration and water table at a shrub-covered bog in southern Ontario, Canada. *Hydrol. Process.* **2005**, *19*, 3533–3550. [CrossRef]
42. Lafleur, P.M.; Roulet, N.T.; Admiral, S.W. Annual cycle of CO_2 exchange at a bog peatland. *J. Geophys. Res.* **2001**, *106*, 3071–3081. [CrossRef]
43. Roulet, N.T.; Lafleur, P.M.; Richard, P.J.H.; Moore, T.R.; Humphreys, E.R.; Bubier, J. Contemporary carbon balance and late Holocene carbon accumulation in a northern peatland. *Glob. Chang. Biol.* **2007**, *13*, 397–411. [CrossRef]
44. Dimitrov, D.D. Modelling of hydrological and thermal controls on CO2 exchange at Mer Bleue bog. Ph.D. Thesis, Department of Renewable Resources, University of Alberta, Edmonton, AB, Canada, 2009.
45. Willmott, C.J. Some comments on the evaluation of model performance. *Bull. Am. Meteorol. Soc.* **1982**, *63*, 1309–1313. [CrossRef]
46. RStudio Cloud. Available online: https://posit.cloud (accessed on 5 July 2024).
47. Small, E. Water relations of plants in raised Sphagnum peat bogs. *Ecology* **1972**, *53*, 726–728. [CrossRef]
48. Titus, J.E.; Wagner, D.J. Carbon balance for two Sphagnum mosses: Water balance resolves a physiological paradox. *Ecology* **1984**, *65*, 1765–1774. [CrossRef]
49. Danise, M. The tradeoff between polyuronic acid content and photosynthesis rates in Sphagnum. Bachelor's Thesis, Department of Biological Sciences, Union College, Schenectady, NY, USA, 2011.
50. Dong, J.; Xiao, X.; Wagle, P.; Zhang, G.; Zhou, Y.; Jin, C.; Torn, M.S.; Meyers, T.P.; Suyker, A.E.; Wang, J.; et al. Comparison of four EVI-based models for estimating gross primary production of maize and soybean croplands and tallgrass prairie under severe drought. *Remote Sens. Environ.* **2015**, *162*, 154–168. [CrossRef]
51. Zhang, L.; Zhou, D.; Fan, J.; Guo, Q.; Chen, S.; Wang, R.; Li, Y. Contrasting the Performance of Eight Satellite-Based GPP Models in Water-Limited and Temperature Limited Grassland Ecosystems. *Remote Sens.* **2019**, *11*, 1333. [CrossRef]
52. Sarkar, D.P.; Shankar, B.U.; Pariba, B.R. Machine learning approach to predict terrestrial gross primary productivity using topographical and remote sensing data. *Ecol. Inform.* **2022**, *70*, 101697. [CrossRef]
53. Talbot, J.; Roulet, N.T.; Sonnentag, O.; Moore, T.R. Increases in aboveground biomass and leaf area 85 years after drainage in a bog. *Botany* **2014**, *92*, 713–721. [CrossRef]
54. Talbot, J.; Richard, P.J.H.; Roulet, N.T.; Booth, R.K. Assessing long-term hydrological and ecological responses to drainage in a raised bog using paleoecology and a hydrosequence. *J. Veg. Sci.* **2010**, *21*, 143–156. [CrossRef]
55. Sonnentag, O.; Chen, J.M.; Roberts, D.A.; Talbot, J.; Halligan, K.Q.; Govind, A. Mapping tree and shrub leaf area indices in an ombrotrophic peatland through multiple endmember spectral unmixing. *Remote Sens. Environ.* **2007**, *109*, 342–360. [CrossRef]
56. Dimitrov, D.D.; Lafleur, P.M. From Ecological Models to Modelling Platforms: Bridging Science, Scientific Programming, and Web Application Development. (Poster) 7th Open Science Meeting, North American Caron Program (NACP) 2021, Session Linkages

among the Air-Land-Water Continuum. Available online: https://cce-datasharing.gsfc.nasa.gov/files/conference_presentations/Poster_Dimitrov__266_21.pdf (accessed on 1 August 2024).
57. Jansson, P.-E.; Karlberg, L. Coupled heat and mass transfer model for soil-plant-atmosphere systems. Royal Institute of Technology, Department of Civil and Environmental Engineering. 2004. Available online: https://www.researchgate.net/publication/304714926 (accessed on 1 August 2024).
58. Thornton, P.E.; Law, B.E.; Gholz, H.L.; Clark, K.L.; Falge, E.; Ellsworth, D.S.; Goldstein, A.H.; Monson, R.K.; Hollinger, D.; Falk, M.; et al. Modeling and measuring the effects of disturbance history and climate on carbon and water budgets in evergreen needleleaf forests. *Agric. For. Meteorol.* **2002**, *113*, 185–222. [CrossRef]
59. SoilGrids REST. Available online: https://rest.isric.org/soilgrids/v2.0/docs (accessed on 8 September 2024).
60. Agro API. Available online: https://agromonitoring.com/ (accessed on 8 September 2024).
61. OpenWeatherMap. Available online: https://openweathermap.org/ (accessed on 8 September 2024).
62. GBIF. Available online: https://www.gbif.org/ (accessed on 8 September 2024).
63. Ngrok. Available online: https://ngrok.com (accessed on 8 September 2024).
64. Shook, K.; Pomeroy, J.W. Synthesis of incoming shortwave radiation for hydrological simulation. *Hydrol. Res.* **2011**, *42*, 433. [CrossRef]
65. Annandale, J.G.; Jovanovic, N.Z.; Benadé, N.; Allen, R.G. Software for missing data analysis of Penman-Monteith reference evapotranspiration. *Irrig. Sci.* **2001**, *21*, 57–67. [CrossRef]
66. Leaflet. Available online: https://leafletjs.com/ (accessed on 8 September 2024).
67. Zhu, X.; Vondrick, C.; Fowlkes, C.C.; Ramanan, D. Do we need more training data? *Int. J. Comput. Vis.* **2016**, *119*, 76–92. [CrossRef]
68. Bailly, A.; Blanc, C.; Francis, E.; Guillotin, T.; Jamal, F.; Wakim, B.; Roy, P. Effects of dataset size and interactions on the prediction performance of logistic regression and deep learning models. *Comput. Methods Programs Biomed.* **2022**, *213*, 106504. [CrossRef]
69. TensorFlow. Available online: https://www.tensorflow.org/ (accessed on 8 September 2024).
70. Yin, X.; Struik, P.C. C_3 and C_4 photosynthesis models: An overview from the perspective of crop modelling. *NJAS–Wagening. J. Life Sci.* **2009**, *57*, 27–38. [CrossRef]
71. Thum, T.; Aalto, T.; Laurila, T.; Aurela, M.; Kolari, P.; Hari, P. Parametrization of two photosynthesis models at the canopy scale in a northern boreal Scots pine forest. *Tellus* **2007**, *59*, 874–890. [CrossRef]
72. Ali, A.A.; Xu, C.; Rogers, A.; McDowell, N.G.; Medlyn, B.E.; Fisher, R.A.; Wullschleger, S.D.; Reich, P.B.; Vrugt, J.A.; Bauerle, W.L.; et al. Global scale environmental control of plant photosynthetic capacity. *Ecol. Appl.* **2015**, *25*, 2349–2365. [CrossRef]
73. Baldocchi, D.D.; Amthor, J.S. Canopy photosynthesis: History, measurements and models. In *Terrestrial Global Productivity*; Roy, J., Saugier, B., Mooney, H.A., Eds.; Academic Press: San Diego, CA, USA, 2001; pp. 9–31.
74. Smith, E. The influence of light and carbon dioxide on photosynthesis. *Gen. Physiol.* **1937**, *20*, 807–830. [CrossRef] [PubMed]
75. Yin, X.; Van Oijen, M.; Schapendonk, A.H.C.M. Extension of a biochemical model for the generalized stoichiometry of electron transport limited C_3 photosynthesis. *Plant Cell Environ.* **2004**, *27*, 1211–1222. [CrossRef]
76. Monteith, J.L.; Unsworth, M.H. *Principles of Environmental Physics*, 2nd ed.; Butterworth-Heinemann, Elsevier: Oxford, UK, 1990.
77. Swinbank, W.C. Long-Wave Radiation from Clear Skies. *Q. J. R. Meteorol. Soc.* **1963**, *89*, 339–348. [CrossRef]
78. Makela, A.; Kolari, P.; Karimaki, J.; Nikinmaa, E.; Peramaki, M.; Hari, P. Modelling five years of weather-driven variation of GPP in a boreal forest. *Agric. For. Meteorol.* **2006**, *139*, 382–398. [CrossRef]
79. Collatz, G.J.; Ball, J.T.; Grivet, C.; Berry, J.A. Physiological and environmental regulation of stomatal conductance, photosynthesis and transpiration—A model that includes a laminar boundary-layer. *Agric. For. Meteorol.* **1991**, *54*, 107–136. [CrossRef]
80. De Kauwe, M.G.; Kala, J.; Lin, Y.-S.; Pitman, A.J.; Medlyn, B.F.; Duursma, R.A.; Abramovitz, G.; Wang, Y.-P.; Miralles, D.G. A test of an optimal stomatal conductance scheme within the CABLE land surface model. *Geosci. Model Dev.* **2015**, *8*, 431–452. [CrossRef]
81. Larcher, W. *Physiological Plant Ecology*; Springer: Berlin, Germany, 2001.
82. Leuning, R. Modelling stomatal behaviour and photosynthesis of Eucalyptus grandis. *Aust. J. Plant Physiol.* **1990**, *17*, 159–175. [CrossRef]
83. Harley, P.C.; Thomas, R.B.; Reynolds, J.F.; Strain, B.R. Modelling photosynthesis of cotton grown in elevated CO_2. *Plant Cell Environ.* **1992**, *15*, 271–282. [CrossRef]
84. Kim, S.-H.; Lieth, J.H. A coupled model of photosynthesis, stomatal conductance and transpiration for a rose leaf (*Rosa hybrida* L.). *Ann. Bot.* **2003**, *91*, 771–781. [CrossRef]
85. Dizengremel, P. Encyclopedia of the Environment. Available online: https://www.encyclopedie-environnement.org/en/author/dizengremel_pierre/ (accessed on 22 July 2024).
86. Silvola, J. CO_2 dependence of photosynthesis in certain forest and peat mosses and simulated photosynthesis at various actual and hypothetical CO_2 concentrations. *Lindbergia* **1985**, *11*, 86–93. Available online: https://www.jstor.org/stable/3682506 (accessed on 30 July 2024).

87. Sveinbjornsson, B. Arctic treeline in a changing climate, in Arctic Ecosystems in a Changing Climate. In *An Ecophysiological Perspective*; Chapin, F.S., Jefferies, R.L., Reynolds, J.F., Shaver, G.R., Svoboda, J., Chu, E.W., Eds.; Academic Press: San Diego, CA, USA, 1992; pp. 239–256.
88. Aber, J.D.; Federer, C.A. A generalized, lumpedparameter model of photosynthesis, evapotranspiration and net primary production in temperate and boreal forest ecosystems. *Oecologia* **1992**, *92*, 463–474. [CrossRef] [PubMed]
89. Thornley, J.H.M. Modelling Allocation with Transport / Conversion Processes. *Silva Fenn.* **1997**, *31*, 341–355. [CrossRef]
90. Sellers, P.J.; Randall, D.A.; Collatz, G.J.; Berry, J.A.; Field, C.B.; Dazlich, D.A.; Zhang, C.; Collelo, G.D.; Bounuoa, L. A Revised Land Surface Parameterization (SiB2) for Atmospheric GCMS. Part I: Model Formulation. *J. Clim.* **1996**, *9*, 676–705. [CrossRef]
91. Bond-Lamberty, B.; Gower, S.T. Estimation of stand-level leaf area for boreal bryophytes. *Oecologia* **2007**, *151*, 584–592. [CrossRef] [PubMed]
92. Chen, W.; Li, J.; Zhang, Y.; Zhou, F.; Koehler, K.; Leblanc, S.; Fraser, R.; Oltof, I.; Zhang, Y.; Wang, J. Relating Biomass and Leaf Area Index to Non-Destructive Measurements for Monitoring Changes in Arctic Vegetation. *Arctic* **2009**, *62*, 281–294. [CrossRef]
93. Konopka, B.; Pajtik, J.; Marusak, R.; Bosel'a, M.; Lukac, M. Specific leaf area and leaf area index in developing stands of Fagus sylvatica L. and Picea abies Karst. *For. Ecol. Manag.* **2016**, *364*, 52–59. [CrossRef]
94. Thornley, J.H.M. Respiration, growth and maintenance in plants. *Nature* **1970**, *227*, 304–305. [CrossRef]
95. Le Roux, X.; Lacointe, A.; Escobar-Gutierrez, A.; Le Dizes, S. Carbon-based models of individual tree growth: A critical appraisal. *Ann. For. Sci.* **2001**, *58*, 469–506. [CrossRef]
96. Arora, V.K.; Boer, J.F. A parameterization of leaf phenology for the terrestrial ecosystem component of climate models. *Glob. Chang. Biol.* **2005**, *11*, 39–59. [CrossRef]
97. Jackson, R.B.; Mooney, H.A.; Schulze, E.-D. A global budget for fine root biomass, surface area, and nutrient contents. *Proc. Natl. Acad. Sci. USA* **1997**, *94*, 7362–7366. [CrossRef]
98. Kozlowski, T.T.; Palardy, S.G. Physiology of Woody Plants. Academic Press: San Diego, CA, USA, 1997.
99. Moore, T.R.; Lafleur, P.M.; Roulet, N.T.; Frolking, S. Dependency of Ecosystem Respiration in a Cool Temperate Bog on Peat Temperature and Water Table. American Geophysical Union, Fall Meeting 2003, abstract id. B22B-04. Available online: https://scholars.unh.edu/earthsci_facpub/452/ (accessed on 24 July 2024).
100. Fan, Y.; Miguez-Macho, G.; Jobbagy, E.G.; Jackson, R.B.; Otero-Casal, C. Hydrologic regulation of plant rooting depth. *Proc. Natl. Acad. Sci. USA* **2017**, *114*, 10572–10577. [CrossRef] [PubMed]
101. Crawford, R.M.M. Metabolic adaptations to anoxia. In *Plant Life in Anaerobic Environments*; Hook, D.D., Crawford, R.M.M., Eds.; Ann Arbor Science Publication: Ann Arbor, MI, USA, 1978; pp. 119–135.
102. Boutin, C.; Keddy, P.A. A functional classification of wetland plants. *J. Veg. Sci.* **1993**, *4*, 591–600. [CrossRef]
103. Mitsch, W.J.; Gosselink, J.G. *Wetlands*; John Wiley & Sons: Hoboken, NJ, USA, 2007.
104. Batzer, D.P.; Baldwin, A.H. *Wetland Habitats in North America: Ecology and Conservation Concerns*; University of California Press: Berkeley, CA, USA; Los Angeles, CA, USA, 2012.
105. Xu, J.; Morris, P.J.; Liu, J.; Holden, J. PEATMAP: Refining estimates of global peatland distribution based on a meta-analysis. *Catena* **2018**, *160*, 134–140. [CrossRef]
106. Naasz, R.; Michel, J.-C.; Charpentier, S. Measuring hysteretic hydraulic properties of peat and pine bark using a transient method. *Soil Sci. Soc. Am. J.* **2005**, *69*, 13–22. [CrossRef]
107. Freeze, R.A.; Cherry, J.A. *Groundwater*; 9780133653120. OCLC 252025686; Prentice-Hall: Englewood Cliffs, NJ, USA, 1979.
108. Wright, N.; Hayashi, M.; Quinton, W.L. Spatial and temporal variations in active layer thawing and their implication on runoff generation in peat-covered permafrost terrain. *Water Resour. Res.* **2009**, *45*, W05414. [CrossRef]
109. Jansson, P.-E. *Simulating Model for Soil Water and Heat Conditions: Description of the Soil Model*; University of Agricultural Sciences: Uppsala, Sweden, 1998; pp. 282–6569.
110. Weiss, R.; Shurpali, N.J.; Sallantaus, T.; Laiho, R.; Laine, J.; Alm, J. Simulation of water table level and peat temperatures in boreal peatlands. *Ecol. Model.* **2006**, *192*, 441–456. [CrossRef]
111. Wang, J.; Lee, W.F.; Ling, P.P. Estimation of thermal diffusivity for greenhouse soil temperature simulation. *Appl. Sci.* **2020**, *10*, 653. [CrossRef]
112. Brooks, A.; Farquhar, G.D. Effect of temperature on the CO_2/O_2 specificity of ribulose-1,5-bisphosphate carboxylase/oxygenase and the rate of respiration in the light. Estimates from gas-exchange measurements on spinach. *Planta* **1985**, *165*, 397–406. [CrossRef]
113. Juutinen, S.; Moore, T.R.; Laine, A.M.; Bubier, J.L.; Tuittila, E.-S.; De Young, A.; Chong, M. Responses of the mosses *Sphagnum capillifolium* and *Polytrichum strictum* to nitrogen deposition in a bog: Growth, ground cover, and CO_2 exchange. *Botany* **2015**, *17*. [CrossRef]
114. Medlyn, B.E.; Dreyer, E.; Ellsworth, D.; Forstreuter, M.; Harley, P.C.; Kirschbaum, M.U.F.; Le Roux, X.; Montpied, P.; Strassemeyer, J.; Walcroft, A.; et al. Temperature response of parameters of a biochemically based model of photosynthesis. II. A review of experimental data. *Plant Cell Environ.* **2002**, *25*, 1167–1179. [CrossRef]

115. Bernacchi, C.J.; Portis, A.R.; Nakano, H.; von Caemerer, S.; Long, S.P. Temperature Response of Mezophyll Conductance. Implications for the Determination of Rubisco Enzyme Kinetics and for Limitations to Photosynthesis in Vivo. *Plant Physiol.* **2002**, *130*, 1992–1998. [CrossRef]
116. Harley, P.C.; Baldocchi, D.D. Scaling carbon dioxide and water vapour exchange from leaf to canopy in a temperate deciduous forest. I. leaf level parametrization. *Plant Cell Environ.* **1995**, *18*, 1146–1156. [CrossRef]
117. Grossman, Y.L.; DeJong, T.M. PEACH: A simulation model of reproductive and vegetative growth in peach trees. *Tree Physiol.* **1994**, *14*, 329–345. [CrossRef]
118. Hauhs, M.; Kastner-Maresch, A.; Rost-Siebert, K. A model relating forest growth to ecosystem-scale budgets of energy and nutrients. *Ecol. Model.* **1995**, *83*, 229–243. [CrossRef]
119. Williams, M. A three-dimensional model of forest development and competition. *Ecol. Model.* **1996**, *89*, 73–98. [CrossRef]
120. Barber, S.A.; Silberbush, M. Plant root morphology and nutrient uptake. In *Roots, Nutrients and Water Influx, and Plant Growth*; Barber, S.A., Bouldin, D.R., Eds.; Number 49; ASA Special Publicatio: Madison, WI, USA, 1984; pp. 65–87. [CrossRef]